AD-A151 926

DYNAMIC RESPONSE OF FLUID

TRANSMISSION LINES

THESIS

Phillip G. Wilkins
Captain, USAF

DTIC FILE COPY

DISTRIBUTION STATEMENT A
Approved for public release;
Distribution Unlimited

DTIC
ELECTE
MAR 28 1985
S D
B

DEPARTMENT OF THE AIR FORCE
AIR UNIVERSITY
AIR FORCE INSTITUTE OF TECHNOLOGY

Wright-Patterson Air Force Base, Ohio

85 03 13 090

REPRODUCED AT GOVERNMENT EXPENSE

AFIT/GAE/AA/84D-28

DYNAMIC RESPONSE OF FLUID TRANSMISSION LINES

THESIS

Phillip G. Wilkins
Captain, USAF

AFIT/GAE/AA/84D-28

DTIC
ELECTE
MAR 28 1985
S D
B

Approved for public release; distribution unlimited

AFIT/GAE/AA/84D-28

DYNAMIC RESPONSE OF FLUID TRANSMISSION LINES

THESIS

Presented to the Faculty of the School of Engineering

of the Air Force Institute of Technology

Air University

In Partial Fulfillment of the

Requirements for the Degree of

Master of Science in Aeronautical Engineering

Phillip G. Wilkins, B.S.

Captain, USAF

December 1984

Approved for public release; distribution unlimited

Preface

This thesis is one of a continuing series of studies conducted at the Air Force Institute of Technology (AFIT) to increase the understanding of frequency response characteristics of pneumatic transmission lines. Better models are sought to enhance the prediction capabilities for various flow conditions and line configurations. The purpose of this study is to investigate the effects of turbulent mean flow and line terminations on the dynamic response of circular pneumatic lines.

Previous studies performed at AFIT, notably those of Moore, Vining, Malanowski and Briski, provided invaluable information and guidance pertaining to the experimental and analytical aspects of this thesis.

I wish to thank a number of individuals whose support made this study possible. No matter how busy, Dr. M. E. Franke was always available for consultation and technical advise. Dr. W. Elrod and Capt. W. Cox contributed welcomed analytical and experimental assistance. A special thanks to my wife Cindy who managed the household and keep our family together through some difficult periods.

Phillip G. Wilkins

Contents

	Page
Preface	ii
List of Figures	v
List of Tables	vi
List of Symbols	vii
Abstract	x
I. Introduction	1
Background	1
Objectives	3
II. Theory	4
Electrical Analogy	4
Blocked and Laminar Flow Lines	6
Turbulent Flow	9
Termination Impedance	16
Computer Analysis	21
III. Experiment	24
Apparatus	24
Test Designation	30
Procedure	30
IV. Results and Discussion	32
Test Conditions	32
Blocked Lines	32
Laminar Mean Flow	35
Turbulent Mean Flow	37
V. Conclusions	43
VI. Recommendations	45
Bibliography	46
Appendix A: Theoretical and Experimental Gain and Phase Shift	48

Page

Appendix B: Orifice Models 106

Appendix C: Computer Program 113

Appendix D: Experimental Equipment 124

Vita 125

DTIC
COPY
INSPECTED
1

Accession For
NTIS GRA&I
DTIC TAB
Unannounced
Justification
By
Distribution/
Availability Codes
Avail and/or
Dist Special
A-1

List of Figures

Figure		Page
1	Electrical Analogy to Fluid Transmission Line	5
2	Transmission Line with Terminal Impedance . .	8
3	Nondimensional Attenuation vs Frequency . . .	11
4	Sudden Area Change	20
5	Test Line	25
6	Termination Devices	26
7	Experimental Apparatus	28
8-13	Blocked Line Frequency Response	49-54
14-21	Response for Laminar Flow, Choked Orifice . .	55-62
22-33	Response for Laminar Flow, Unchoked Orifice .	63-74
34-37	Response of Open Lines with Laminar Flow . .	75-78
38-40	Effect of Constant LRC Component Variation .	79-81
41-48	Response of Turbulent Flow with Orifice . . .	82-89
49-64	Response of Open Lines with Turbulent Flow .	90-105
65	Comparison of Orifice Impedance Models . . .	112

List of Tables

Table		Page
I	Transfer Functions for Selected Terminal Conditions	18
II	Test Line Dimensions	27
III	Test Summary	33

List of Symbols

Symbol	Description	Units
A	line cross-sectional area	in
a	adiabatic speed of sound	in/sec
B	phase angle	radians
C	capacitance/unit length	in^4/lbf
C_a	adiabatic capacitance/unit length	in^4/lbf
C_i	isothermal capacitance/unit length	in^4/lbf
C_T	turbulent capacitance/unit length	in^4/lbf
D	inside line diameter	in
f	friction factor	dimensionless
G	conductance/unit length	$in^4/lbf\text{-}sec$
g	pressure gain	dimensionless
g_{db}	pressure gain in decibels	decibels
h_t	temperature distribution factor	dimensionless
h_v	velocity distribution factor	dimensionless
j	$(-1)^{0.5}$	dimensionless
k	ratio of specific heats	dimensionless
K_{LT}	inertance constant	dimensionless
L	inertance/unit length	$lbf\text{-}sec^2/in^6$
L_a	adiabatic inertance/unit length	$lbf\text{-}sec^2/in^6$
L_T	turbulent inertance/unit length	$lbf\text{-}sec^2/in^6$
M	mass flow rate	lbm/sec
n	polytropic exponent	dimensionless

Symbol	Description	Units
P	pressure	psia
P_a	ambient pressure	psia
P_{in}	inlet pressure	psia
P_L	pressure drop across load	psi
P_R	receiving pressure	psig
P_S	sending pressure	psig
P_T	static line pressure	psig
Q	volumetric flow rate	cis
R	resistance/unit length	$lbf\text{-}sec/in^6$
R_{AC}	AC resistance/unit length	$lbf\text{-}sec/in^6$
R_{DC}	DC resistance/unit length	$lbf\text{-}sec/in^6$
R_g	gas constant for air	$in^2/sec^2/R$
Re	Reynolds number	dimensionless
RC	reflection coefficient	dimensionless
r	inside line radius	in
T_a	ambient temperature	$^\circ R$
u	velocity	in/sec
V	volume	in^3
x	distance in downstream direction	in
Y	admittance/unit length	$in^4/lbf\text{-}sec$
Z	impedance/unit length	$lbf\text{-}sec/in^6$
Z_c	characteristic impedance/unit length	$lbf\text{-}sec/in^6$
Z_{in}	input impedance	$lbf\text{-}sec/in^5$
Z_L	load impedance	$lbf\text{-}sec/in^5$
Z_R	radiation impedance	$lbf\text{-}sec/in^5$

Symbol	Description	Units
α	attenuation/unit length	neper/in
β	phase shift/unit length	rad/in
Γ	propagation operator/unit length	1/in
μ	dynamic viscosity	lbf-sec/in^2
ν	kinematic viscosity	in^2/sec
Ω	nondimensional frequency	dimensionless
Ω_B	nondimensional break frequency	dimensionless
ω	angular frequency	rad/sec
ω_ν	characteristic frequency	rad/sec
ρ	density	lbf-sec^2/in^4
σ	(Prandtl number)$^{.05}$	dimensionless
$\theta_\circ$	radiation function, real	dimensionless
$\chi_\circ$	radiation function, imaginary	dimensionless

Abstract

Experimental frequency response data were obtained for straight pneumatic transmission lines of circular cross-section. Three 24 in. long lines with inside diameters of 0.041, 0.119 and 0.195 in. were tested at Reynolds numbers varying from 0 to 15000.

The experimental data were compared with theoretical predictions obtained from the distributed parameter, small signal equations for the blocked and laminar mean flow cases. Several models were used to predict the effects of turbulent mean flow. The prediction capability and limitations of two turbulent flow models, that include the effects of the Reynolds number, but not frequency, were investigated and discussed.

Methods for determining the end impedance of open and orifice terminated lines with mean flow were studied. The relatively simple approach of reflection coefficients gave satisfactory results for both choked and unchoked flow in orifices. The radiation impedance associated with open lines was found to be negligible for all test cases.

DYNAMIC RESPONSE OF FLUID TRANSMISSION LINES

I. Introduction

Background

A periodic pressure signal propagating in a fluid filled line exhibits changes both in magnitude, defined as gain, and in phase angle, known as phase shift, along the length of the line. The signal may be information, as in a fluidics circuit or instrumentation system, noise in an air duct or even an undesired pulsation due to a pump or valve. It is essential to many system designs to accurately predict the gain and phase shift to assess the impact on desired operation.

The gain and phase shift are dependent on such parameters as line geometry, signal frequency, fluid medium and flow conditions. Early investigations were limited to the field of acoustics. Instrumentation applications led to later studies, many of which involved liquids. The relatively young field of fluidics brought renewed interest in the dynamic response of fluid systems. Many studies have been conducted over a wide range of signal frequencies using circular, annular and rectangular lines with, primarily, air or water as the fluid medium.

The dynamic response of blocked, no mean flow, lines has been accurately predicted by the equations developed by Nichols (Ref 1) and later modified by Krishnaiyer and Lechner (Ref 2). These equations also apply to lines in which the signals are imposed on a laminar mean flow.

Brown, Margolis and Shaw (Ref 3), Moore (Ref 4) and Briski (Ref 5), among others, showed that application of these equations to cases involving turbulent mean flow lead to good agreement at higher frequencies, but under predicted the attention at lower frequencies. Brown, et al. (Ref 3) developed a somewhat complicated procedure for predicting turbulent flow response by considering two and three-region boundary layer models. Moore (Ref 4) described three frequency regimes based on boundary layer thickness and used a constant inertance, resistance and capacitance (LRC) model to predict the increased attenuation of the turbulent flow, compared to the laminar case, at lower frequencies. Briski (Ref 5) modified the constant LRC model to account for the effects of mean flow on the resistance.

All fluid lines are terminated in some fashion. Vining (Ref 6) studied means to determine the impedance of orifices with mean air flow. The proper determination of the terminal impedance was shown to be an important factor in modeling the line.

Objectives

The following objectives were established to study the dynamic response of pneumatic transmission lines.

1. Investigate means of determining the impedance of various termination and flow combinations.

2. Modify existing computer program to incorporate revised theoretical models and techniques for determining the pressure drop and Reynolds number of a line.

3. Experimentally determine gain and phase shift for various test line configurations and flow conditions.

4. Present simple models to predict the response of lines with turbulent mean flow.

5. Assess response predictions for blocked, laminar and turbulent mean flow cases by comparison with experimental data.

II. Theory

Electrical Analogy

Electrical transmission theory is well developed and can be found in great detail in King (Ref 7) among others. Electrical theory can be applied to the study of fluid transmission lines by considering pressure to be analogous to potential and volumetric flow rate to represent the current. Ohm's Law then becomes

$$\Delta P = zQ \tag{1}$$

or

$$Q = y \Delta P \tag{2}$$

where z is the complex series impedance, y is the complex admittance, ΔP is the pressure change and Q is the volumetric flow rate. The above equations expressed as a function of the length, x, are

$$dP/dx = ZQ = (R + j\omega L)Q \tag{3}$$

or

$$dQ/dx = YP = (G + j\omega C)P \tag{4}$$

where R, L, G and C are the resistance, inertance, conductance and capacitance per unit length of line. The analogous circuit for a fluid transmission line is shown in Fig 1.

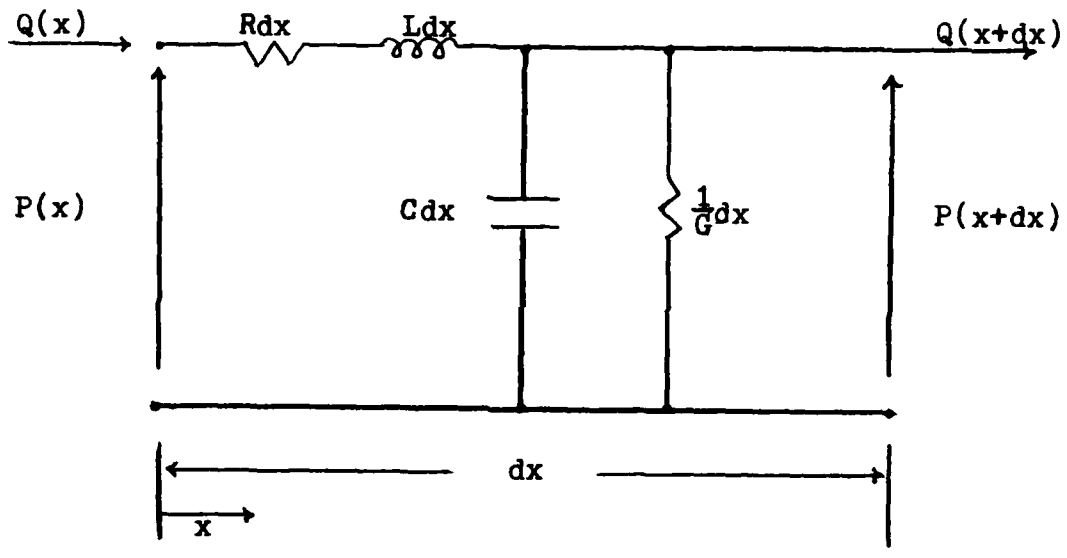

Figure 1 Electrical Analogy for Fluid Transmission Lines

Blocked and Laminar Flow Lines

Values for Z and Y may be obtained for circular blocked lines and those with laminar mean flow by using the equations of Nichols (Ref 1). This approach involves the use of Bessel functions and becomes rather complicated. Krishnaiyer and Lechner (Ref 2) present modifications that have been shown to give accurate predictions for Z and Y for the frequency range $\omega > \omega_\nu/10$ where ω_ν is the characteristic frequency defined as

$$\omega_\nu = 32\ \nu/D^2 \tag{5}$$

where D is the line diameter.

The modified equations are given as

$$Z = (8\pi/A^2)(DR) + j((\omega\rho/A) + (8\pi\mu/A^2)(DL)) \tag{6}$$

and

$$Y = -\frac{\left[\omega(k-1)\ \frac{A}{kP}\right]}{(DC)^2 + (DG)^2}\ (DG) + j\omega\frac{\left[\frac{A}{kP} + (k-1)\left(\frac{A}{kP}\right)(DC)\right]}{(DC)^2 + (DG)^2} \tag{7}$$

where the quantities DR, DL, DG and DC are described in terms of velocity and temperature parameters, are respectively

$$DR = 3/8 + h_\nu/4 + 3/(8\ h_\nu) \tag{8}$$

$$DL = h_\nu/4 - 15/(64h_\nu) \tag{9}$$

$$DG = h_t/2 - 1/(4h_t) \tag{10}$$

$$DC = 1/4 + h_t/2 + 1/(4h_t) \tag{11}$$

where

$$h_\nu = 2(\omega/\omega_\nu)^{0.5} \tag{12}$$

and

$$h_t = \sigma h_\nu \tag{13}$$

The line may now be described by a characteristic impedance defined as

$$Z_C = (Z/Y)^{.05} \tag{14}$$

and a propagation operator

$$\Gamma = (ZY)^{0.5} = \alpha + j\beta \tag{15}$$

where α and β are the attenuation and phase shift per unit length. These parameters, along with the terminal impedance and line length will be used later to determine gain and phase shift.

Kirshner and Katz (Ref 8) give the input impedance for the general case of a line with a terminal impedance Z_L, as shown in Fig 2, as

$$Z_{in} = P_{in}/Q_{in} = Z_C(Z_L \cosh\Gamma\ell + Z_C \sinh\Gamma\ell)/(Z_L \sinh\Gamma\ell + Z_C \cosh\Gamma\ell) \tag{16}$$

The transfer function relating the value of P at any x along the line to the inlet pressure becomes

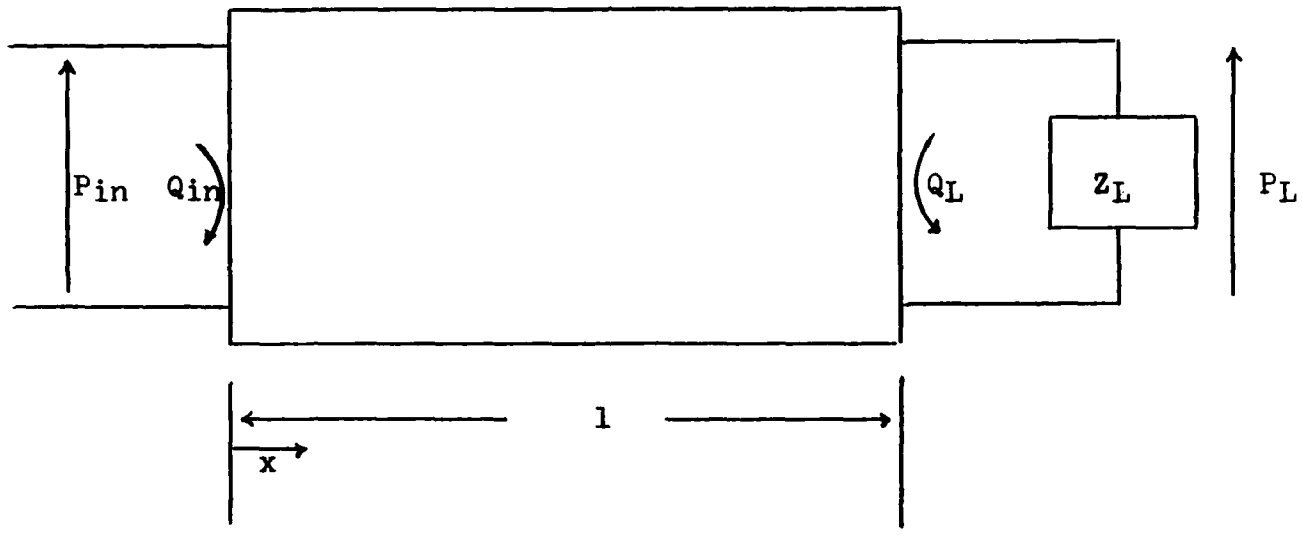

Figure 2 Transmission Line with Terminal Impedance

$$P/P_{in} = [\sinh\Gamma\ell(1-x/\ell) + (Z_L/Z_c)\cosh\Gamma\ell(1-x/\ell)]/ \quad (17)$$
$$[\sinh\Gamma\ell + (Z_L/Z_c)\cosh\Gamma\ell]$$

The pressure gain is the magnitude of equation (17)

$$g = |P/P_{in}| \quad (18)$$

or expressed in decibels

$$g_{db} = 20\ LOG_{10}|P/P_{in}| \quad (19)$$

The corresponding phase shift is the angle formed in the complex plane by the real and imaginary parts of the transfer function

$$B = TAN^{-1}[Im(P/P_{in})/Re(P/P_{in})] \quad (20)$$

Turbulent Flow

Equations (6) and (7) yield accurate predictions for the response of blocked and laminar flow cases. Attempts to extend their application to turbulent mean flow underestimate the experimentally observed attenuation, (Ref 3-5).

The laminar steady state fully developed flow has a parabolic velocity profile with a boundary layer thickness equal to the radius. The dynamic boundary layer, created when a periodic signal is imposed on the steady state, or mean, flow, becomes thinner, that is the gradients near the wall increase, as the frequency increases. Therefore, for all frequencies of practical interest, the dynamic

layer is much thinner than the steady state and therefore dictates the response behavior. Equations (6) and (7) are seen to be dependent on the signal frequency but not the Reynolds number.

For turbulent flow, however, the steady state velocity profile becomes dependent on the Reynolds number. As the Reynolds number increases, the boundary layer becomes thinner until in the limiting case of an infinite Reynolds number a uniform profile, or slug flow, is obtained. When a periodic signal is imposed on turbulent flow, the dynamic layer may or may not be thinner than the steady state layer. Since the response is dictated by the thinner layer, one would expect to observe different behavior due to frequency and Reynolds number combinations.

A plot of nondimensional attenuation versus nondimensional frequency, Ω , presented by Brown, et al. (Ref 3) is shown in Fig 3. Future use of the terms attenuation and frequency will refer to these nondimensional parameters. Moore (Ref 4), as suggested by Brown, et al. (Ref 3), divides the frequency spectrum into three regions; low, mid and high.

In the low frequency region, the dynamic boundary layer is thicker than the steady state layer. The high frequency region exhibits the same behavior as the laminar flow due to the fact that the dynamic layer has grown much

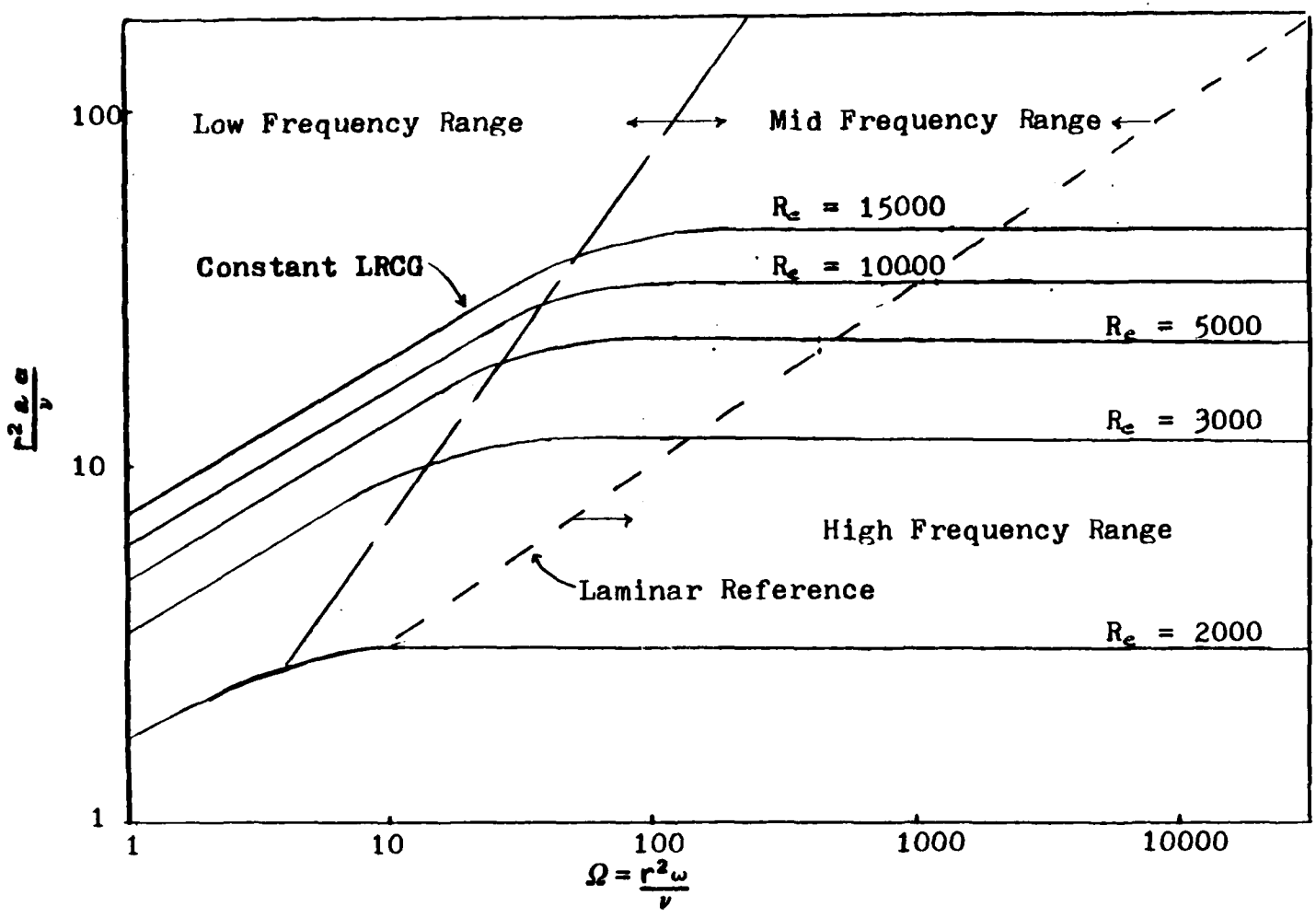

Figure 3 Nondimensional Attenuation vs Frequency

thinner than the steady state layer. The mid frequency range is characterized by dynamic and steady state layers of comparable thickness.

Moore (Ref 4) applied a constant LRC model to both the low and mid frequency regions. This approach used a steady state (DC) resistance

$$R_{DC} = f \, Re \, \mu / 2 \, A \, D^2 \tag{21}$$

which by using the Blasius resistance formula, as presented by Schlichting (Ref 9), for turbulent flow in smooth lines

$$f = 0.3164 \, Re^{-0.25} \tag{22}$$

was written as

$$R_{DC} = 0.3164 \, Re^{0.75} \, \mu / (2 \, A \, D^2) \tag{23}$$

The capacitance was assumed to be

$$C = (k/n) C_a \tag{24}$$

where n is the polytropic exponent obtained from the thermodynamic process description

$$PV^n = \text{constant} \tag{25}$$

and C_a is the adiabatic capacitance defined as

$$C_a = A/(kP) \tag{26}$$

The value of n varies from k at high frequencies to 1.0 for the isothermal process though to exist at low frequencies (Ref 4).

The adiabatic inertance used is defined as

$$L_a = \rho/A \tag{27}$$

As the model name implies, the conductance was neglected. This choice, as well as that of isothermal capacitance and adiabatic inertance, was based on analysis of the laminar case at low frequency (Ref 4)

Using equations (3) and (4), the turbulent impedance and admittance can be expressed as

$$Z = R_{DC} + j\omega L_a \tag{28}$$

and

$$Y = j\omega C \tag{29}$$

The gain and phase shift can now be determined through the use of equations (14)-(28). The laminar model, as shown experimentally by Brown, et al. (Ref 3) and Funk and Wood (Ref 10), among others, accurately describes the response behavior at frequencies above the break frequency, Ω_B, which is defined as the frequency at which the attenuation predictions of the laminar, equations (6) and (7), and the turbulent, in this case the constant LRC, models are equal. At frequencies below the

break frequency, however, the laminar model under predicts the attenuation.

As shown by Briski (Ref 5), the attenuation predicted by the constant LRC model is also lower than that observed experimentally. Modifications to the constant LRC model will be presented in an effort to improve the prediction capability in the low and mid frequency regions. Although L, R, C and G have been shown to be frequency dependent (Ref 4), this study will employ only constant values to maintain the simplicity of the constant LRC model.

The mid frequency region of Fig 3 is characterized by a rather flat attenuation curve dependent upon the Reynolds number only. Therefore, only the Reynolds number dependency of each of the components will be investigated.

To account for the variation in resistance due to Reynolds number, a linearized or incremental (AC) resistance was proposed (Ref 11)

$$R_{AC} = R_{DC} + Re((\partial / \partial Re) R_{DC}) \qquad (30)$$

which, using the DC resistance of equation (23), reduces to

$$R_{AC} = 1.75 \; R_{DC} \qquad (31)$$

Based on the effect of the velocity profile on the inertance, Moore and Franke (Ref 12) give the inertance

as

$$L_T = K_{LT} L_a \tag{32}$$

where K_{LT} is the inertance constant

$$K_{LT} = (f^{0.5}+1)(f^{0.5}+2)^2/[4(2f^{0.5}+1)] \tag{33}$$

K_{LT} is seen to vary from 1.33 for laminar flows with parabolic velocity profiles to 1.0 as the Reynolds number goes to infinity and the profile approaches that of slug flow (Ref 12). Since the friction factor is Reynolds number dependent, the inertance is also shown to be a function of the Reynolds number.

The conductance accounts for the effects of radial heat transfer of a gas. The increased attenuation due to the radial heat transfer is well understood for laminar flow and is incorporated in equations (6) and (7). Moore (Ref 4) assumed the conductance for turbulent flow to be negligible based on the small values observed for laminar flow with small signal frequencies. Brown, et al. (Ref 3) presents the conductance for turbulent flow as

$$G = ((k-1)C_a L_a \omega^2)/(R_{AC} + j\,\omega L_T) \tag{34}$$

which reduces to the following for cases where the quantity (R_{AC}/ω) is much smaller than L_T

$$G = ((k-1)R_{AC}C_a L_a/L_T^2) - j\,\omega\,((k-1)C_a K_{LT} L_a^2/L_T^2) \tag{35}$$

The imaginary part of the conductance can be combined with the isothermal capacitance to form a turbulent capacitance

$$C_T = kC_a[1-(k-1)/(K_{LT}k)] \qquad (36)$$

which is seen to be Reynolds number dependent through the inertance constant. The real part of the conductance is Reynolds number dependent by virtue of both the resistance and inertance constant.

Two models for turbulent mean flow can now be presented. The modified constant LRC model consists of the turbulent inertance from equation (32), AC resistance of equation (31) and turbulent capacitance given by equation (36). The constant LRCG model adds the real part of the conductance from equation (35) to the components of the modified constant LRC model. All components in both models are seen to be functions of the Reynolds number not of frequency.

Terminal Impedance

The steady state DC terminal impedance of a fluid line can be expressed as

$$Z_L = P_L/Q_L + j\ 0 \qquad (37)$$

where P_L is the pressure drop across the termination. Franke, Malanowski and Martin (Ref 13), among others, have

shown it more applicable to use an incremental or linearized AC expression when dealing with dynamic systems

$$Z_L = (\Delta P_L)/\Delta Q_L + j\,0 \qquad (38)$$

For blocked lines, $Q_L = 0$ and $Z_L = \infty$; while for the other extreme case of an open line, P_L and Z_L are taken to be zero.

The effect of the terminal impedance on the pressure gain can be seen in Table I, from (Ref 8), in which the transfer functions for the special cases of blocked, open and matched lines are given. The matched line has a terminal impedance equal to its characteristic impedance and the line appears infinite in length to the input; therefore, no waves are reflected, no standing wave pattern is created and only exponential decay results.

Acoustic theory states the existence of a finite impedance associated with the open line. The air in the open end of the line can be thought of as a massless piston radiating some energy into free space while reflecting some back into the line. Morse and Ingard (Ref 14) give this radiation impedance as

$$Z_R = (\rho a/A)(\theta_o - j\,\chi_o) \qquad (39)$$

where θ_o and χ_o are termed radiation functions. By approximating the values of these functions for the case of a flanged exit, defined as a flush opening in an

Table I

Transfer Functions for Selected Terminal Conditions

Case	Z_L	$\frac{P}{P_{in}}$
Blocked	∞	$\frac{\cosh \Gamma \ell (1-(x/\ell))}{\sinh \Gamma \ell}$
Open	0	$\frac{\sinh \Gamma \ell (1-x/\ell)}{\sinh \Gamma \ell}$
Matched	Z_C	$\mathrm{EXP}[-\Gamma \ell (x/\ell)]$

infinite wall, the real portion is assumed to be negligible while the imaginary part becomes

$$X_o = 0.4\ (D\,\omega/a) \tag{40}$$

The resultant expression for the terminal impedance of an open line is taken to be

$$Z_R = -j\,\omega\,0.4\ (\rho\,D\,\omega/A) \tag{41}$$

Kinsler and Frey (Ref 15) discuss using reflection coefficients to obtain impedance values. Referring to the notation of Fig 4

$$Z_L = (\rho\,a/A)_1\ [(1+RC)/(1-RC)] + j\ 0 \tag{42}$$

where RC is the reflection coefficient for the sudden area change from line 1 to line 2. For the case where line 2 is terminated by its characteristic impedance

$$RC = (A_1 - A_2)/(A_1 + A_2) \tag{43}$$

The use of reflection coefficients simplifies the difficult problem of determining the impedance of an orifice with compressible flow. For cases in which the flow was choked by the orifice, the entire orifice diameter was assumed to contain sonic flow. Katz, Hausner and Eisenberg (Ref 16) indicate that reflected waves from a boundary, which propagate upstream at the speed of sound, will be swept downstream by the sonic flow.

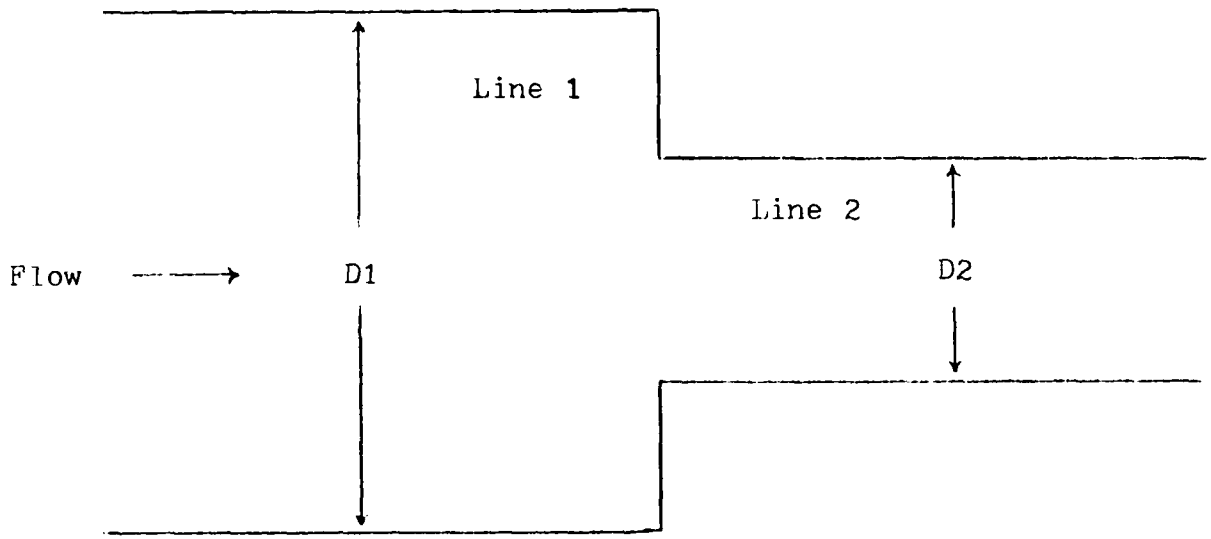

Figure 4 Sudden Area Change

Therefore, the line will appear infinite, or matched, to the input and use of equation (43) is justified.

Determination of the impedance for the case where the pressure ratio across the orifice is insufficient to choke the flow is not as straightforward. For these cases, the orifice was considered as an infinitesimally short open line, with a corresponding reflection coefficient of -1. The remainder of the interface presents a blocked line, reflection coefficient of +1, to the input. The two values are then averaged by area to obtain the composite reflection coefficient

$$RC = (A_1-2A_2)/(A_1+A_2) \qquad (44)$$

Equation (43) is actually obtained in the same fashion by using the fact that the reflection coefficient for a matched line is 0.

Appendix B outlines various orifice impedance models considered for both choked and unchoked cases.

Computer Analysis

An existing computer program, developed by Malanowski (Ref 17) and modified by Briski (Ref 5), was used to determine the attenuation and phase, and then theoretical gain and phase shift. The program uses the laminar model, equations (6) and (7), for the blocked and laminar flow cases. For the turbulent flow cases, attenuation is

calculated by the laminar and selected turbulent model for each frequency. The attenuations are then compared and the largest is used to find the gain and phase shift. As a result, the turbulent model predicts the response up to the break frequency at which point the program shifts to the laminar model.

The program divides the line into a number of short line segments over which it is reasonable to assume constant average values of certain properties to simplify calculations. Since the input pressure to each of the segments is required by the main part of the program, modifications were made to obtain the pressure along the line given a measured line inlet pressure and mass flow rate, which yields the Reynolds number.

Schlichting (Ref 9) gives the pressure drop in a line as

$$\Delta P = f\ (\Delta x)\ \rho (u^2/2D) \tag{45}$$

For laminar flow in smooth lines, the friction factor is

$$f = 64/Re \tag{46}$$

The pressure change for laminar flow then becomes

$$\Delta P = -32(\Delta x)\ \mu^2 (Re/\rho D^3) \tag{47}$$

Using the Blasius resistance formula, the pressure

change for turbulent flow in smooth lines is seen to be

$$\Delta P = -0.1582(\Delta x)\ \mu^2(Re^{1.75}/\rho\ D^3) \qquad (48)$$

Assuming constant temperature and Reynolds number in the short line segment of length x, equation (47) is integrated to give for laminar flow

$$\Delta P = P_{in}-[P_{in}^2+64(\Delta x)\ \mu^2 Re T_a(R_g/D^3)]^{0.5} \qquad (49)$$

where P_{in} is the inlet pressure to the line segment and R_g is the gas constant for air. The corresponding equation for turbulent flow is found from equation (48) to be

$$\Delta P = P_{in}-[P_{in}^2+0.3164\ (\Delta x)\ \mu^2\ Re^{1.75} T_a(R_g/D^3)]^{0.5} \qquad (50)$$

Using the measured pressure at the beginning of the line, the program marches along the line and calculates the inlet pressure for each line segment.

A complete listing of the program is presented in Appendix C.

III. Experiment

Apparatus

Experimental data for this study consisted of pressure measurements taken at the inlet and exit planes of several stainless steel lines. The dynamic pressures at these locations, termed the sending and receiving pressures, were a result of the standing wave pattern created by the periodic signal imposed upstream of the inlet plane. Three lines were used, each 24 in. long and having inside diameters of 0.041, 0.119 or 0.195 in. Each line was supported at both ends by plexiglass blocks which were machined to provide mounting locations for pressure transducers, air supply connections and interchangeable termination devices. Fig 5 depicts the test lines for which the dimensions can be found in Table II. Special devices were used in each of the three lines to create blocked, open and two orifice terminated conditions. Details of the devices are presented in Fig 6 with corresponding dimensions listed in Table II.

Referring to Fig 7, the sending wave analyzer provided an input signal of known frequency, as verified by a frequency counter, to the pneumatic driver assembly. The driver assembly amplified and conditioned the input and imposed sinusoidal pressure signals on the mean air

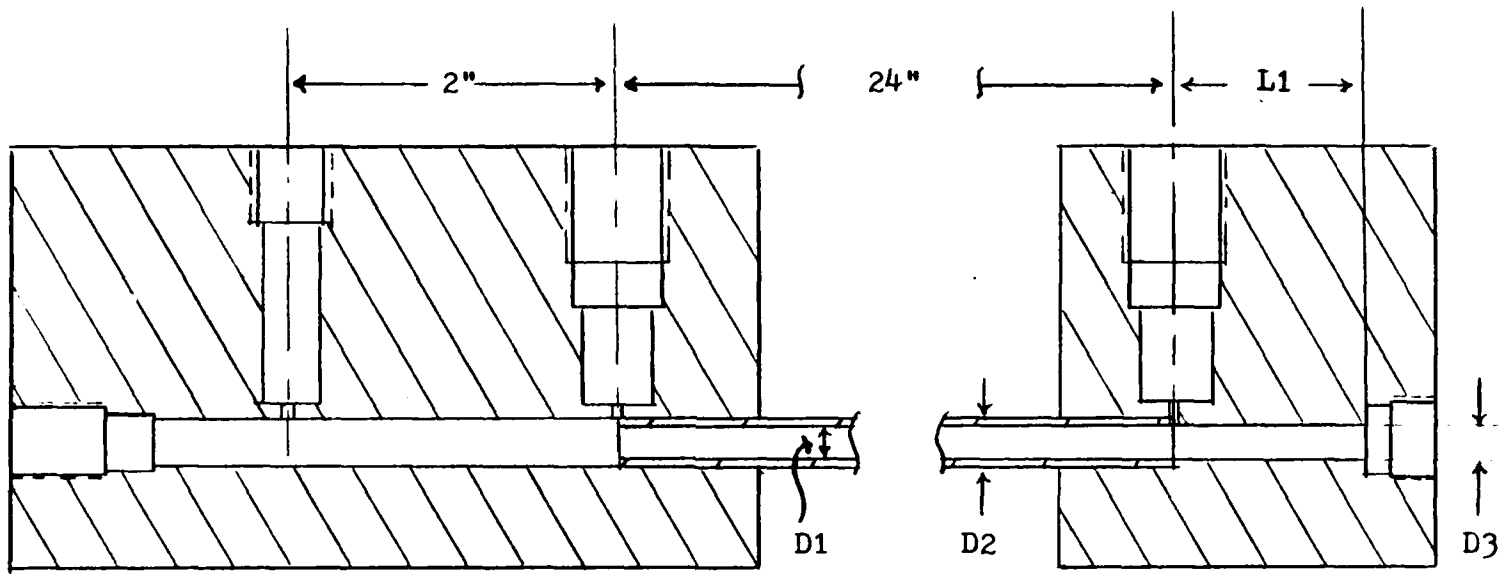

Figure 5 Test Line

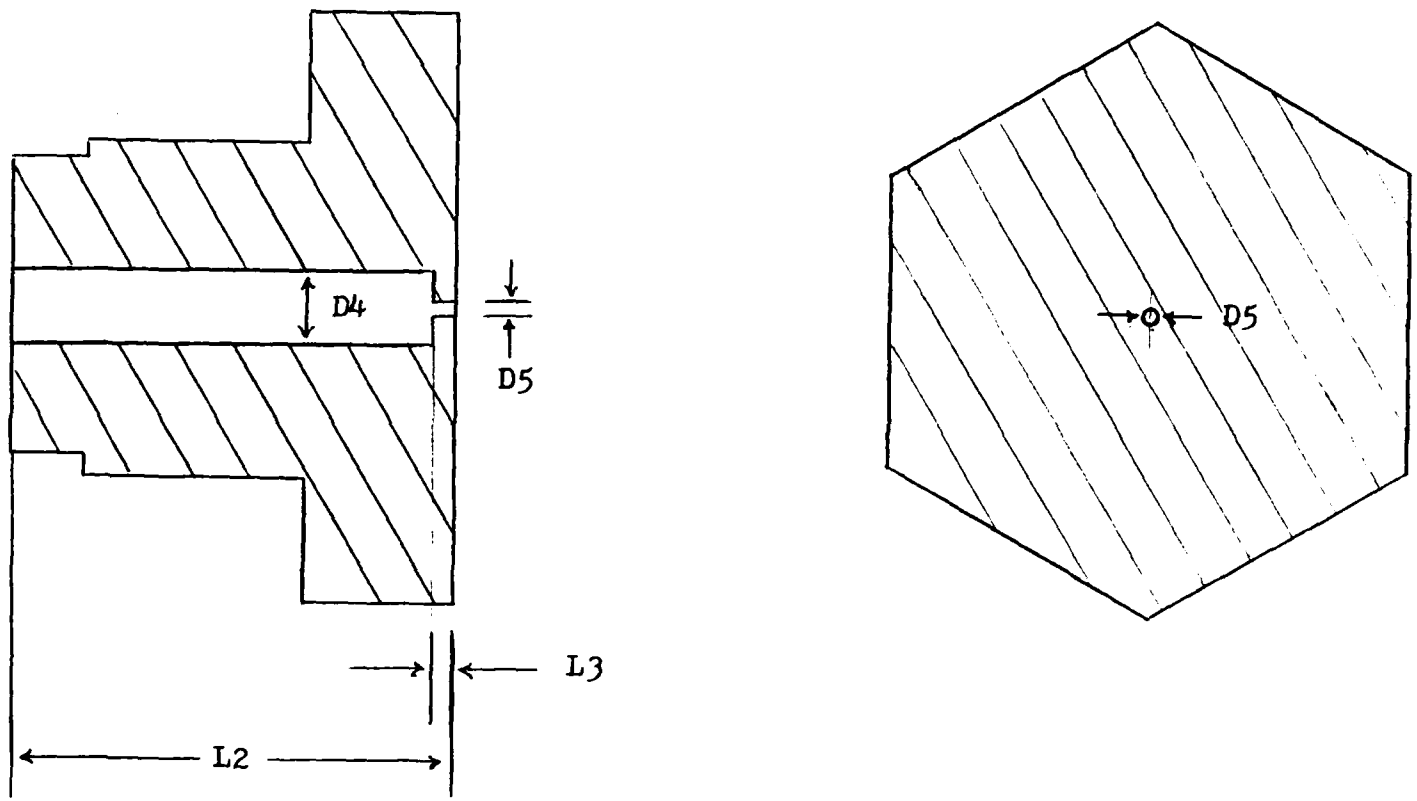

Figure 6 Termination Devices

Table II

Test Line Dimensions

Line Number	Termination Number	D1	D2	D3	D4	D5	L1	L2	L3
1	0	0.041	0.065	0.043	0	0	1.005	0	0
	1	"	"	"	0.043	0.0135	"	0.603	0.060
	2	"	"	"	"	0.016		0.606	0.060
	3	"	"	"	"	0.043	"	0.665	0
2	0	0.119	0.190	0.120	0	0	0.994	0	0
	1	"	"	"	0.120	0.0135	"	0.600	0.060
	2	"	"	"	"	0.016	"	0.604	0.060
	3	"	"	"	"	0.120	"	0.663	0
3	0	0.195	0.251	0.196	0	0	1.001	0	0
	1	"	"	"	0.196	0.0135	"	0.605	0.060
	2	"	"	"	"	0.016	"	0.606	0.060
	3	"	"	"	"	0.196	"	0.663	0

all dimensions in inches

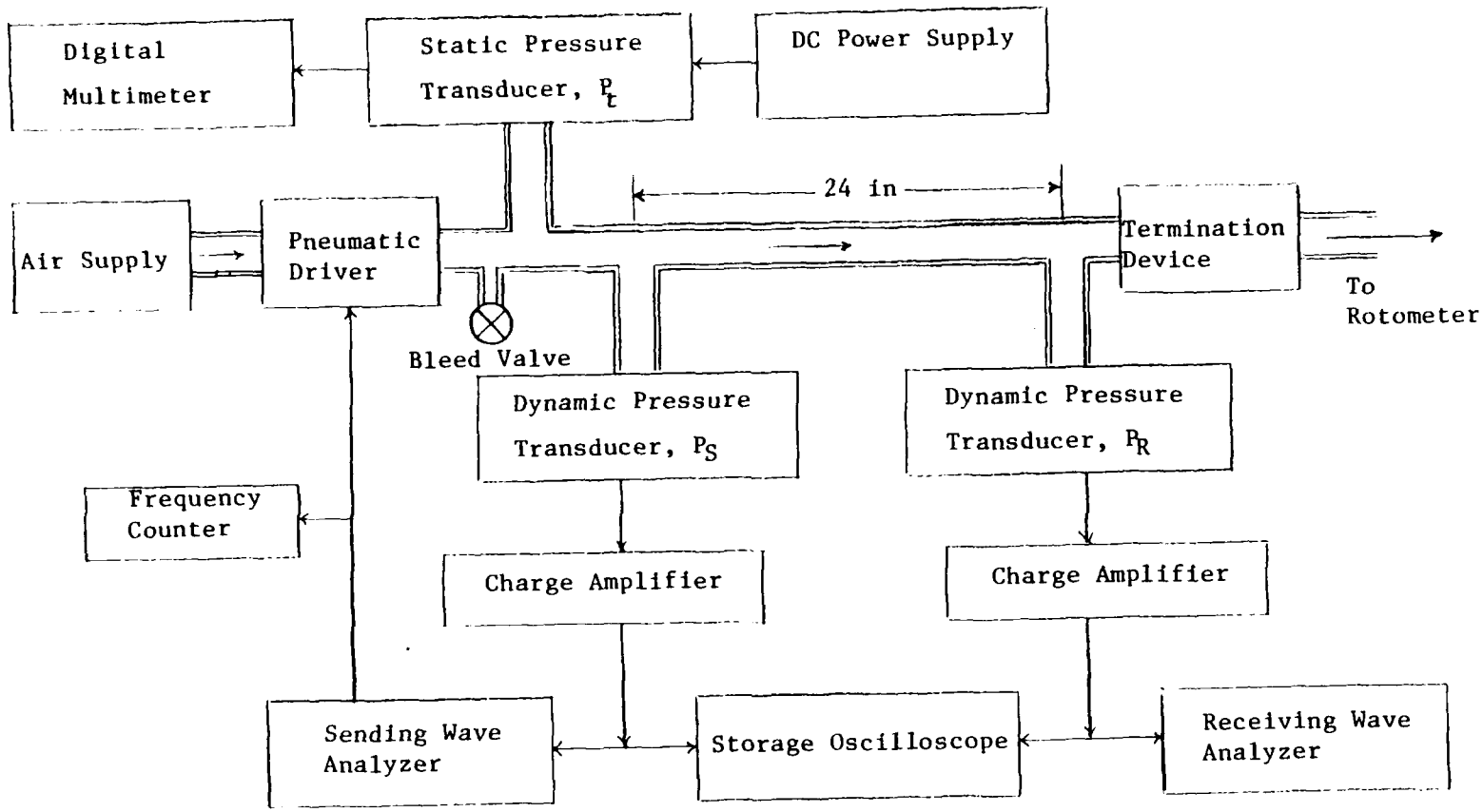

Figure 7 Experimental Apparatus

flow passing through the driver. Piezoelectric transducers were used to measure the dynamic sending and receiving pressures, P_S and P_R. The transducer outputs were routed to charge amplifiers, which converted the charge output of the transducers into a voltage, and then to the wave analyzers for display as RMS values and to the storage oscilloscope, where the waveforms could be compared.

The mass flow rate through the test line was determined using a rotometer that had been calibrated against a gasometer, also known as a bell prover. Since the dynamic response of the line was altered by its presence, the rotometer was removed prior to each test run. The rotometer losses were small enough that its removal did not significantly change the measured mass flow rate. Variations in the air supply during the test were monitored by the static pressure transducer.

For the blocked line cases, a change in the test set up was required. Since the driver required through flow for proper operation, a bypass valve located between the driver and line was opened effectively turning the test line into a blocked branch to a line with mean flow.

A complete list of the major instrumentation used can be found in Appendix D.

Test Designation

A 5-digit code was used to describe each test case. The first digit gave the line number; 1 for the 0.041, 2 for 0.119 and 3 for 0.195 in. inside diameter lines. The second digit indicated the termination employed; 0 for blocked, 1 and 2 for 0.0135 and 0.016 in diameter orifices and 3 for open lines. The last three digits gave the nominal Reynolds number in hundreds. For example, the 12020 case was the 0.041 in test line fitted with a 0.0135 in orifice termination tested at a Reynolds number of 2000.

Procedure

Since the usable frequency range of the driver assembly was limited to 0 to 1000 Hz, the remaining means to vary Ω involved line radius and kinematic viscosity. For a given line, assuming constant absolute viscosity and perfect gas behavior, the range was dictated by line pressure and temperature, taken to be P_T and T_a respectively. As seen in Fig 3, increasing the line pressure in a given line will allow higher Ω values. For turbulent mean flow cases, however, increases in P_T yield increases in attenuation below the break frequency, the start of laminar behavior. This point, termed Ω_B, is then shifted to correspondingly higher values which may exceed the maximum possible with the given line. Since it is of particular interest to investigate the response of

turbulent flow cases in the mid frequency range, orifice terminations are used to increase the P_T and change the Reynolds number. Reynolds numbers are limited by a 50 psig line pressure constraint imposed by the static transducer and test lines. The air supply was manually regulated to provide the mass flow required to obtain the desired Reynolds number. The rotometer was then removed from the line and fluctuations in the line pressure were monitored by the static pressure transducer.

The frequency of the sending wave analyzer, and therefore the signal, was varied from 20 to 1000 Hz in 20 Hz increments. At each increment, the frequency of the receiving wave analyzer was adjusted to provide the maximum voltage reading. The delay time between the sending and receiving waveforms was read off the oscilloscope. The RMS voltages displayed on the wave analyzers and delay time were recorded before moving to the next frequency. These data became part of the input file for the computer program and were used to generate the experimental gain and phase shift.

IV. Results and Discussion

Test Conditions

Table III summarizes the line configurations and test conditions that were used in an attempt to examine various regions of Fig 3. The range of nondimensional frequency spanned by each turbulent test case is also presented. Referring to Fig 3, it is seen that the majority of the data collected is within the mid frequency range.

Blocked Lines

Fig 8-13 give the predicted and experimentally obtained gain and phase shift plotted versus frequency for the three blocked line cases. These figures, along with those for laminar and turbulent mean flow cases, are found in Appendix A. The prediction capabilities of equations (6) and (7) have been demonstrated by many studies to be excellent for blocked lines; hence providing a very reliable means to assess the experimental data collection techniques and evaluate the line model. Fig 10-13 show good agreement between theoretical and experimental values for the two larger diameter lines. Fig 8 and 9, however, show greater deviation for line 1, the 0.041 in. diameter line, which is probably attributable to the increased difficulty of accurately modeling the smaller line dimensions.

Table III

Test Summary

Case	P_a psia	T_a °F	P_T psig	Mx10000 lbm/sec	Re	Ω_{MIN}	Ω_{MAX}
10000	14.36	70.0	0.790	0.0	0	2.28	113.9
11010	14.37	72.0	2.960	0.315	927	2.59	129.9
11020	14.37	72.0	10.17	0.65	1914	3.68	183.9
11030	14.36	73.0	21.67	1.002	2968	5.39	269.6
11050	14.28	71.0	44.95	1.657	4912	8.89	444.9
12010	14.31	72.0	2.230	0.339	998	2.48	123.9
12020	14.31	72.0	7.170	0.696	2044	3.22	160.9
12050	14.30	72.0	31.79	1.692	4992	6.91	345.6
12070	14.30	71.5	49.06	2.338	6904	9.50	475.5
20000	14.29	73.0	0.807	0.0	0	19.02	951.3
21020	14.30	73.0	50.57	1.962	2025	81.75	4087.5
22010	14.40	74.0	10.82	0.948	980	31.72	1586.1
22020	14.23	71.0	36.58	1.989	2052	64.27	3213.6
23020	14.23	71.5	0.068	2.012	2068	18.07	903.5
23030	14.41	73.0	0.147	2.988	2553	18.31	915.5
23050	14.43	74.0	0.661	4.982	6091	18.98	949.1
23070	14.32	73.0	0.910	6.426	7326	19.19	959.6
23100	14.28	73.0	1.656	9.675	10450	20.08	1004.1
23150	14.28	73.0	3.186	14.50	15616	22.01	1100.5
30000	14.29	74.0	0.797	0.0	0	50.96	2955.2
31005	14.30	74.0	14.58	0.772	486	97.54	4877.2
31010	14.34	72.0	39.04	1.563	985	180.9	9048.6
32010	14.33	71.0	26.03	1.556	980	137.1	6854.5

Table III

continued

Case	P_a psia	T_a °F	P_T psig	Mx10000 lbm/sec	Re	Ω_{MIN}	Ω_{MAX}
33020	14.30	72.0	0.019	2.831	1818	48.54	2427.3
33050	14.26	71.0	0.124	7.641	5334	48.86	2442.9
33070	14.25	70.0	0.208	11.17	7177	49.20	2460.1
33100	14.24	70.0	0.384	15.49	10226	49.77	2488.3

Laminar Mean Flow

Fig 14-21 present predicted and measured gain and phase shift for the cases of laminar mean flow in which the flow is assumed to be choked in the orifice. Schlieren techniques were applied to several cases to confirm sonic flow at the the orifice exit.

As for the blocked lines, equations (6) and (7) were used to predict response. From the blocked line analysis, the line models and experiment are seen to be reasonably accurate. Therefore, the effect of the terminating impedance could be determined.

For comparison, the terminal impedance was calculated using two different models. The classic expression for the steady state impedance of an orifice is found from Bernoulli's equation to be

$$Z_L = [\rho \Delta P/(2A_o^2 C_d^2)]^{0.5} + j\,0 \qquad (51)$$

where A_o is the orifice area and C_d is the discharge coefficient. The AC value is shown by equation (38) to be twice the value obtained in equation (51). Fig 14-21 display response using terminal impedances obtained through the appropriate reflection coefficient, equations (42) and (43) and the AC values of equation (51).

Although the AC values vary from approximately equal to more than twice those found using reflection coefficients, the response for the two impedances is seen

to change very little. This is due to the ratio of orifice to line area. As this ratio goes to zero, the line will appear blocked. For lines that are blocked, or almost blocked, a certain impedance value exists above which response changes are negligible.

For cases in which the pressure ratio across the orifice is insufficient to choke to flow, equation (42) can again be used to find the terminating impedance if the reflection coefficient from equation (44) is used. The impedances for these cases are larger than those for the choked cases and are therefore seen to be in better agreement with the AC impedance values.

Fig 22-33 present experimental gain and phase shift, as well as theoretical predictions using the terminal impedance equal to the AC values of equation (38) and impedance found using reflection coefficients in equation (42), for the unchoked orifice cases. The theory, using either terminal impedance, is seen in Fig 22-29 to predict higher attenuation than that observed experimentally for line 1. The theoretical predictions for lines 2 and 3, diameters of 0.119 and 0.195 in. respectively, are seen in Fig 30-33 to be in much better agreement with experimental data. The overprediction of attenuation for the line 1 case is similar to that seen in Fig 8-9 for the same line in the blocked configuration. Since only the terminal impedance was changed in going from the blocked

to orifice case, it appears the deviations in Fig 22-29 are related to the problem of properly modeling line 1.

Cases of laminar flow through open lines offer an opportunity to assess the effect of using the radiation impedance as given by equation (41) versus the value given by equation (38) which becomes identically zero for open lines. The radiation impedance is seen to be quite small at all dimensional frequencies of this study and as shown by Fig 34-37 may be neglected. The radiation impedance will, however, be used, along with that found using reflection coefficients for orifices, for the remainder of this study.

Turbulent Mean Flow

The blocked and laminar cases were used to verify the experiment, line model and terminating impedance. As an initial step in determining turbulent flow response, the components of the constant LRC model are varied individually.

Fig 39 shows the effect of varying the resistance on the gain predictions for an open line. AC and DC resistances, from equations (23) and (31) respectively, were used with the adiabatic inertance and isothermal capacitance. As seen by Briski (Ref 5), use of the AC resistance yields predicted peak gain magnitudes near those seen experimentally but occurring at lower frequencies. This shift would describe the response of a

similiar line of longer length. Since the response of the line is actually dictated by the product of the propagation operator and line length, as seen in equation (17), an increase in either increases the effective line length. The increased attenuation resulting from the AC resistance is seen to delay the transition to the high frequency laminar behavior from , in this case, approximately 340 Hz for the DC resistance to a frequency beyond the 1000 Hz test limit.

Fig 39 illustrates the effect of using either the isothermal or the turbulent capacitance with the AC resistance and adiabatic inertance. The use of the smaller turbulent capacitance, given by equation (36), results in a smaller propagation operator which effectively shortens the line. The peak gain magnitudes are seen to be reduced very little and now occur at slightly higher frequencies than the experimental data. Attenuation remains sufficiently high enough to inhibit transition below 1000 Hz.

Fig 40 shows the effect of varying the inertance. The adiabatic and turbulent inertance, equations (27) and (32) respectively, were used with the AC resistance and turbulent capacitance to obtain the theoretical gain predictions. For this case of Reynolds number equal to 10000, the turbulent inertance is only approximately 3 % greater than the adiabatic value and therefore results in

only a slight increase in the effective line length. The attenuation shows no appreciable change.

The combination of AC resistance, turbulent capacitance and turbulent inertance will be referred to as the modified constant LRC model. The modified constant LRC incorporates the imaginary part of the conductance, within the turbulent capacitance, but neglects the real part. Adding the real part of equation (35) to the modified constant LRC model yields the constant LRCG model.

Fig 55 shows the gain predictions for the modified constant LRC and constant LRCG models for the case presented in Fig 38-40. The constant LRCG model predicts higher attenuation than the modified constant LRC model and a slightly shorter effective line length.

The modified constant LRC, constant LRCG and laminar, from equations (6) and (7), models are used to generate theoretical gain and phase shift for turbulent mean flow in orifice terminated lines, Fig 41-48, and open lines, Fig 49-64.

The predictions for cases involving line 1 are again seen to be in poor agreement with experimental data. Fig 41 shows the laminar model to predict a higher attenuation than seen experimentally. This is similar to the behavior of the laminar cases for line 1 as shown in Fig 22-29. The low attenuation predicted by the laminar model at low

frequencies in Fig 43-48 is as expected (Ref 3-6) but is accompanied by a most unexpected increase in the propagation operator.

This behavior may be due to several factors; the errors in modeling line 1, errors in determining the terminal impedance and/or the possibility of appreciable roughness in the line. The friction factor given by equation (22) is applicable to turbulent flow in smooth lines. If the lines are not smooth, the actual friction factor is larger with the deviation from the smooth values increasing with Reynolds number. Since the computer program assumes smooth lines to calculate pressure drops along the line, the theory would not yield accurate predictions if the line were sufficiently rough.

Due to these problems, line 1 can not be used to assess, with adequate confidence, the prediction capabilities of the constant LRCG and modified constant LRC models.

Fig 49-64 show experimental theoretical gain and phase shift for open line cases for lines 2 and 3, diameters of 0.119 and 0.195 in. The laminar model predictions are as expected indicating little line model error and insignificant roughness effects. Since the roughness effects are a function of the relative roughness, defined as the line roughness divided by the line diameter, the larger lines would exhibit less increase in friction

factor than the smaller line with comparable line roughness.

Fig 49-64 show the modified constant LRC model to predict less attenuation than the constant LRCG model. The laminar model is shown to correctly predict the effective line length while the modified constant LRC and constant LRCG models slightly underpredict the propagation operator.

Examination of the assumptions and simplifications made in the formulation of both the modified constant LRC and constant LRCG models reveals some possible explanations for the degraded prediction capabilities for certain cases. To obtain equation (35) from equation (34), the term (R_{AC}/ω) was assumed to be much smaller than the turbulent inertance. However, in cases of large Reynolds number and/or small line diameter, the AC resistance can become large enough to violate this assumption. Also, this assumption does not hold for very low frequencies. The inclusion of this term will tend to lower the conductance resulting in lower attenuation. Comparison of the two larger lines tested at a Reynolds number of 5000, Fig 51 and 59, indicate increasing overprediction of the attenuation as the line size is decreased. Fig 49-58 are seen to indicate similar increases in attenuation error due to increasing Reynolds number. The 0.195 in diameter line is apparently large

enough that the term in question may be ignored at the frequencies and Reynolds numbers tested. Incorporation of this term should enhance the prediction capability of both models but stray from the original intent of keeping the components frequency independent.

V. Conclusions

1. The impedance of orifices with and without choked flow could be adequately determined using reflection coefficients. The small radiation impedance associated with the open lines tested could be neglected for frequencies less than 1000 Hz.

2. The laminar model, using the Krishnaiyer and Lechner equations, gave accurate predictions for blocked test lines and lines tested with laminar mean flow. Attempts to apply this model to turbulent mean flow cases resulted in good agreement with experimental data at higher frequencies, but significant underprediction of the attenuation at lower frequencies.

3. The modified constant LRC model, consisting of the turbulent inertance, AC resistance and turbulent capacitance, was seen to predict higher attenuation than the laminar model for turbulent mean flow cases at lower frequencies. As a result, deviation between theoretical and experimental peak gain magnitudes was reduced, for the cases tested, by at least 50 % while introducing less than 3 % error in the frequency at which the peaks occur.

4. The constant LRCG model, which adds the real part of the conductance to the modified constant LRCG model,

further increases the attenuation resulting in peak gain magnitudes approximately 3 db less than those predicted by the modified constant LRC model and, in most cases, well below the experimental values.

5) The modified constant LRC and constant LRCG models account for the effects of Reynolds number, but not frequency, on the individual components. The applicable frequency range of both models is limited by the combination of Reynolds number, density and line diameter due to certain assumptions made to eliminate frequency dependence.

VI. Recommendations

1. The effect of including the frequency dependent terms of the conductance should be investigated. The improvement in prediction capability should be weighed against the increased complexity introduced.

2. Experimental data points should be extended into the low frequency range. Present instrumentation, in particular the wave analyzers, prevents accurate readings at the extremely low frequencies required to explore this region with the lines used this study. Therefore, using current instrumentation, smaller line diameters must be considered to lower the nondimensional frequency.

3. Automated data collection equipment should be used to increase accuracy, facilitate low frequency measurements, standardize experimental procedures and significantly reduce time requirements while providing more data points. An experimental data base could then be established, using reliable and repeatable results obtained through standardized test procedures, that future studies could draw upon and contribute to.

4. The effect of line roughness on the response of turbulent flow lines should be investigated in greater detail.

Bibliography

1. Nichols, N. B., "The Linear Properties of Pneumatic Transmission Lines," Transactions of the Instrument Society of America, Vol. 1, 1962, pp 5-14

2. Krishnaiyer, R. and Lechner, T. J., Jr. "An Experimental Evaluation of Fluidic Transmission Line Theory." Advances in Fluidics. Edited by F. T. Brown et al. New York: American Society of Mechanical Engineers, 1967.

3. Brown, F. T., Margolis, D. L., and Shah, R. P., "Small Amplitude Frequency Behavior of Fluid Lines with Turbulent Flow." Journal of Basic Engineering, Trans. ASME, December 1969, pp 678-693.

4. Moore, E. F. "The Small Signal Response of Fluid Transmission Lines Including Developed Mean Flow Effects." PhD Dissertation. School of Engineering, Air Force Institute of Technology (AU), Wright-Patterson AFB OH, June 1977.

5. Briski, M. S., "Effects of Mean Flow on the Dynamic Characteristics of Fluid Transmission Lines." Ms Thesis, School of Engineering, Air Force Institute of Technology (AU), Wright-Patterson AFB OH, December, 1983.

6. Vining, J. D., "Through Flow Effects on the Dynamic Characteristics of Pneumatic Transmission Lines." Ms Thesis, School of Engineering, Air Force Institute of Technology (AU), Wright-Patterson AFB, OH, June 1975.

7. King, R. W. P., Transmission-Line Theory. New York: McGraw-Hill Book Company, 1955.

8. Kirshner, J. M. and Katz, S., Design Theory of Fluidic Components. New York: Academic Press, 1975.

9. Schlichting, H., Boundary Layer Theory. New York: McGraw-Hill Book Company, 1979.

10. Funk, J. E. and Wood, D. J., "Frequency Response of Fluid Lines with Turbulent Flow." Journal of Fluids Engineering, Trans. ASME, Series I, Vol. 96, No. 4, December 1974, pp 365-369.

11. Franke, M. E., Private Communications. Air Force Institute of Technology (AU), Wright-Patterson AFB OH, March 1984 - November 1984.

12. Moore, E. F., and Franke, M. E., "Approximations for Frequency Dependent Attenuation in Circular and Noncircular Lines with Turbulent Mean Flow." Unpublished paper, date unknown.

13. Franke, M. E., Malanowski, A. J. and Martin, P. S., "Effects of Temperature, End-Conditions, FLow, and Branching on the Frequency Response of Pneumatic Lines." Journal of Dynamic Systems, Measurement and Control, Trans. ASME, March 1972, pp 15-20.

14. Morse, P. M. and Ingard, K. U., Theoretical Acoustics. New York: McGraw-Hill Book Company, 1968.

15. Kinsler, L. E. and Frey, A. R., Fundamentals of Acoustics. New York: John Wiley and Sons, Inc., 1972.

16. Malanowski, A. J., "The Dynamic Response of Fluidic Networks." Ms Thesis, School of Engineering, Air Force Institute of Technology (AU), Wright-Patterson AFB, OH March 1971.

17. Katz, S., Hausner, A., and Eisenberg, N. A., "The Effect of Through-Flow on Signal Propagation in Fluid Lines." Proceedings. of the Fluidic State-of-the-Art Symposium, 30 Sep - 4 Oct 74. Harry Diamond Laboratories, Washington, D. C.: pp 269-297.

18. Funk, J. E., Wood, D. J. and Chao, S. P., "The Transient Response of Orifices and Very Short Lines." Journal of Basic Engineering, Trans. ASME, June 1972, pp 483-491.

19. Shaprio, A. H., The Dynamics and Thermodynamics of Compressible Fluid FLow. New York: J. Wiley and Sons, 1953.

Appendix A

Experimental and Theoretical Gain and Phase vs Frequency For Blocked, Laminar and Turbulent Mean Flow Cases.

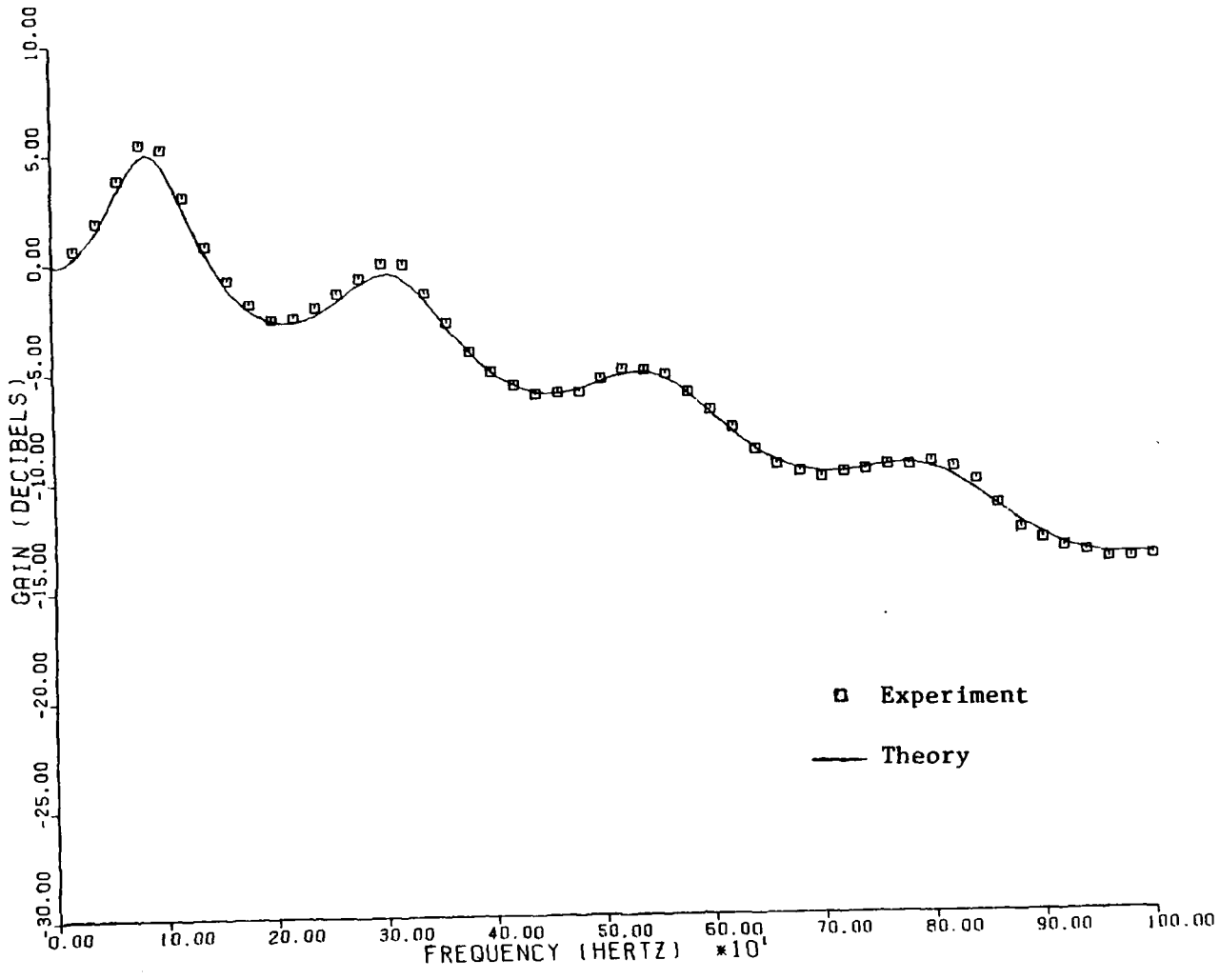

Figure 8 Experimental and Theoretical Gain vs Frequency for Case 10000

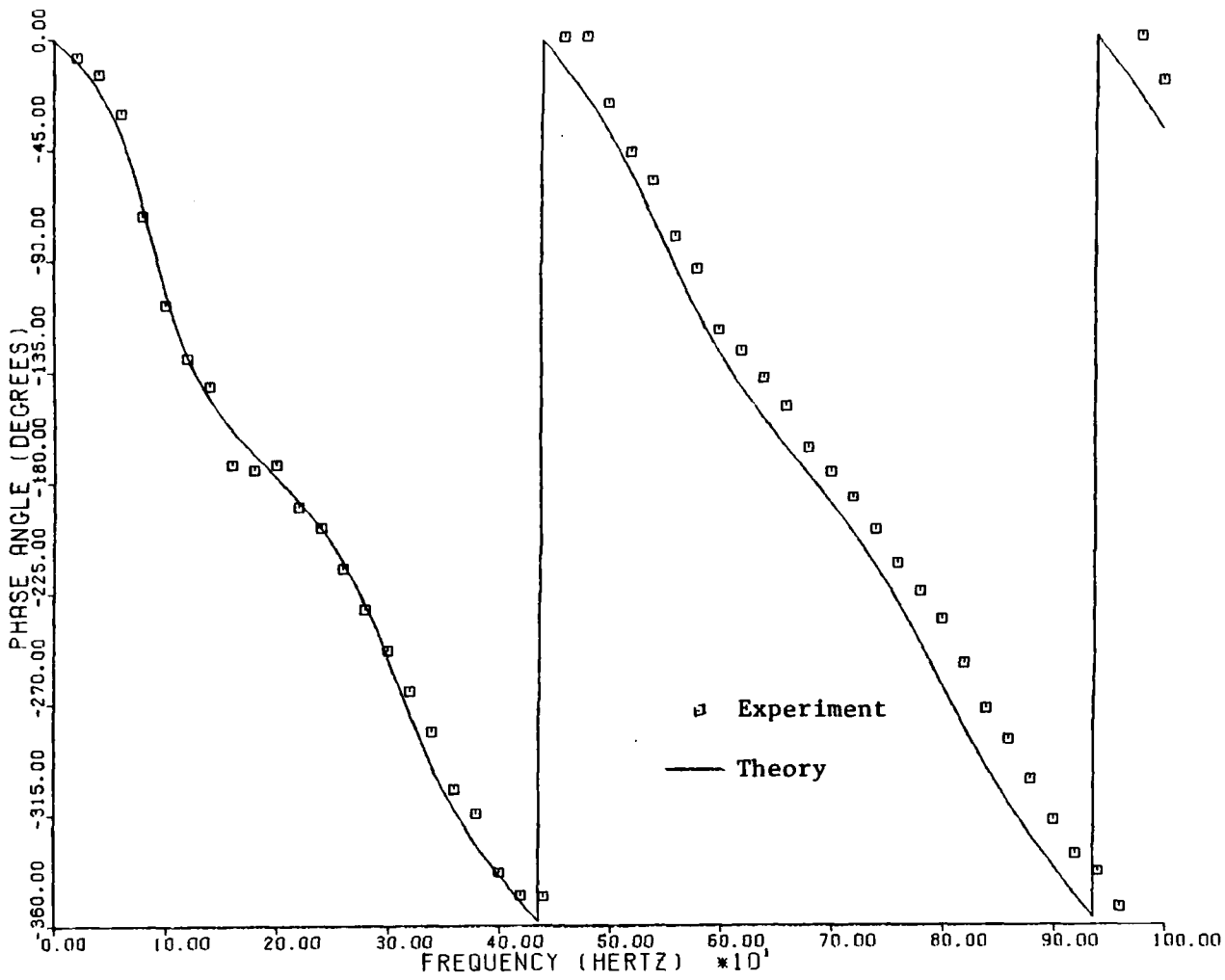

Figure 9 Experimental and Theoretical Phase vs Frequency for Case 10000

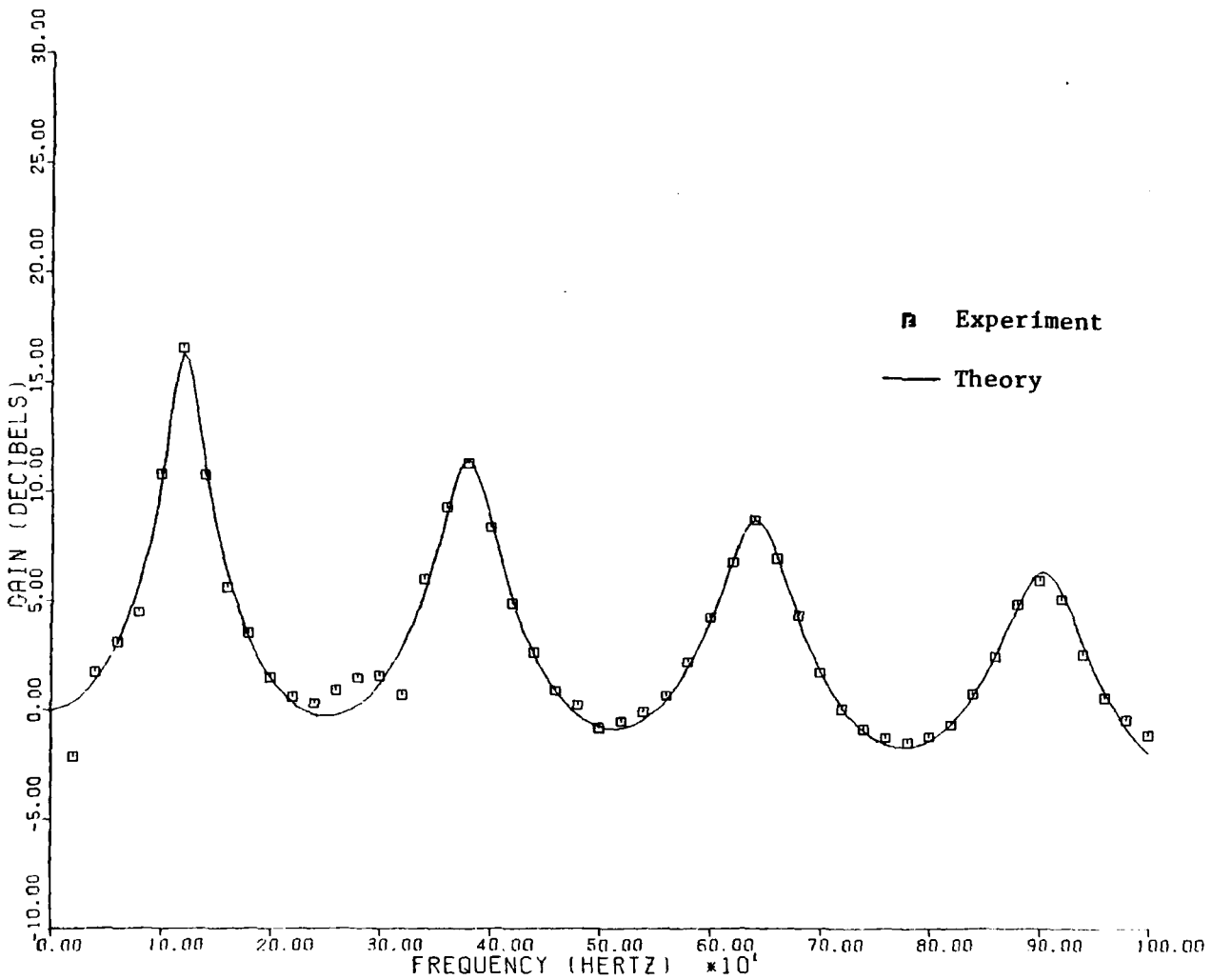

Figure 10 Experimental and Theoretical Gain vs Frequency for Case 20000

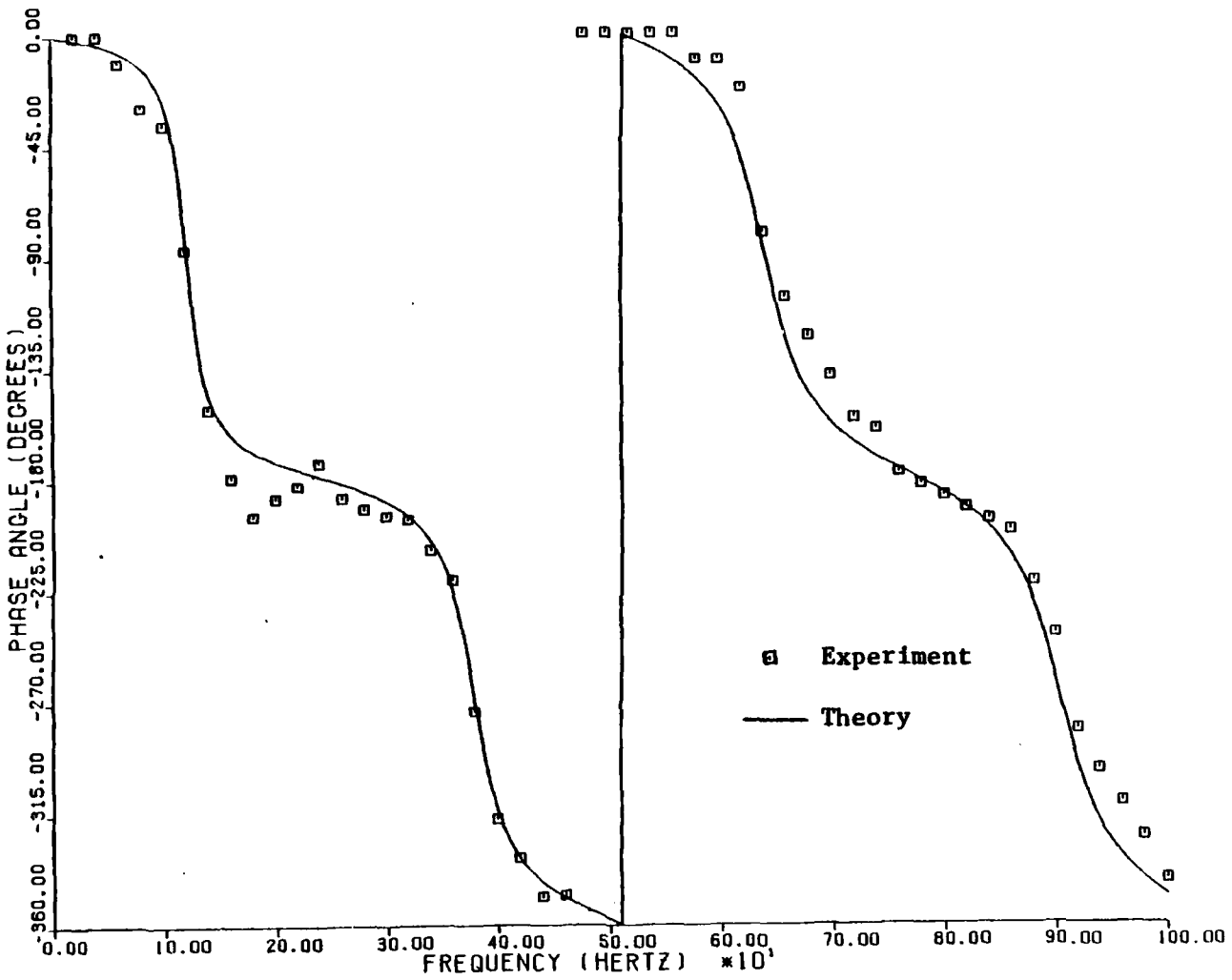

Figure 11 Experimental and Theoretical Phase vs Frequency for Case 20000

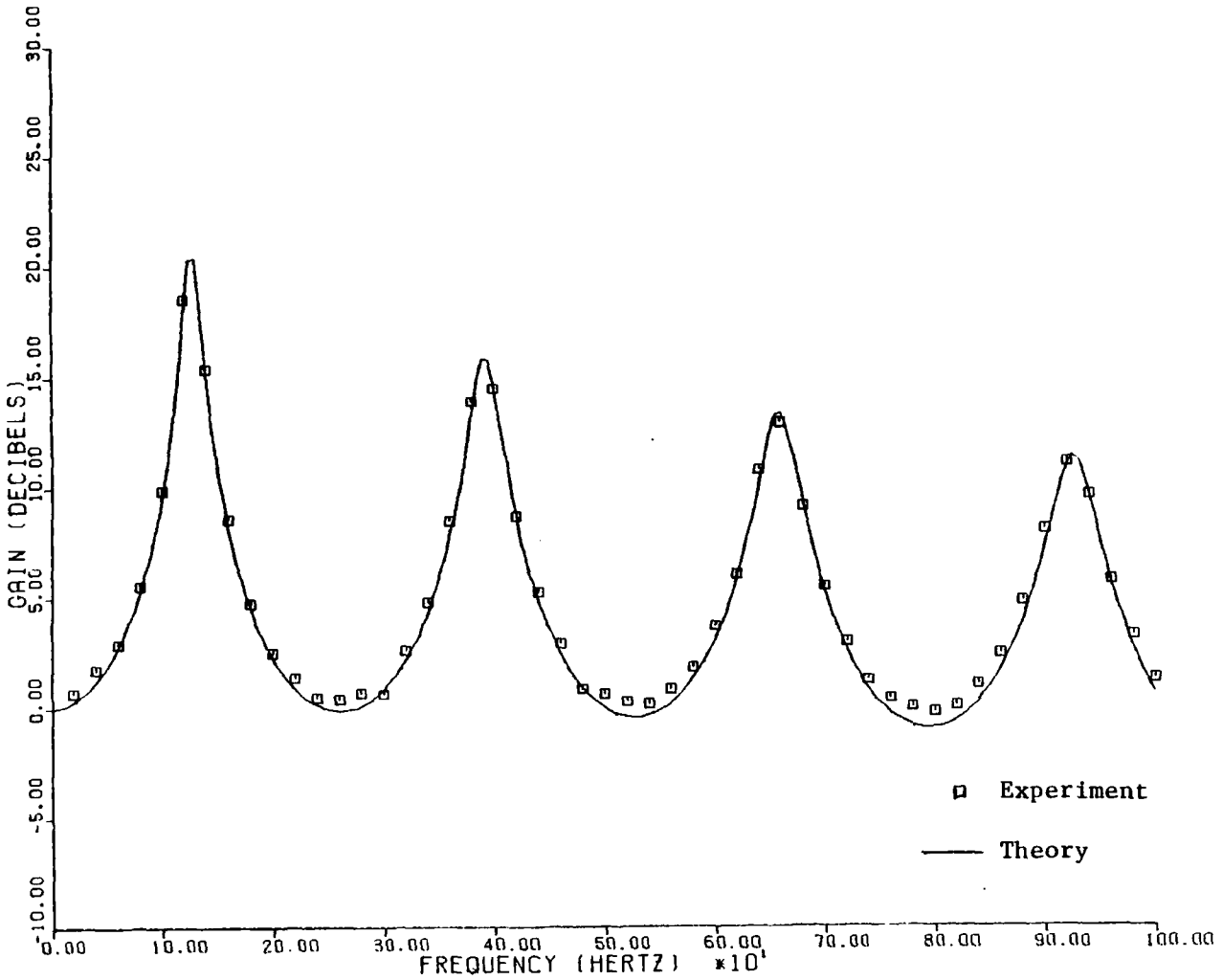

Figure 12 Experimental and Theoretical Gain vs Frequency for Case 30000

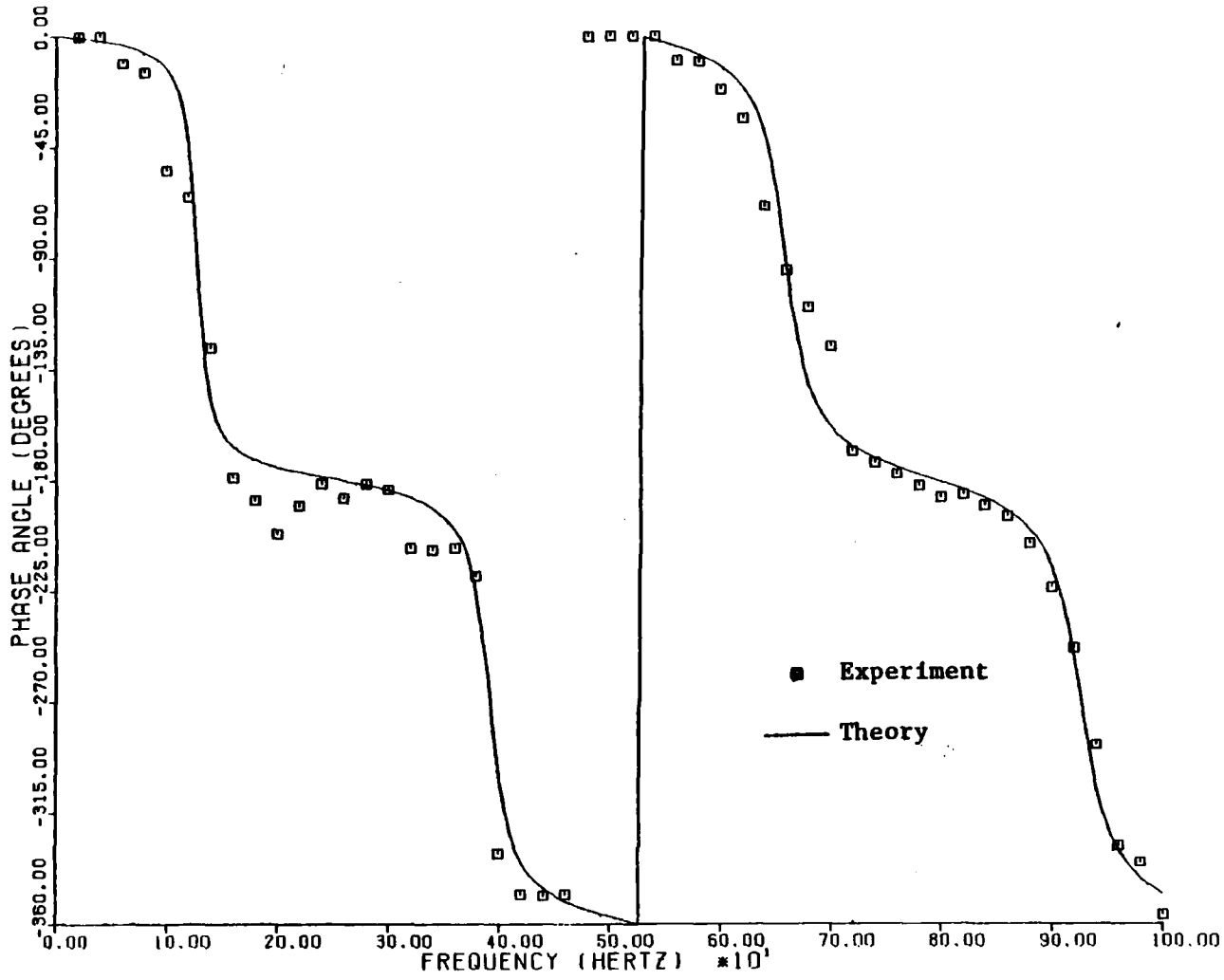

Figure 13 Experimental and Theoretical Phase vs Frequency for Case 30000

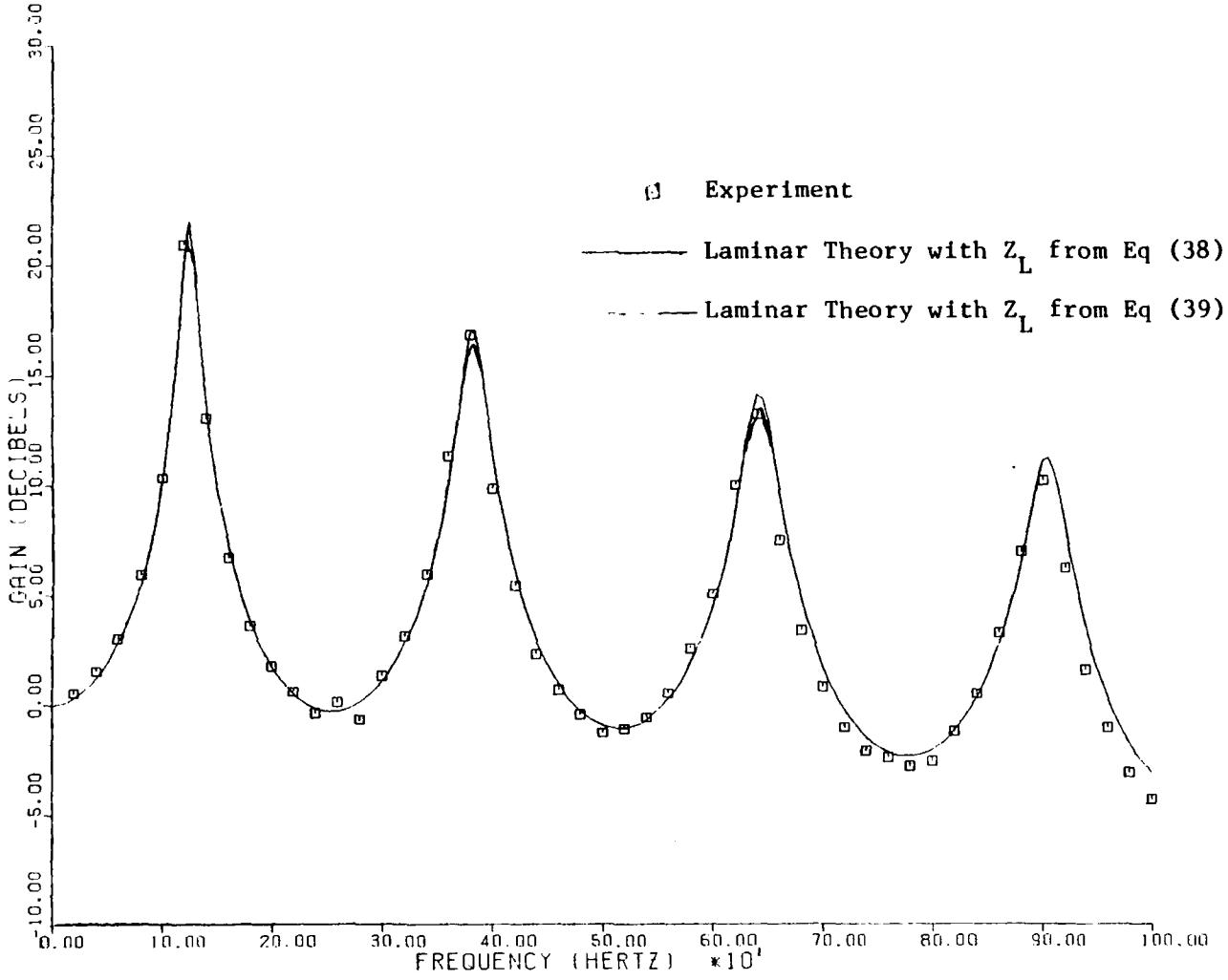

Figure 14 Experimental and Theoretical Gain vs Frequency for Case 21020

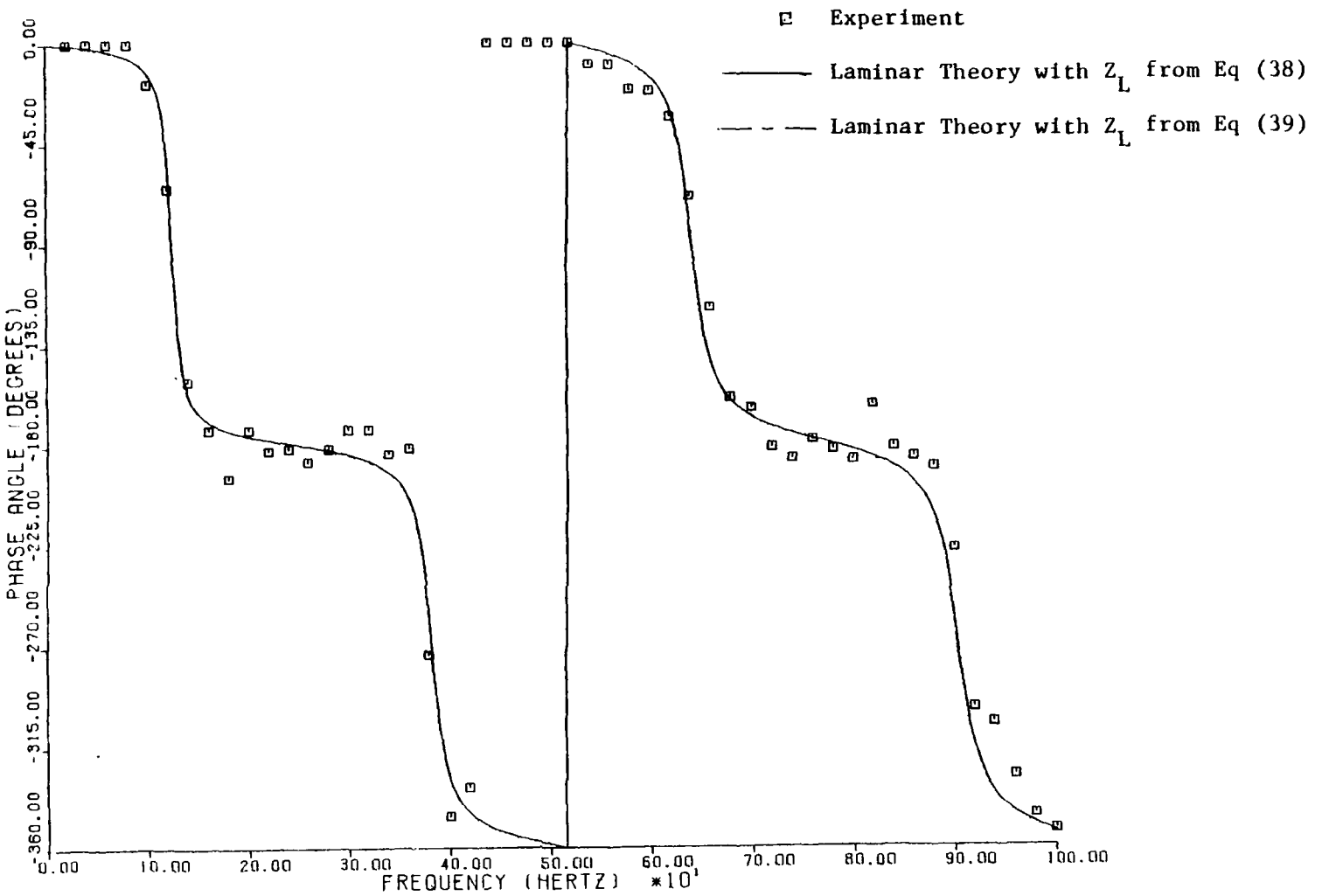

Figure 15 Experimental and Theoretical Phase vs Frequency for Case 21020

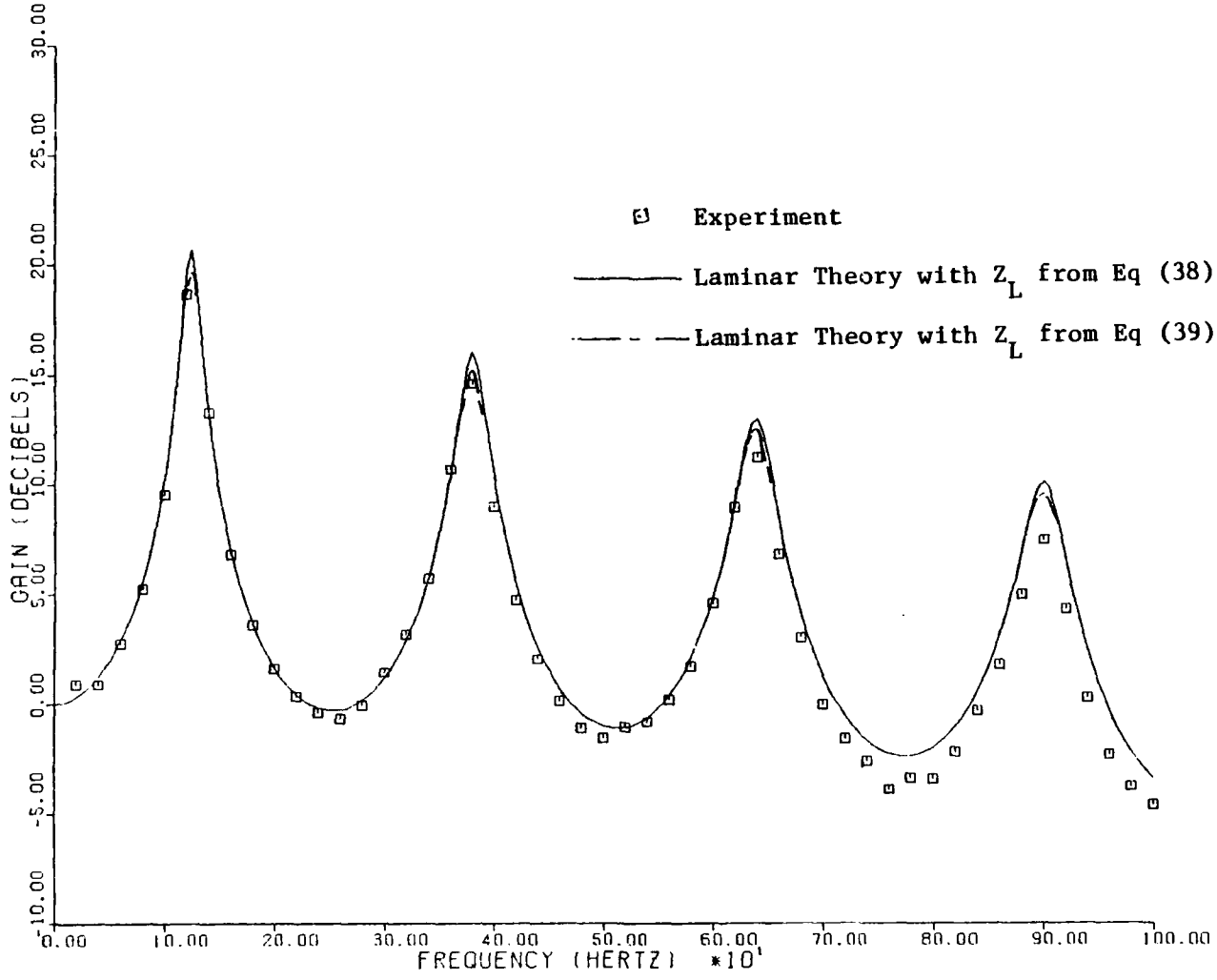

Figure 16 Experimental and Theoretical Gain vs Frequency for Case 22020

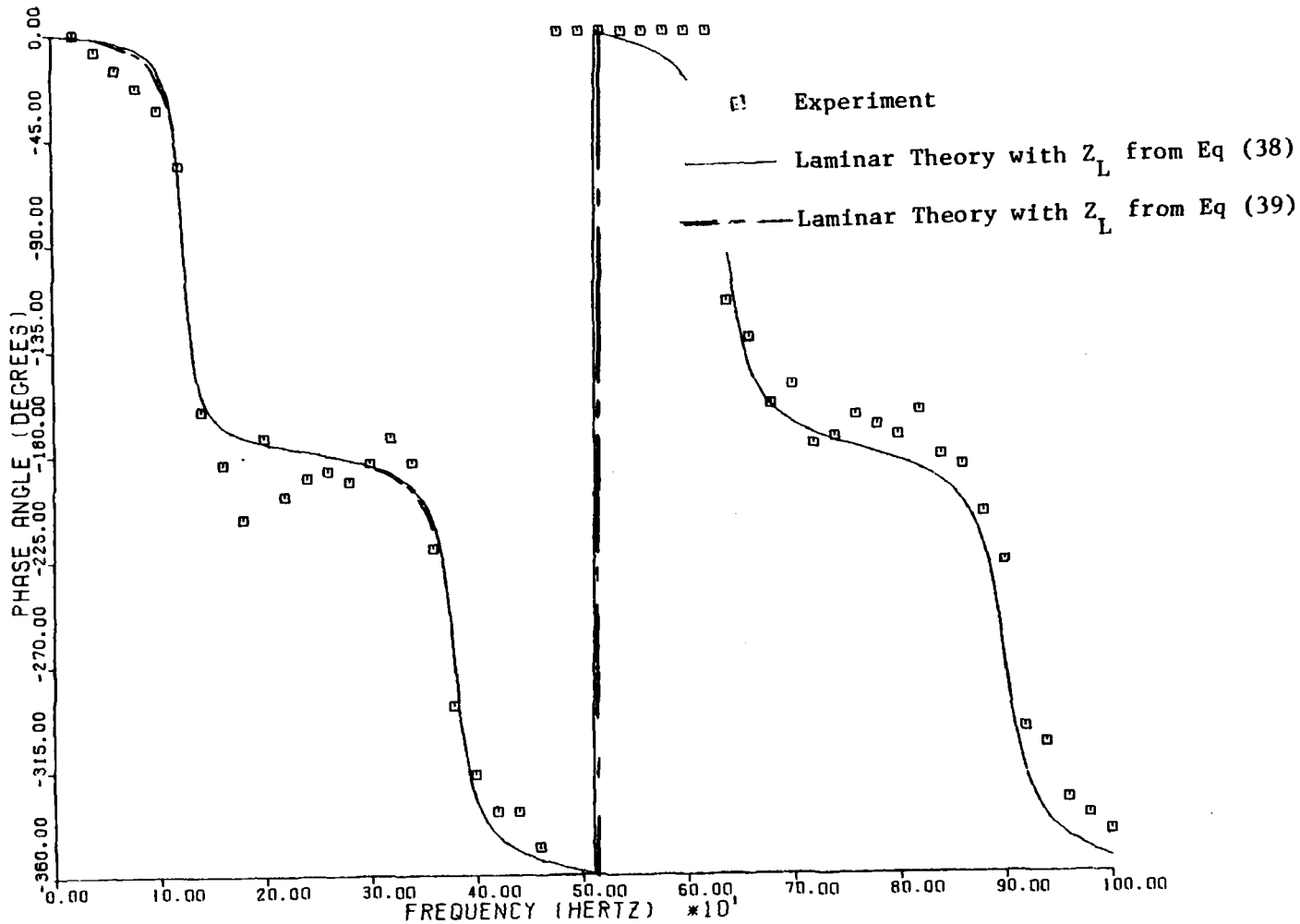

Figure 17 Experimental and Theoretical Phase vs Frequency for Case 22020

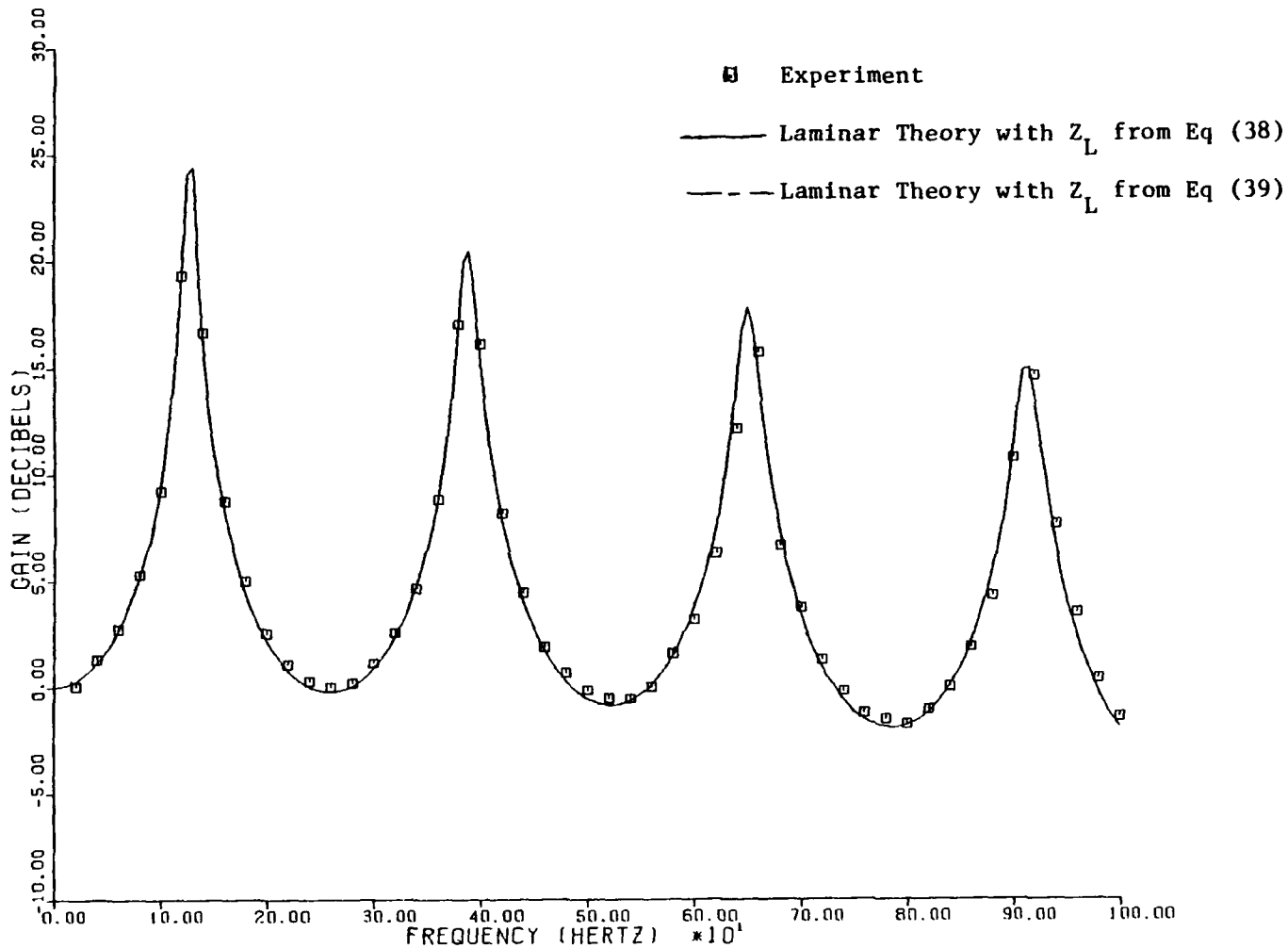

Figure 18 Experimental and Theoretical Gain vs Frequency for Case 31010

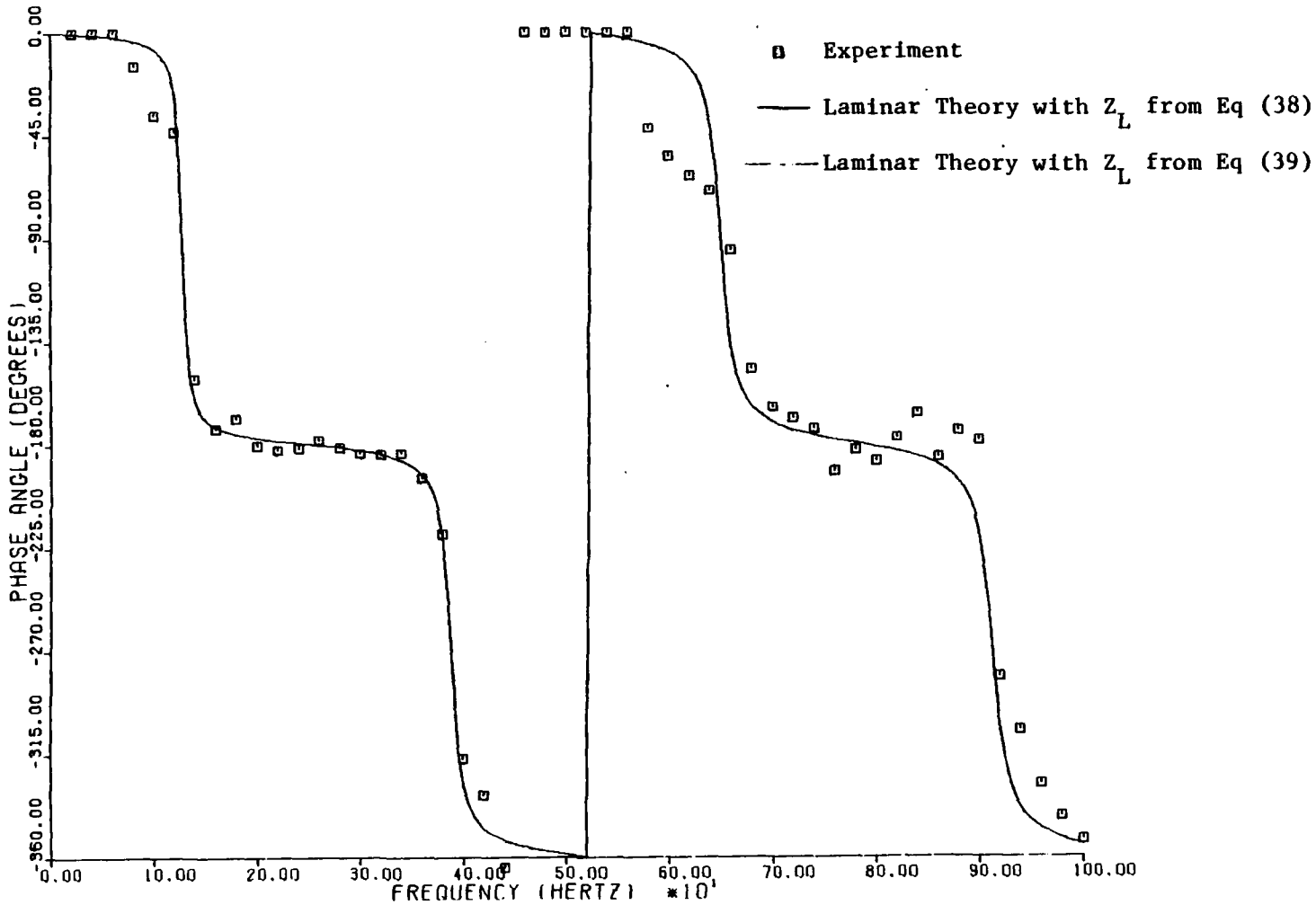

Figure 19 Experimental and Theoretical Phase vs Frequency for Case 31010

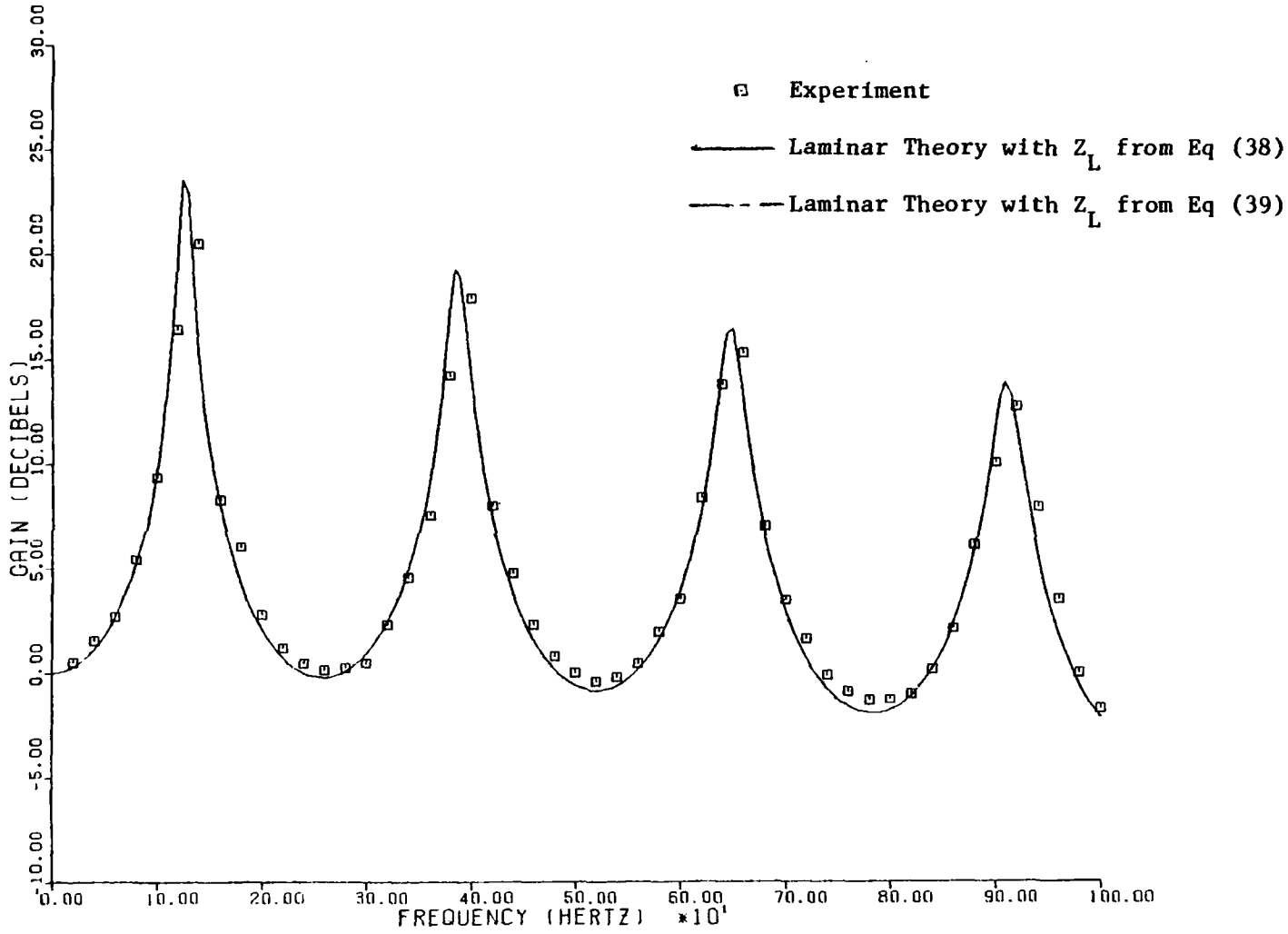

Figure 20 Experimental and Theoretical Gain vs Frequency for Case 32010

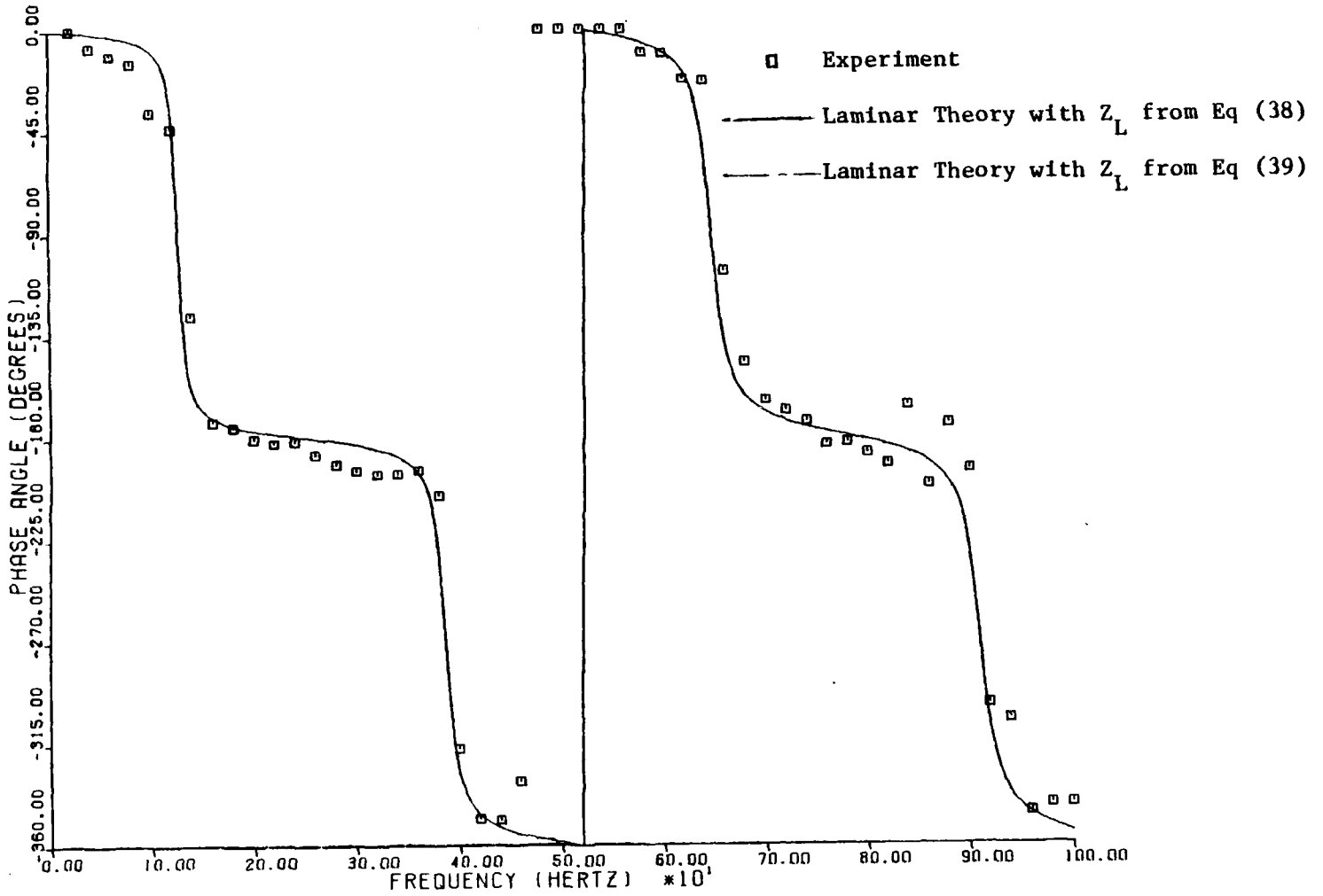

Figure 21 Experimental and Theoretical Phase vs Frequency for Case 32010

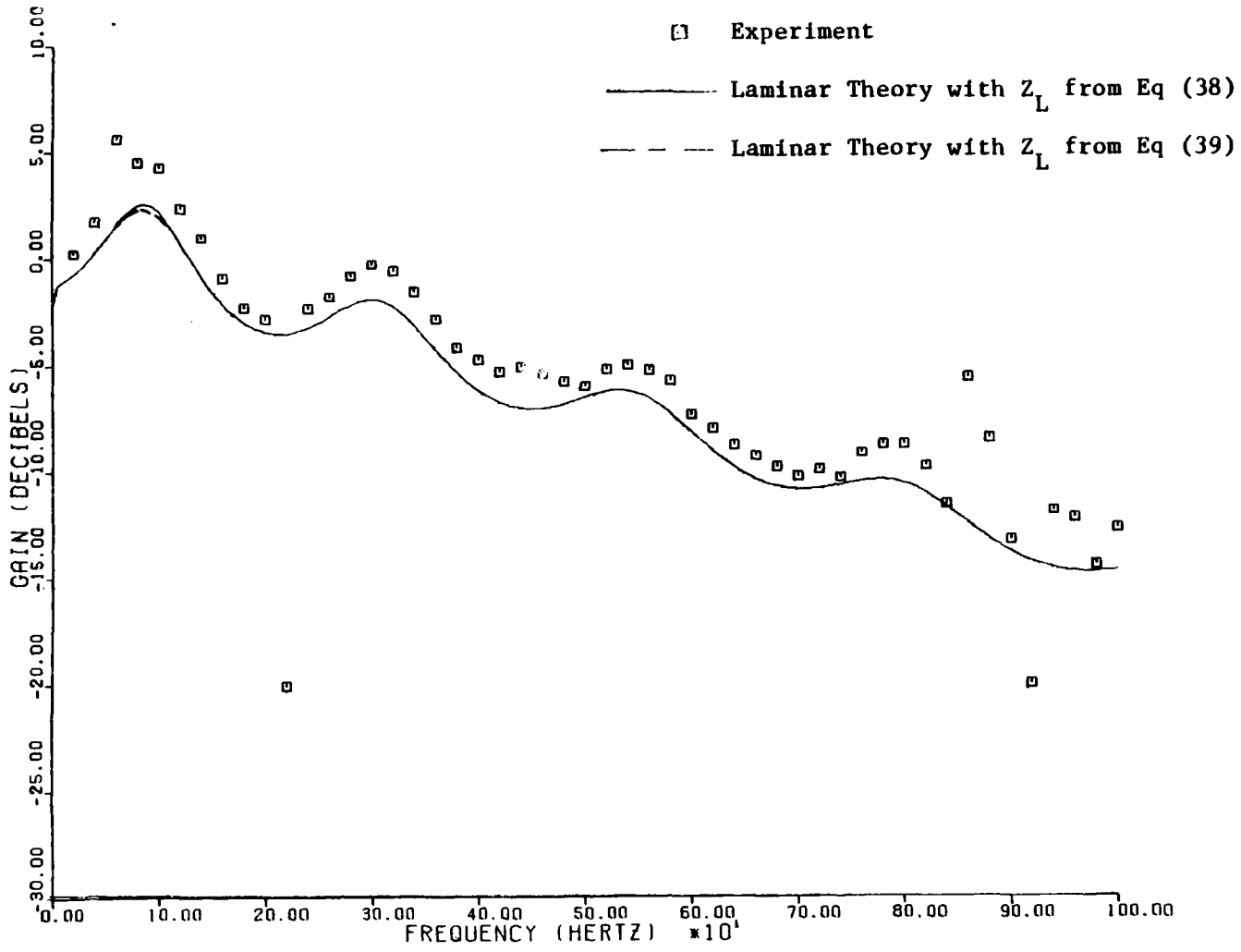

Figure 22 Experimental and Theoretical Gain vs Frequency for Case 11010

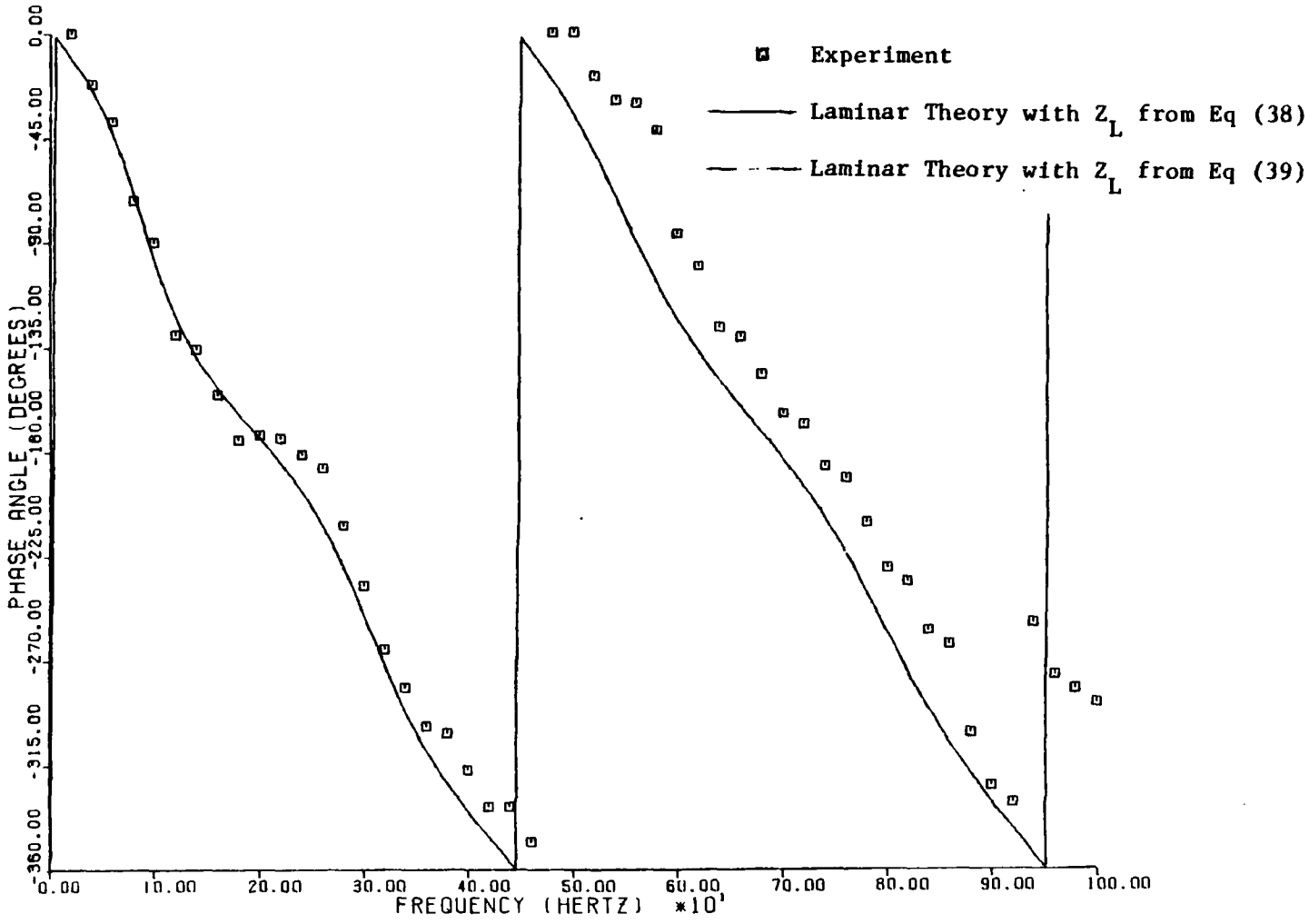

Figure 23 Experimental and Theoretical Phase vs Frequency for Case 11010

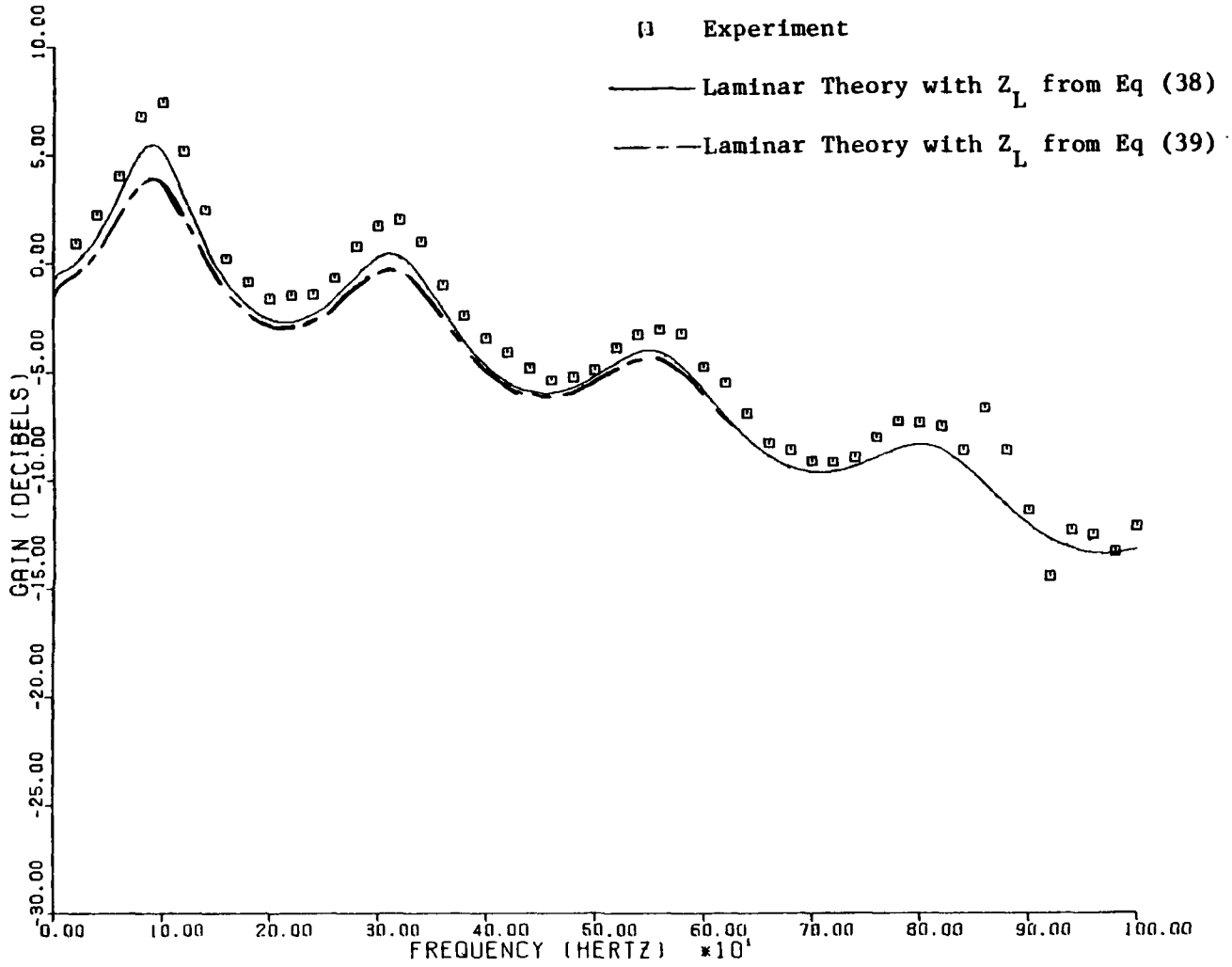

Figure 24 Experimental and Theoretical Gain vs Frequency for Case 11020

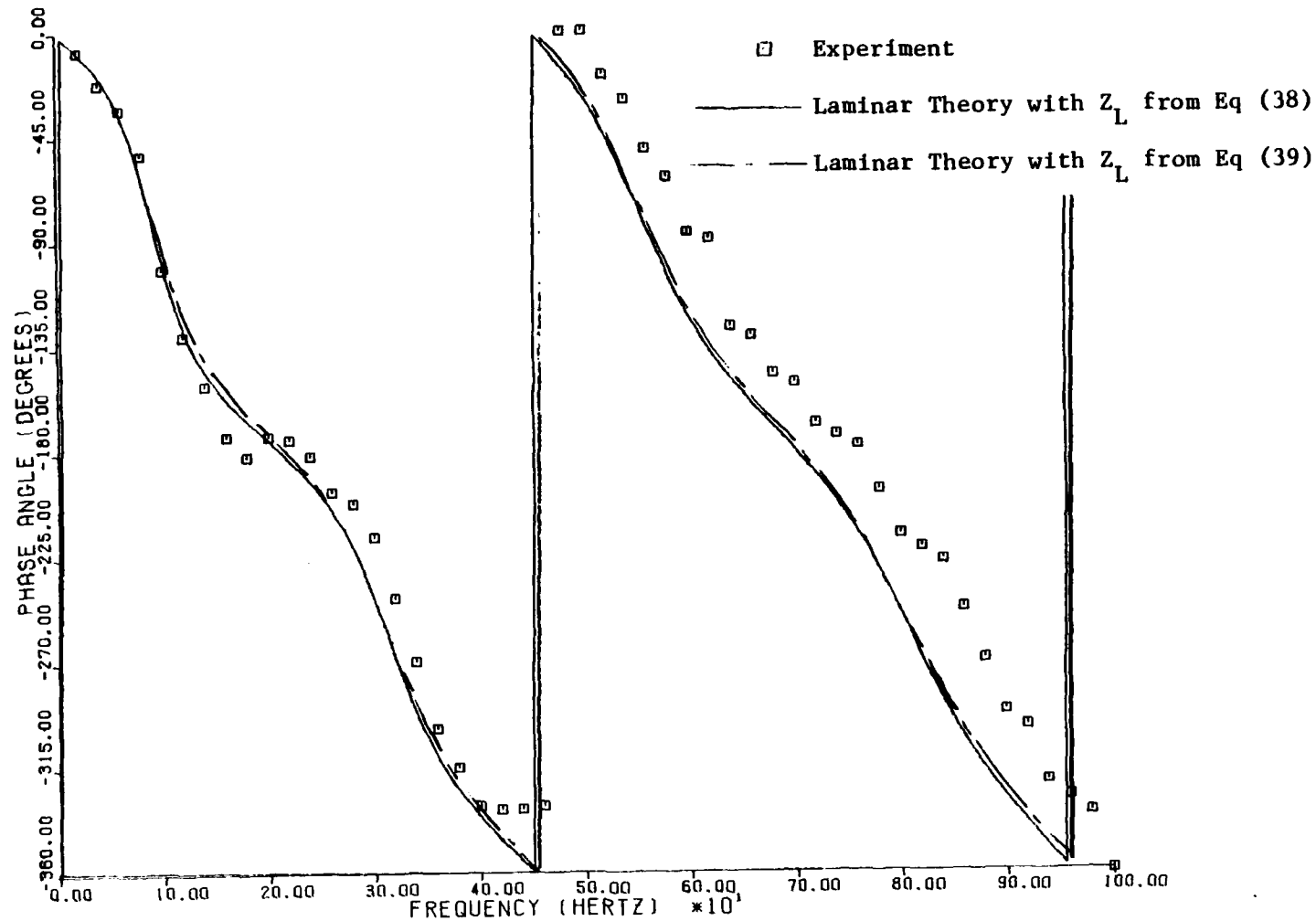

Figure 25 Experimental and Theoretical Phase vs Frequency for Case 11020

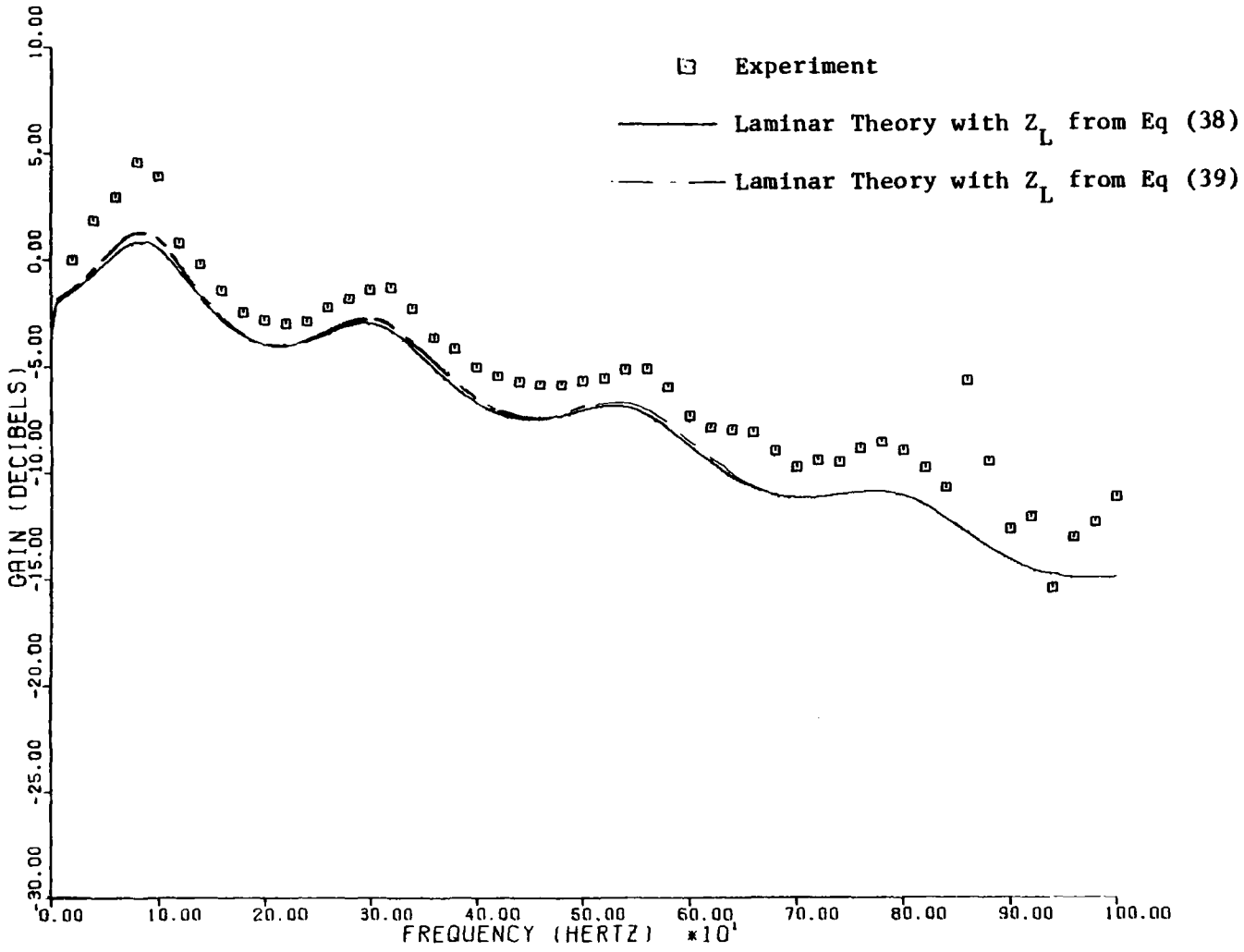

Figure 26 Experimental and Theoretical Gain vs Frequency for Case 12010

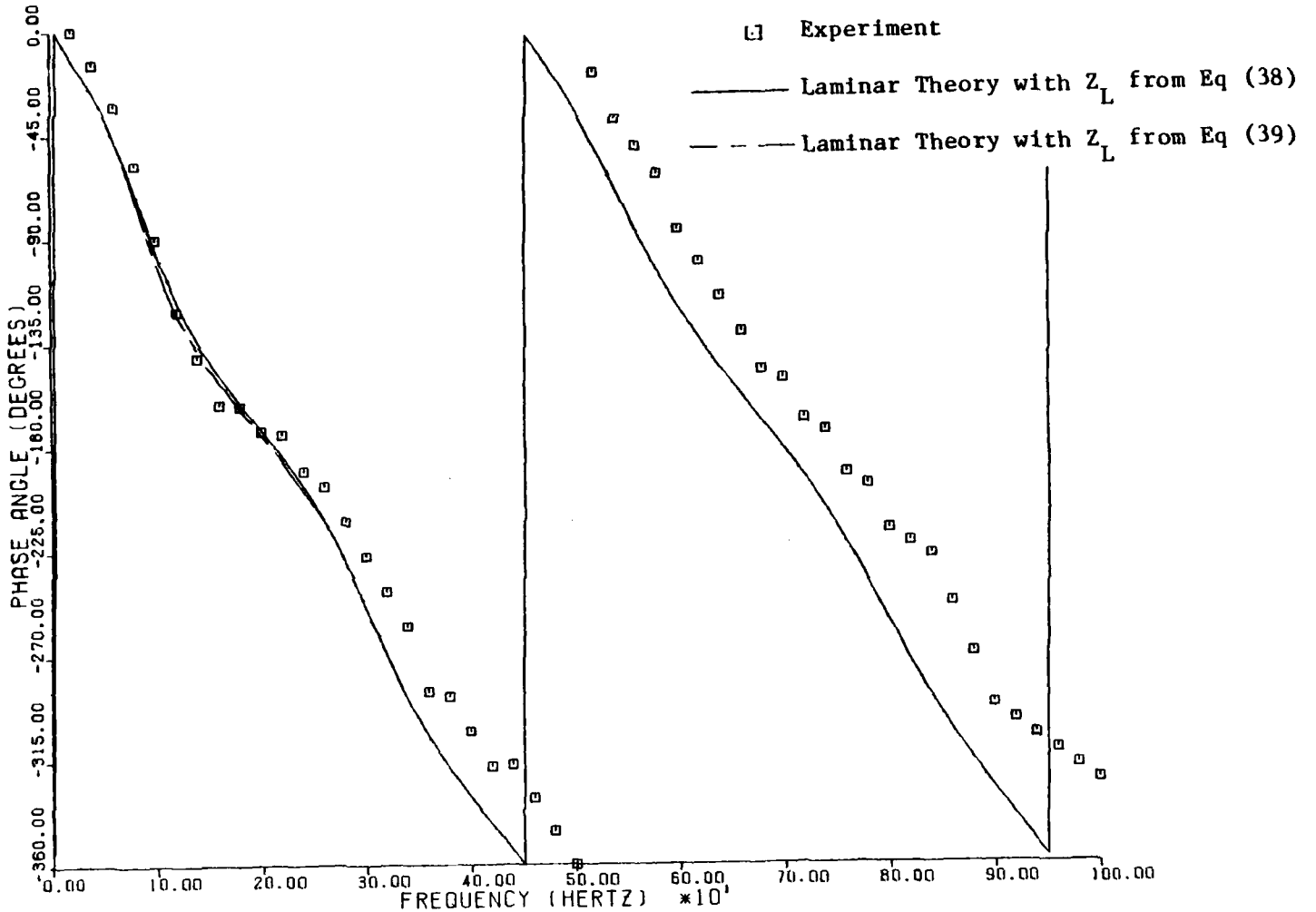

Figure 27 Experimental and Theoretical Phase vs Frequency for Case 12010

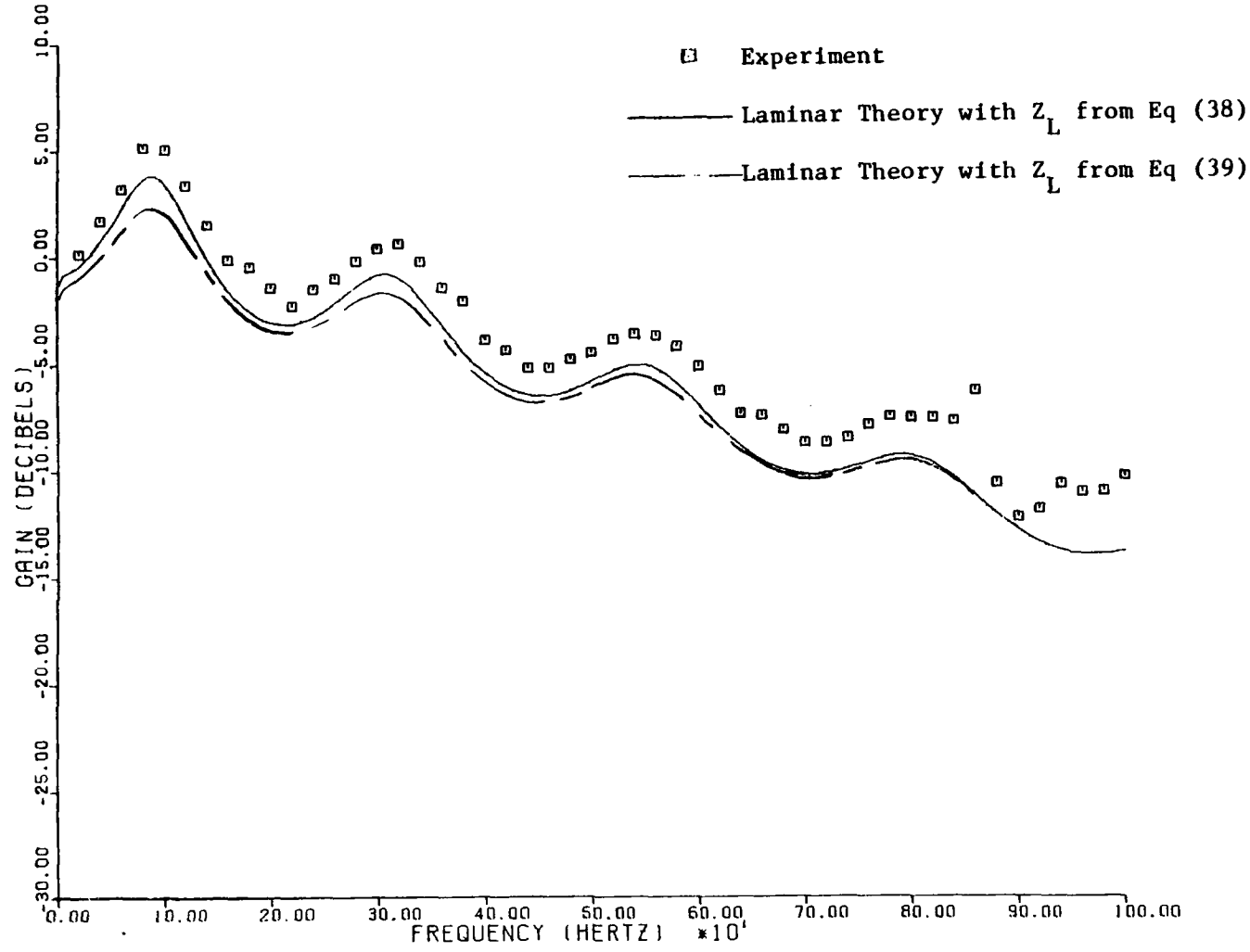

Figure 28 Experimental and Theoretical Gain vs Frequency for Case 12020

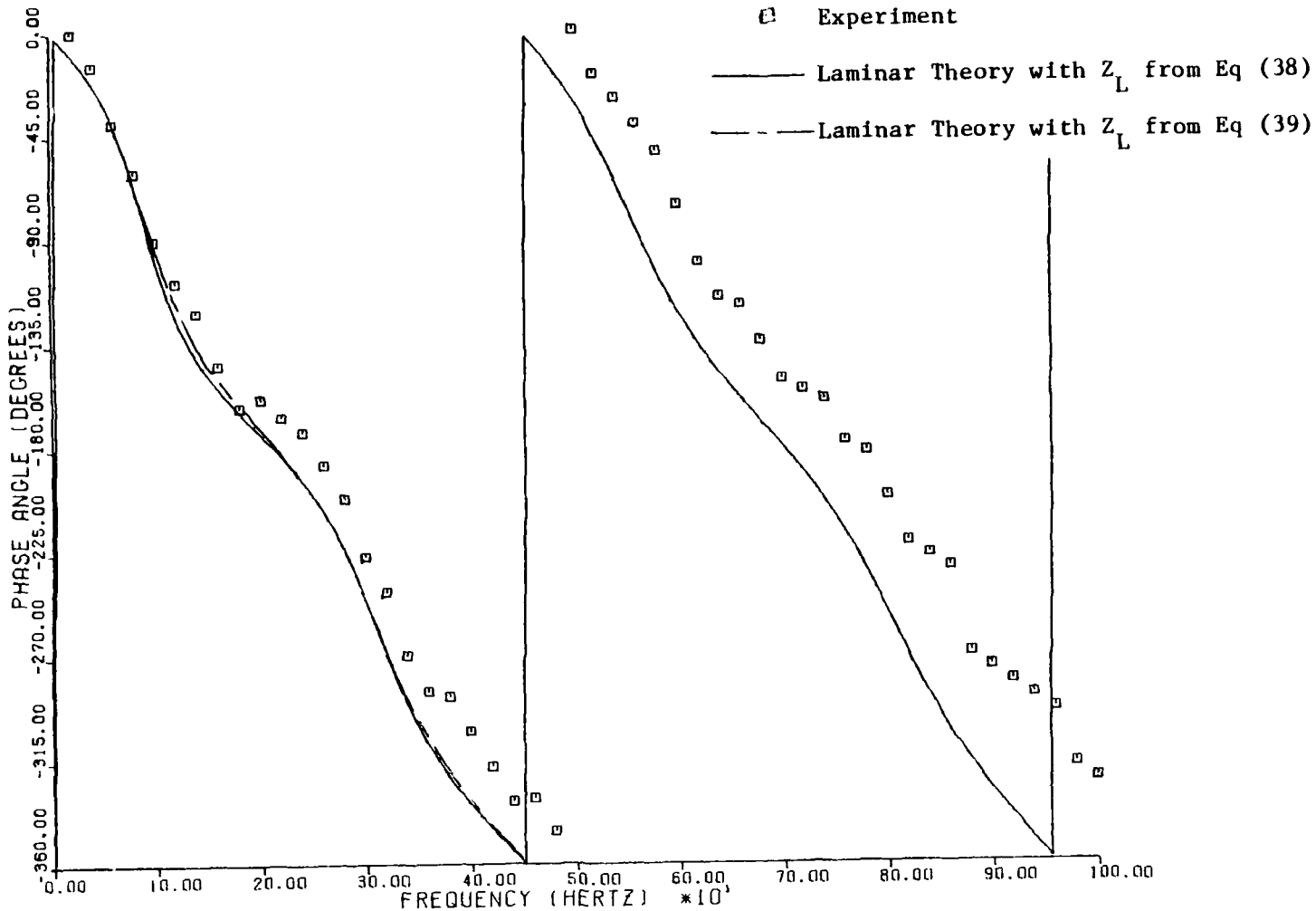

Figure 29 Experimental and Theoretical Phase vs Frequency for Case 12020

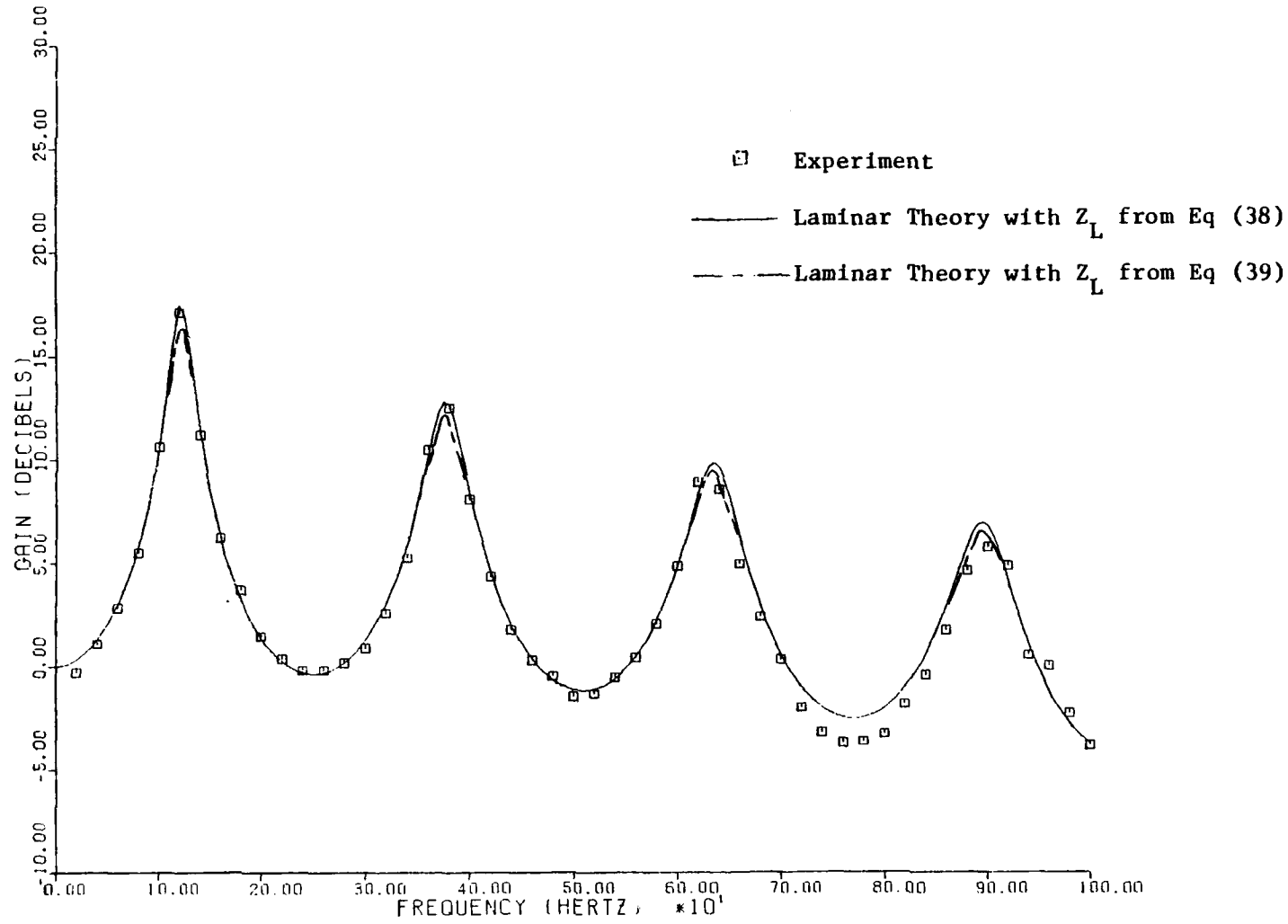

Figure 30 Experimental and Theoretical Gain vs Frequency for Case 22010

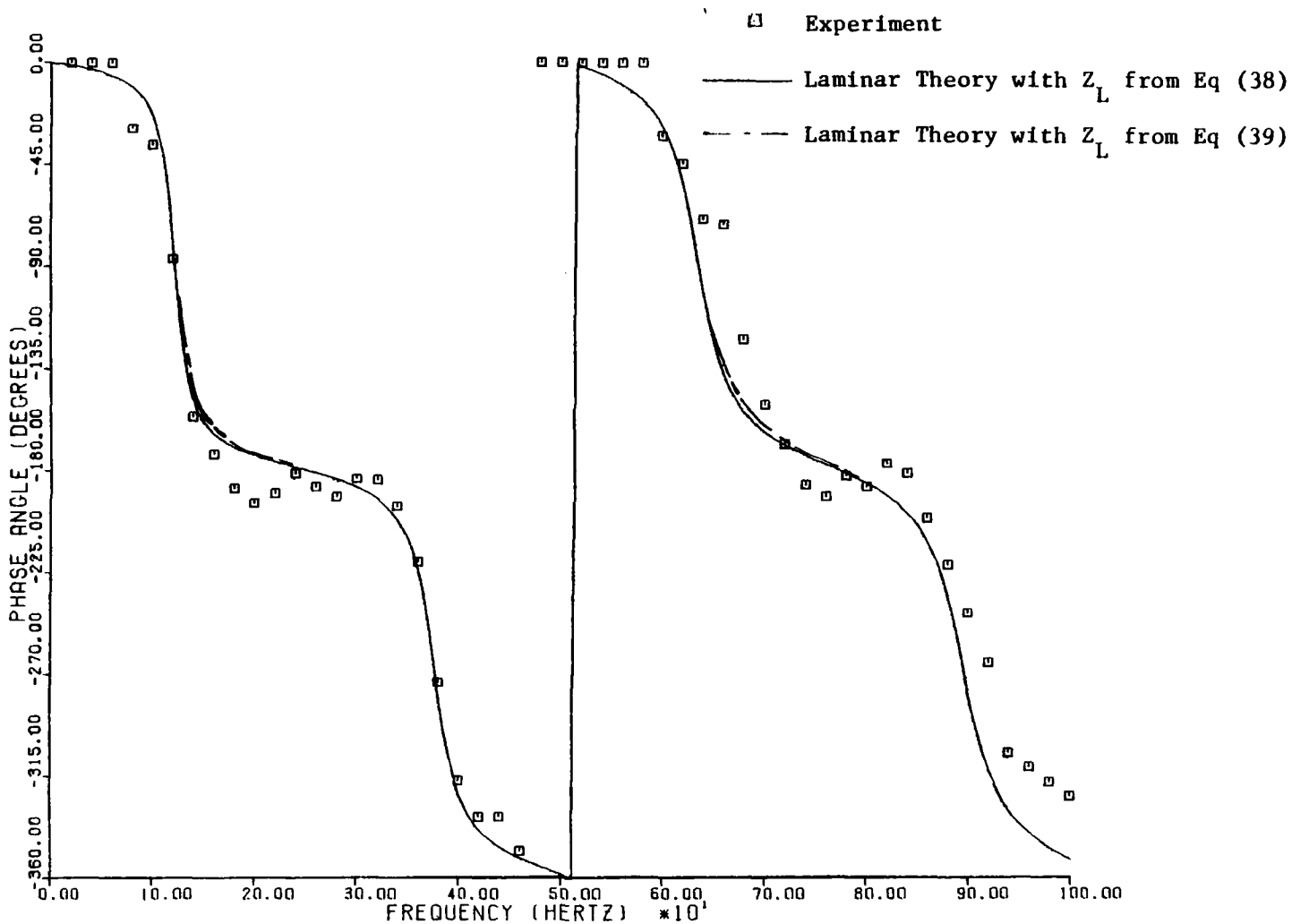

Figure 31 Experimental and Theoretical Phase vs Frequency for Case 22010

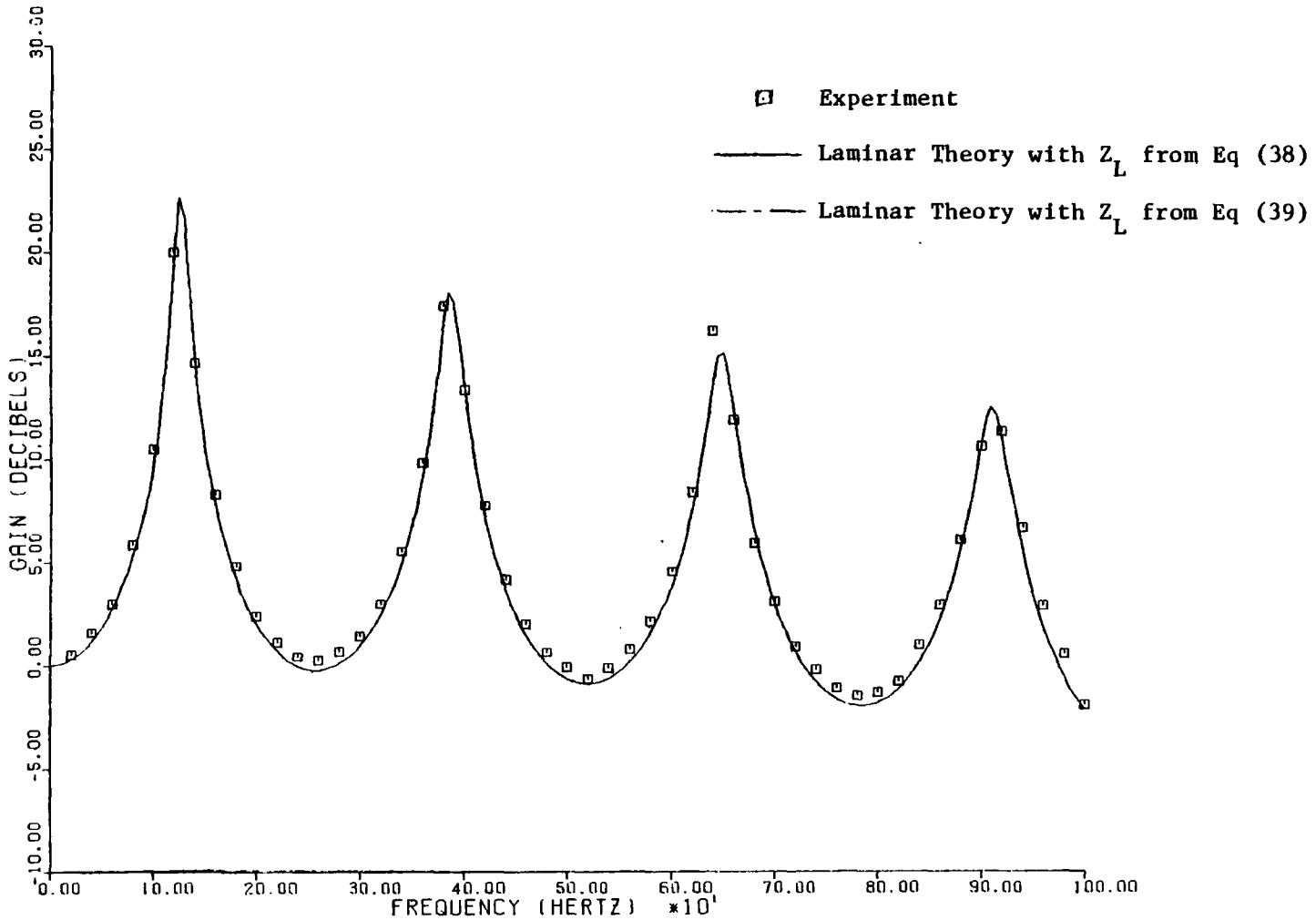

Figure 32 Experimental and Theoretical Gain vs Frequency for Case 31005

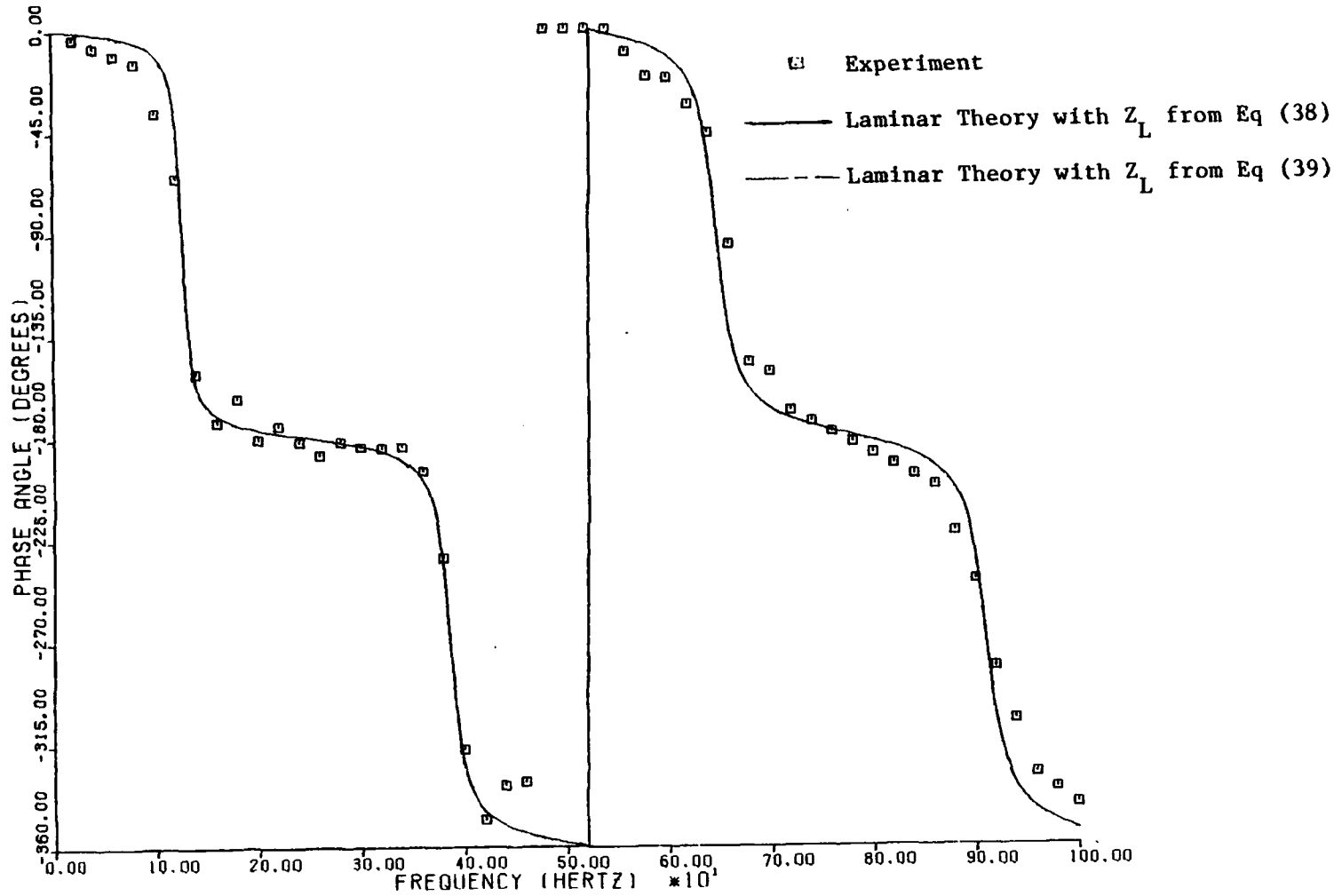

Figure 33 Experimental and Theoretical Phase vs Frequency for Case 31005

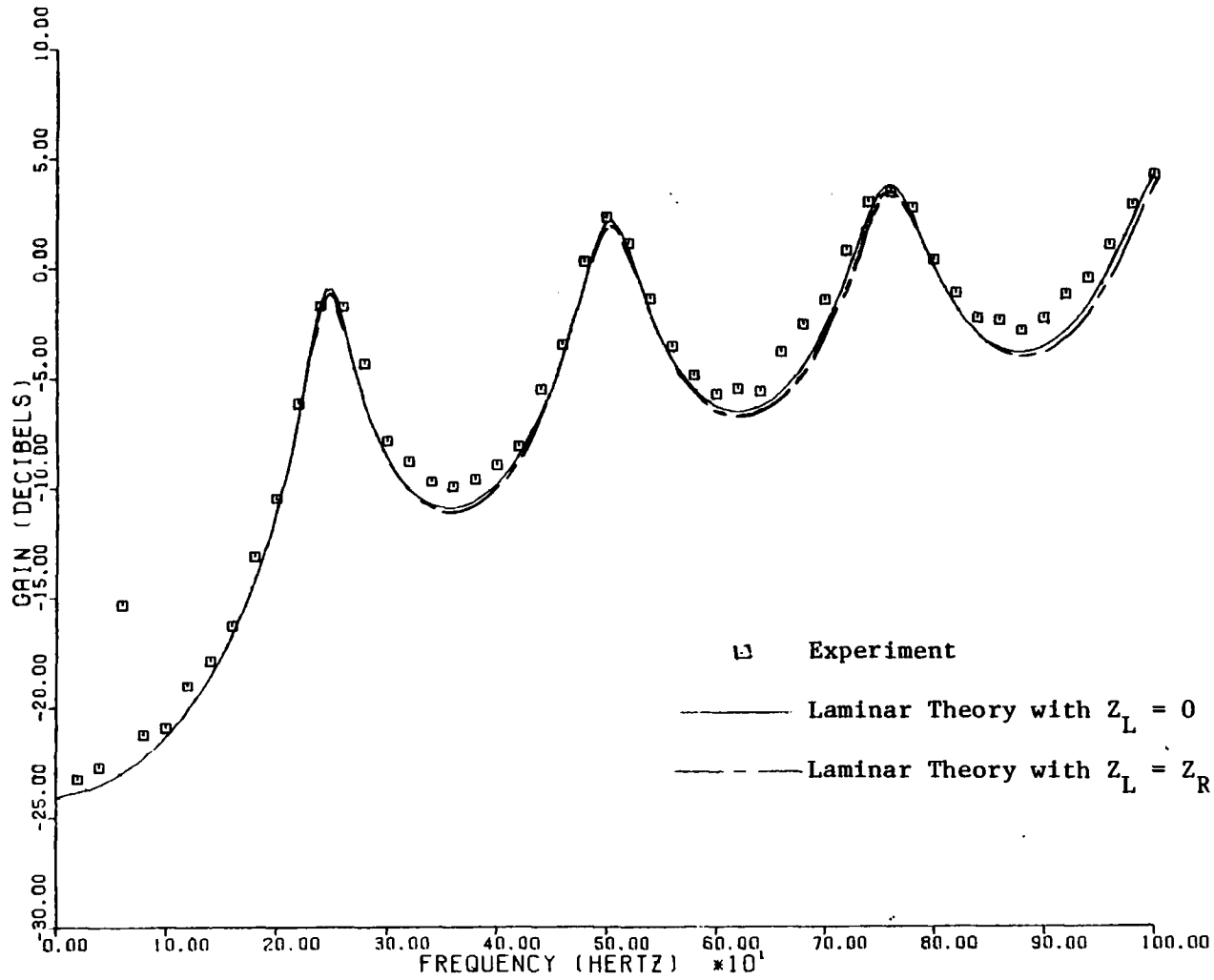

Figure 34 Experimental and Theoretical Gain vs Frequency for Case 23020

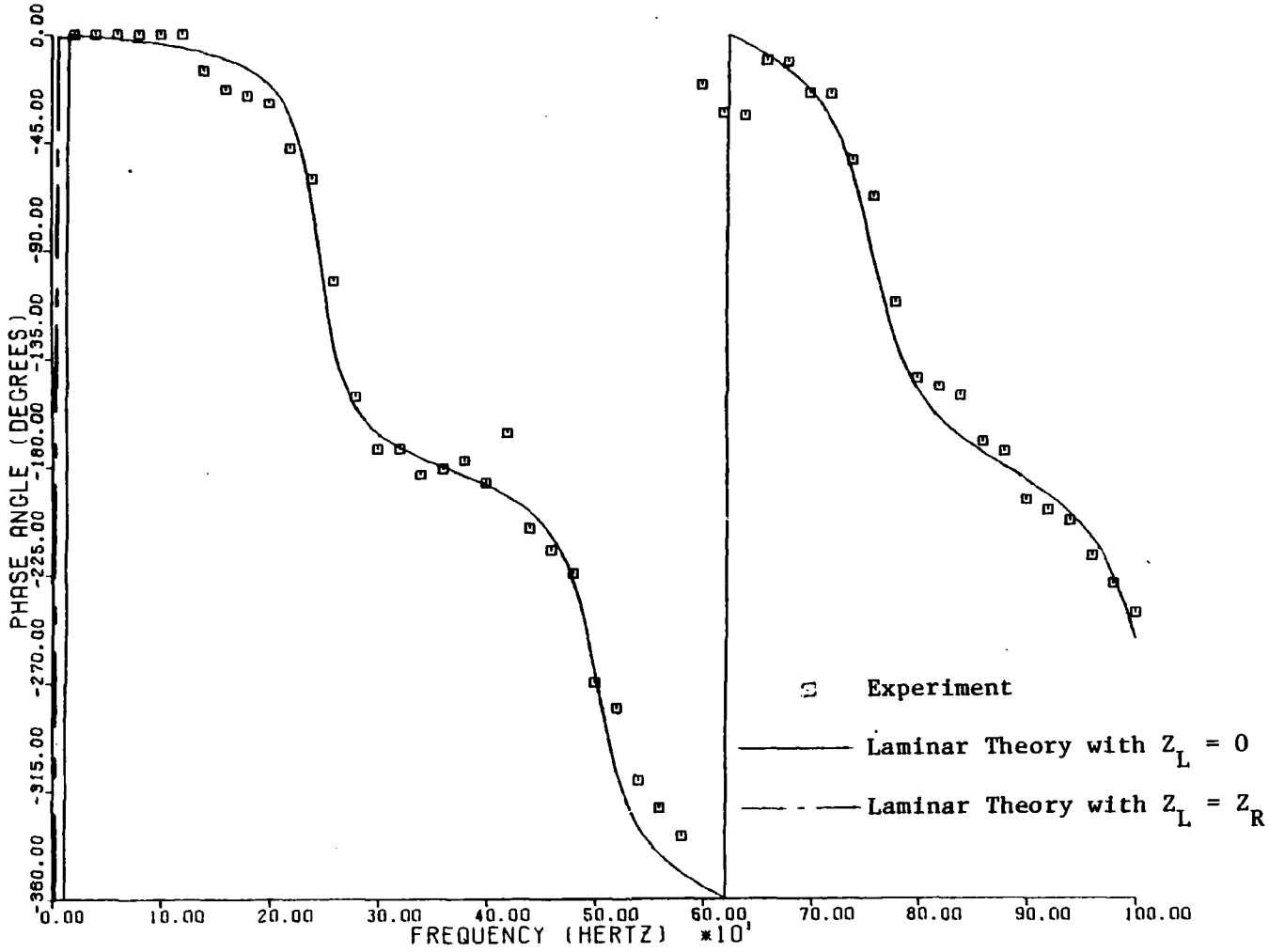

Figure 35 Experimental and Theoretical Phase vs Frequency for Case 23020

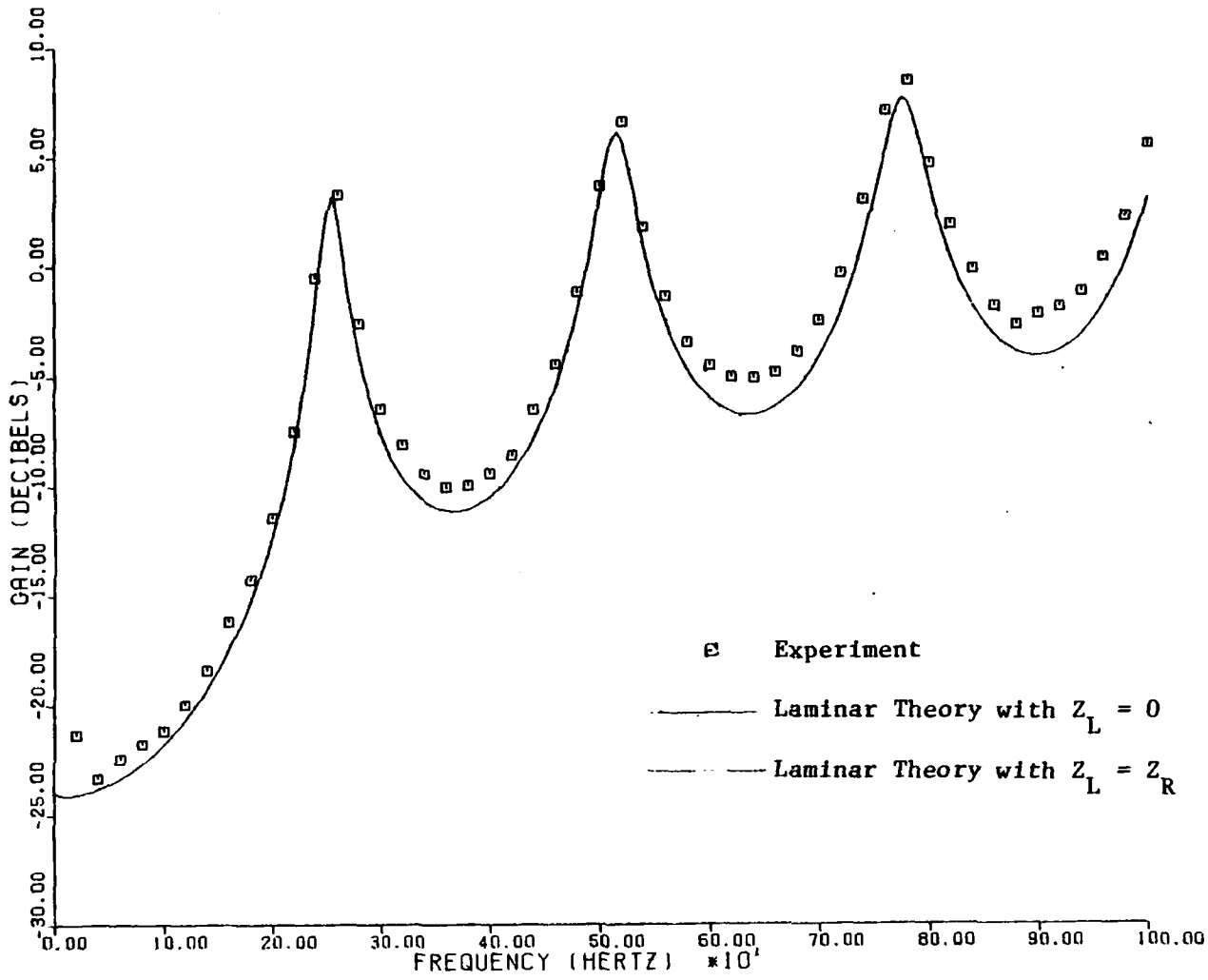

Figure 36 Experimental and Theoretical Gain vs Frequency for Case 33020

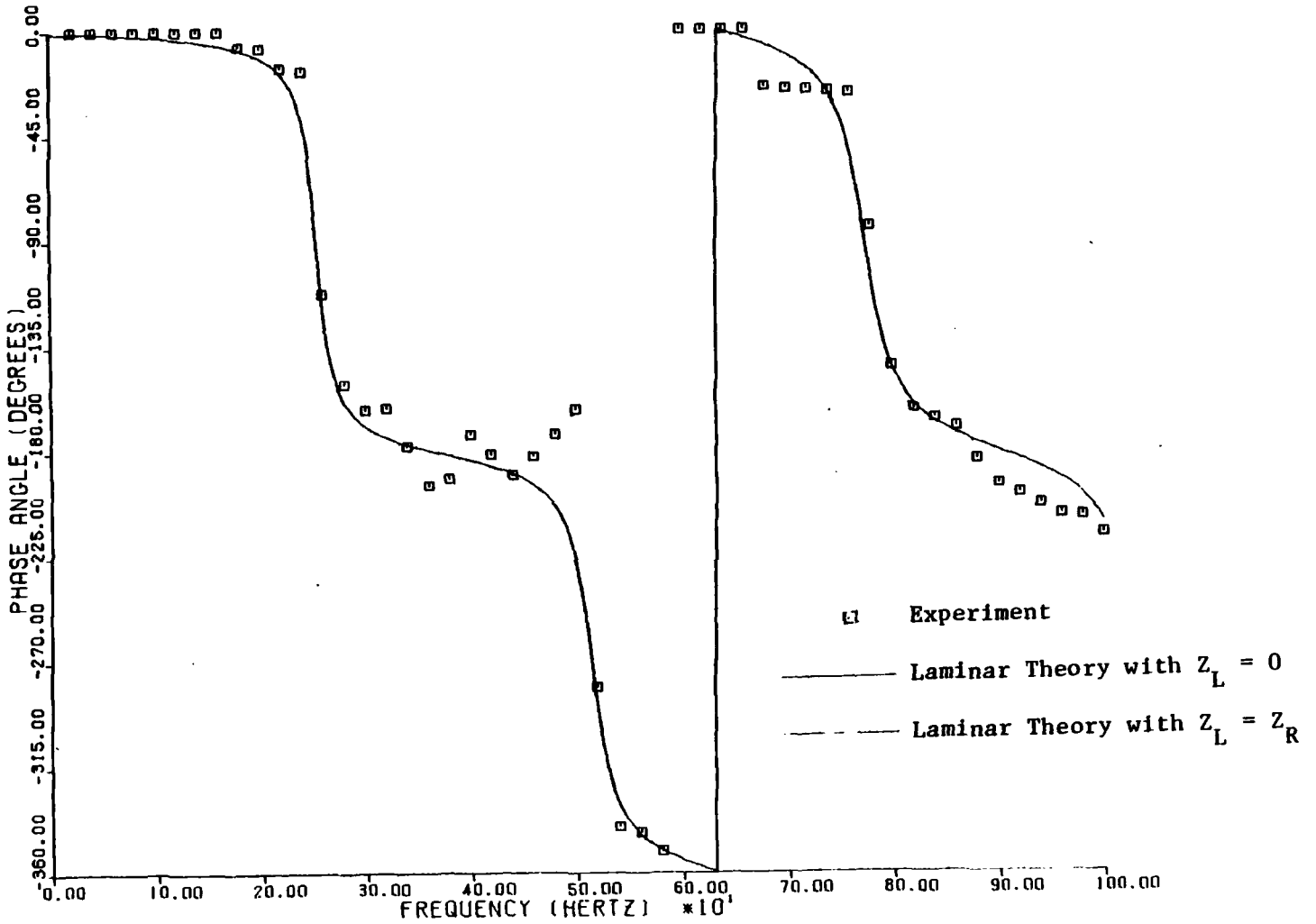

Figure 37 Experimental and Theoretical Phase vs Frequency for Case 33020

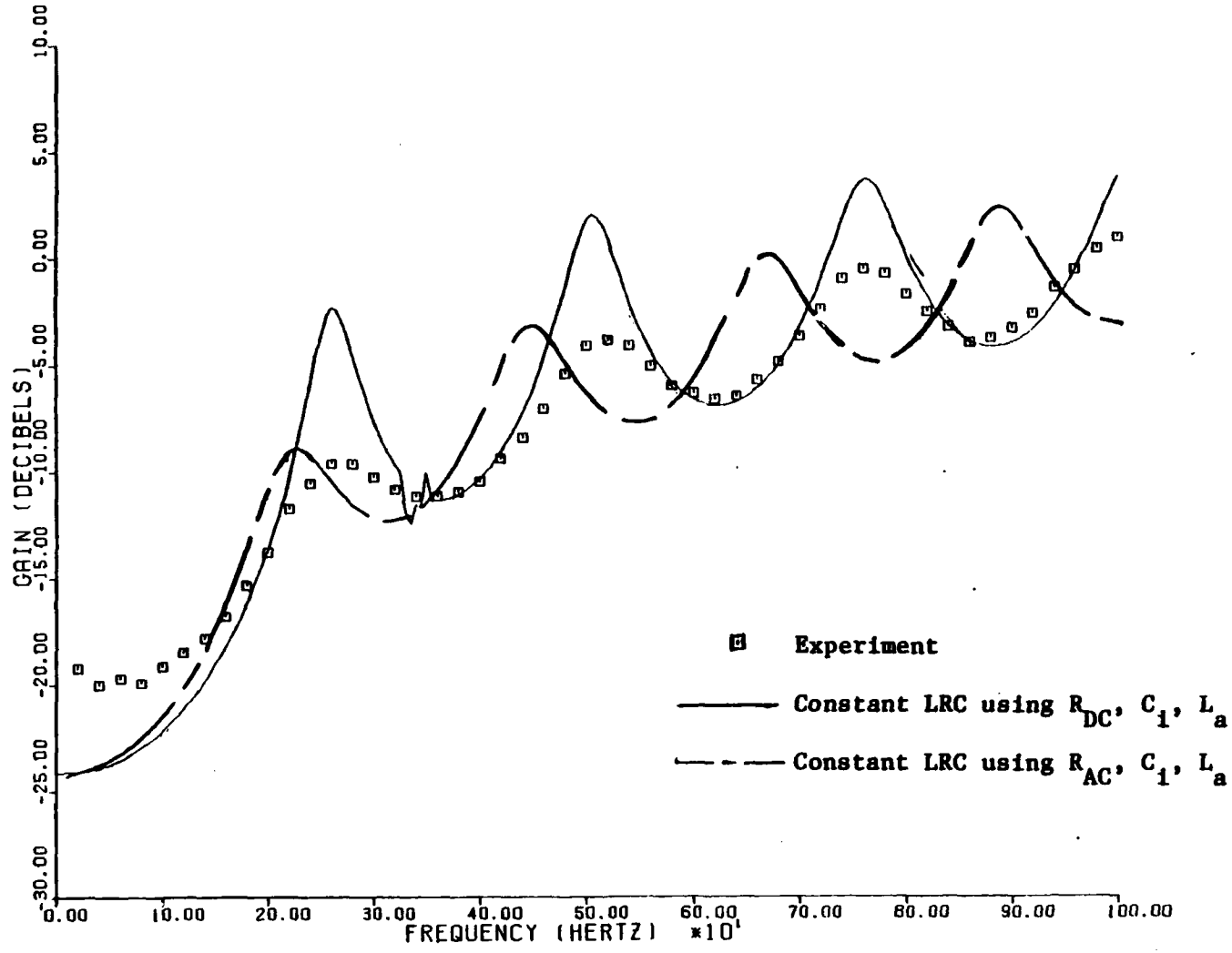

Figure 38 Experimental and Theoretical Gain vs Frequency for Case 23100

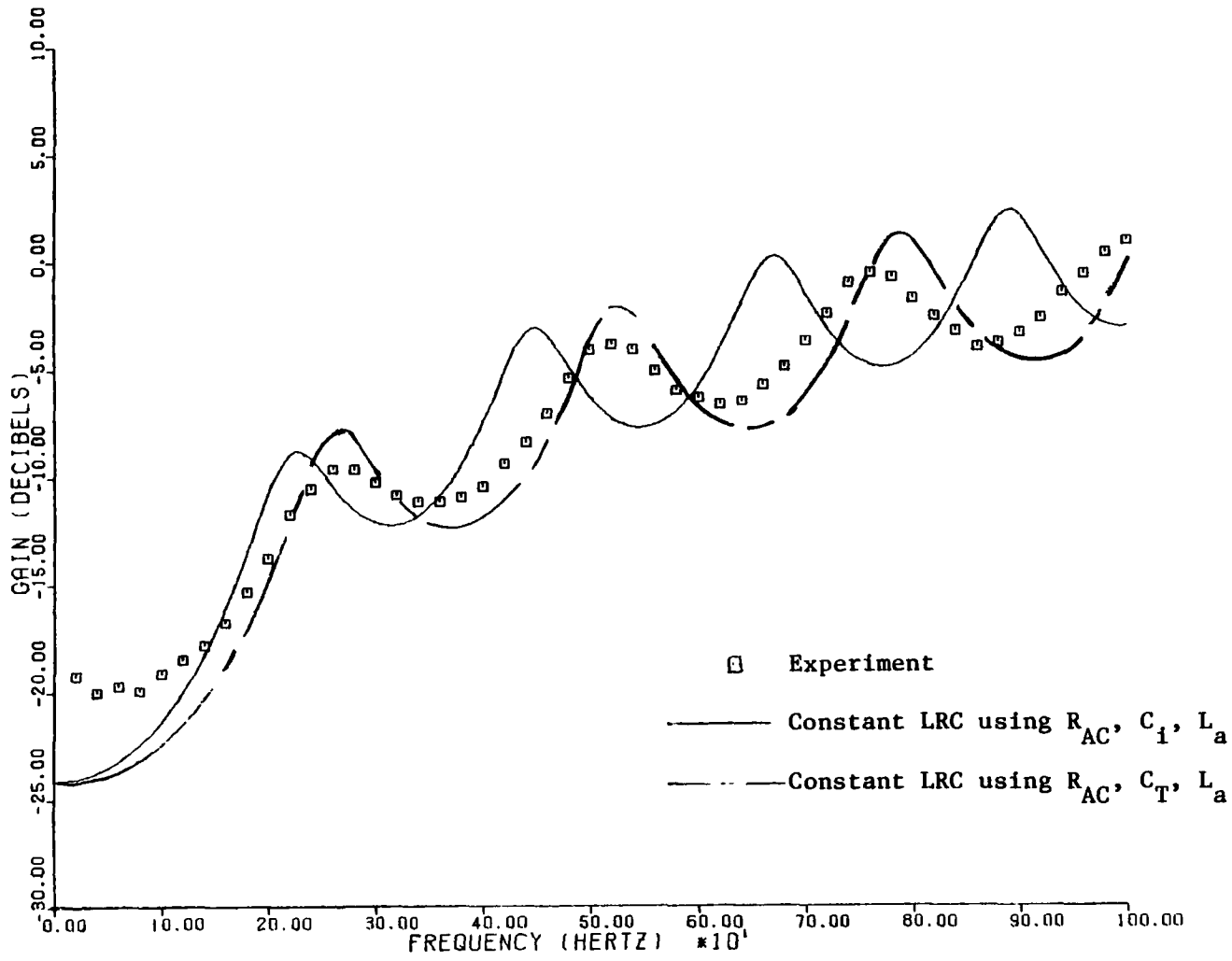

Figure 39 Experimental and Theoretical Gain vs Frequency for Case 23100

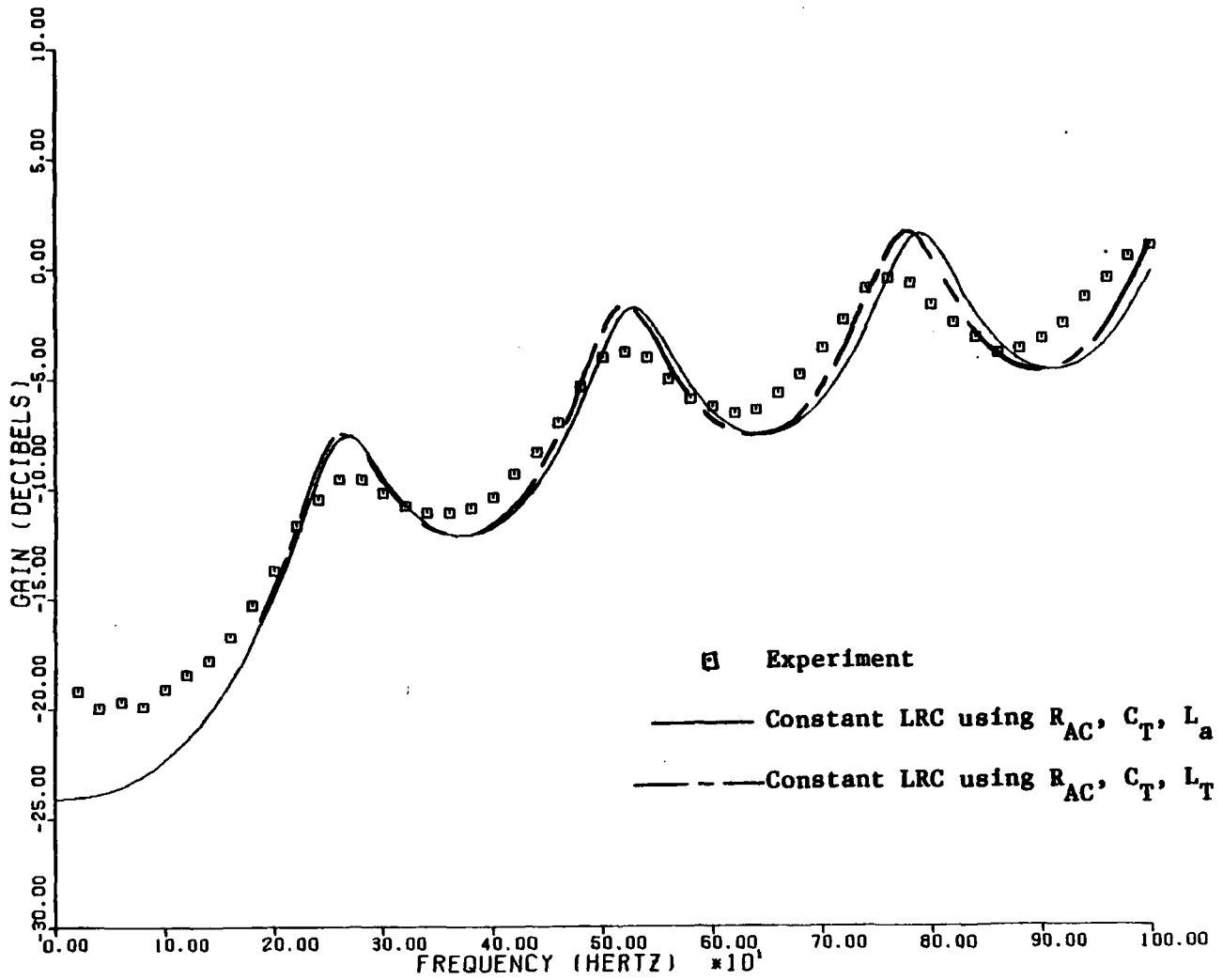

Figure 40 Experimental and Theoretical Gain vs Frequency for Case 23100

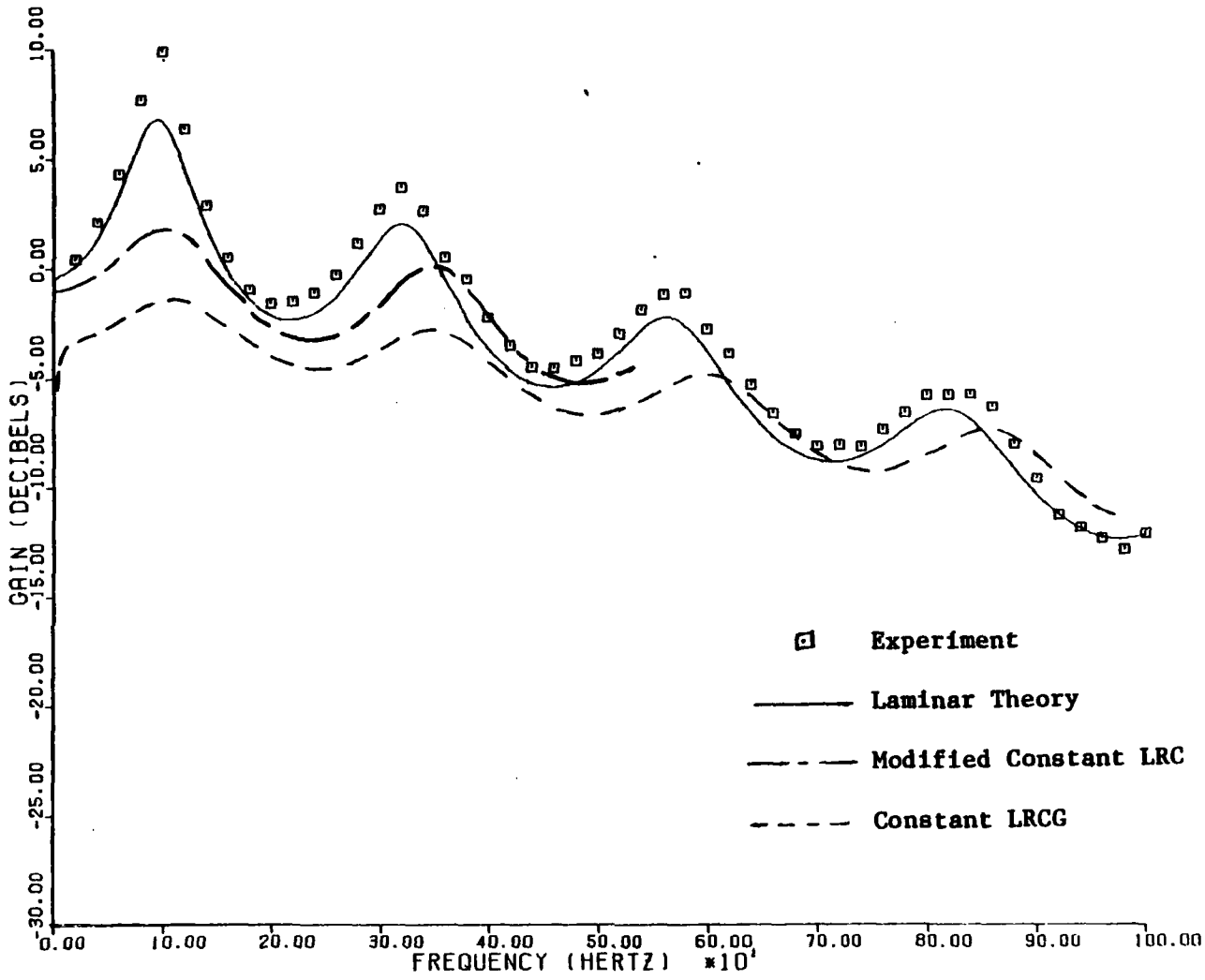

Figure 41 Experimental and Theoretical Gain vs Frequency for Case 11030

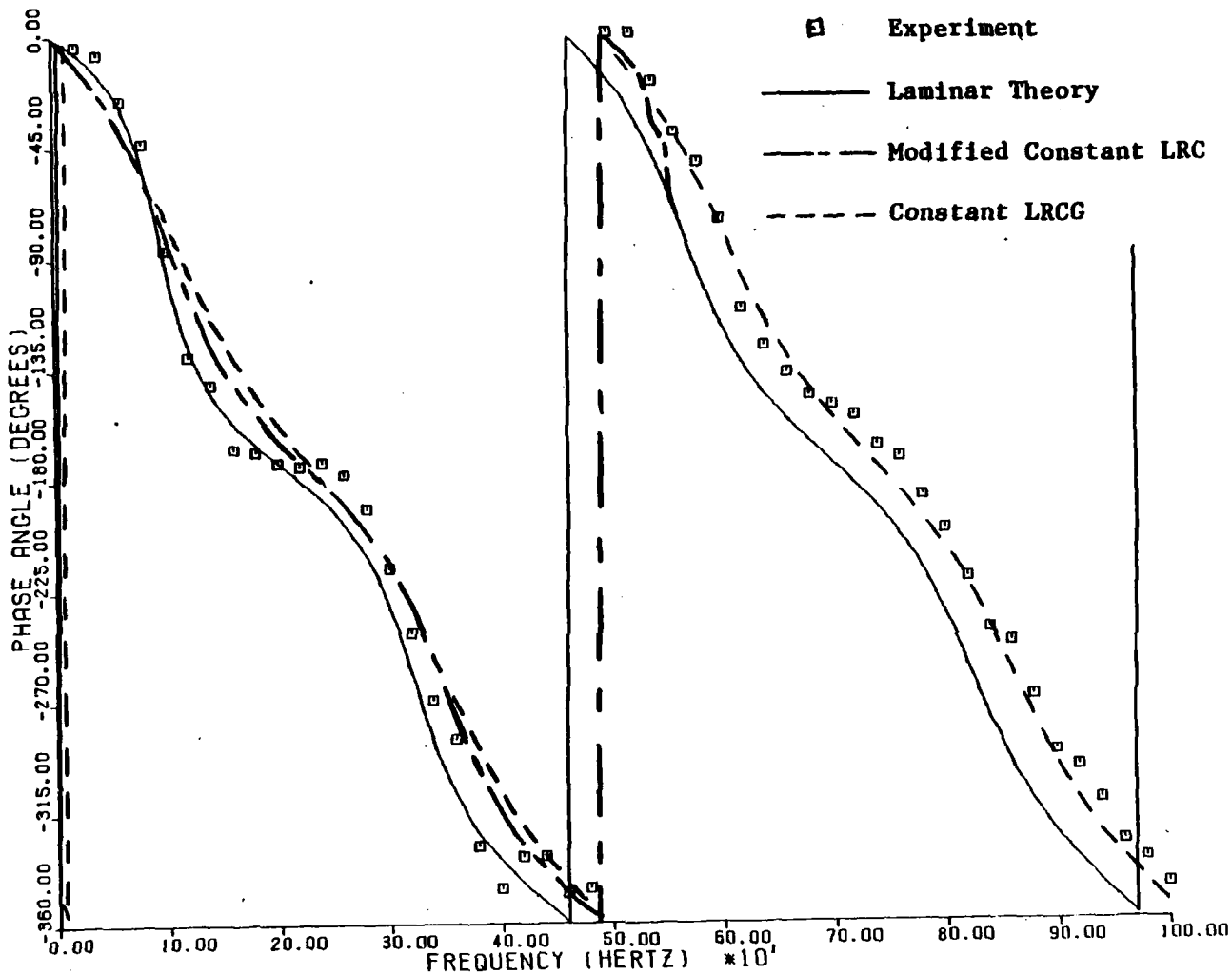

Figure 42 Experimental and Theoretical Phase vs Frequency for Case 11030

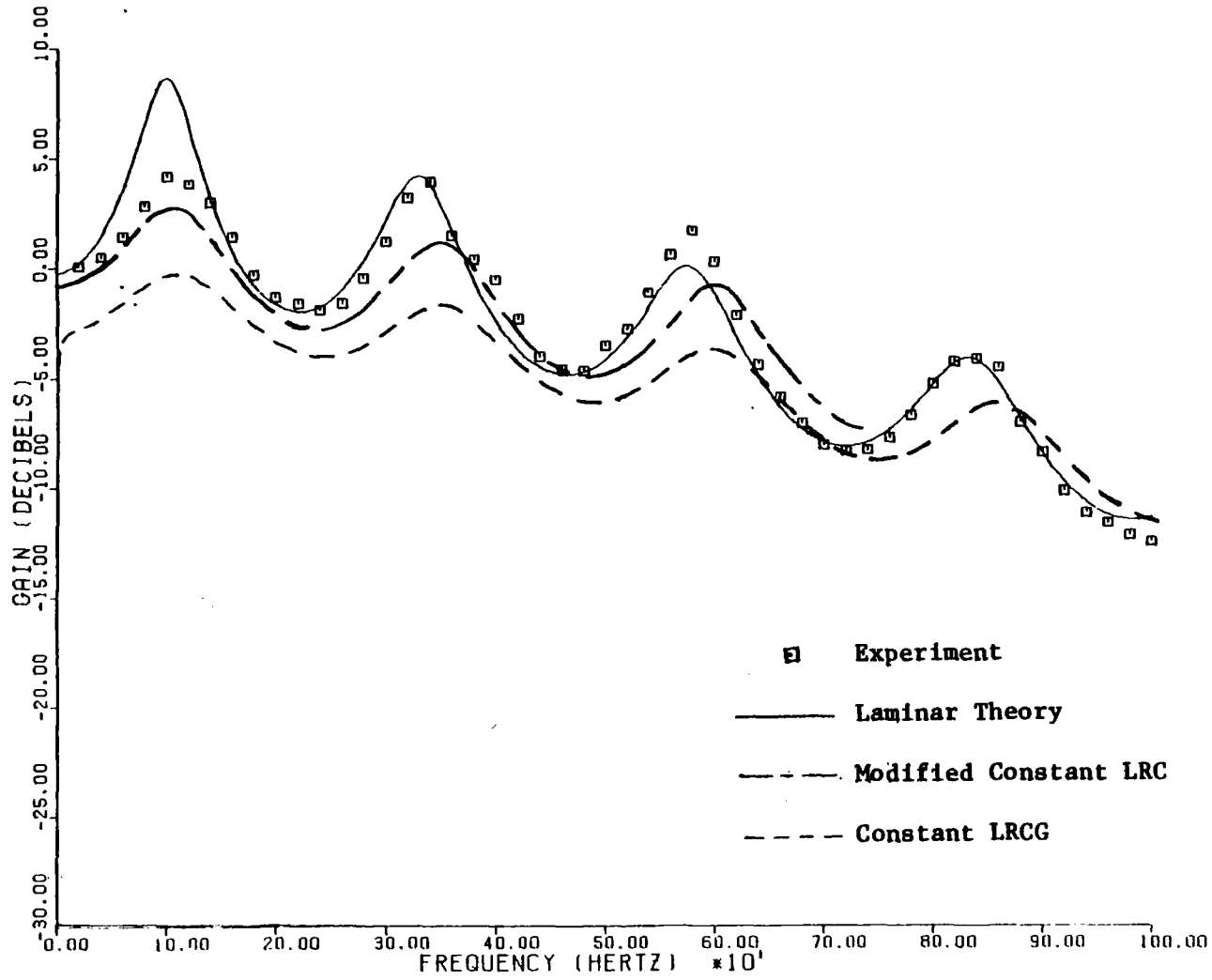

Figure 43 Experimental and Theoretical Gain vs Frequency for Case 11050

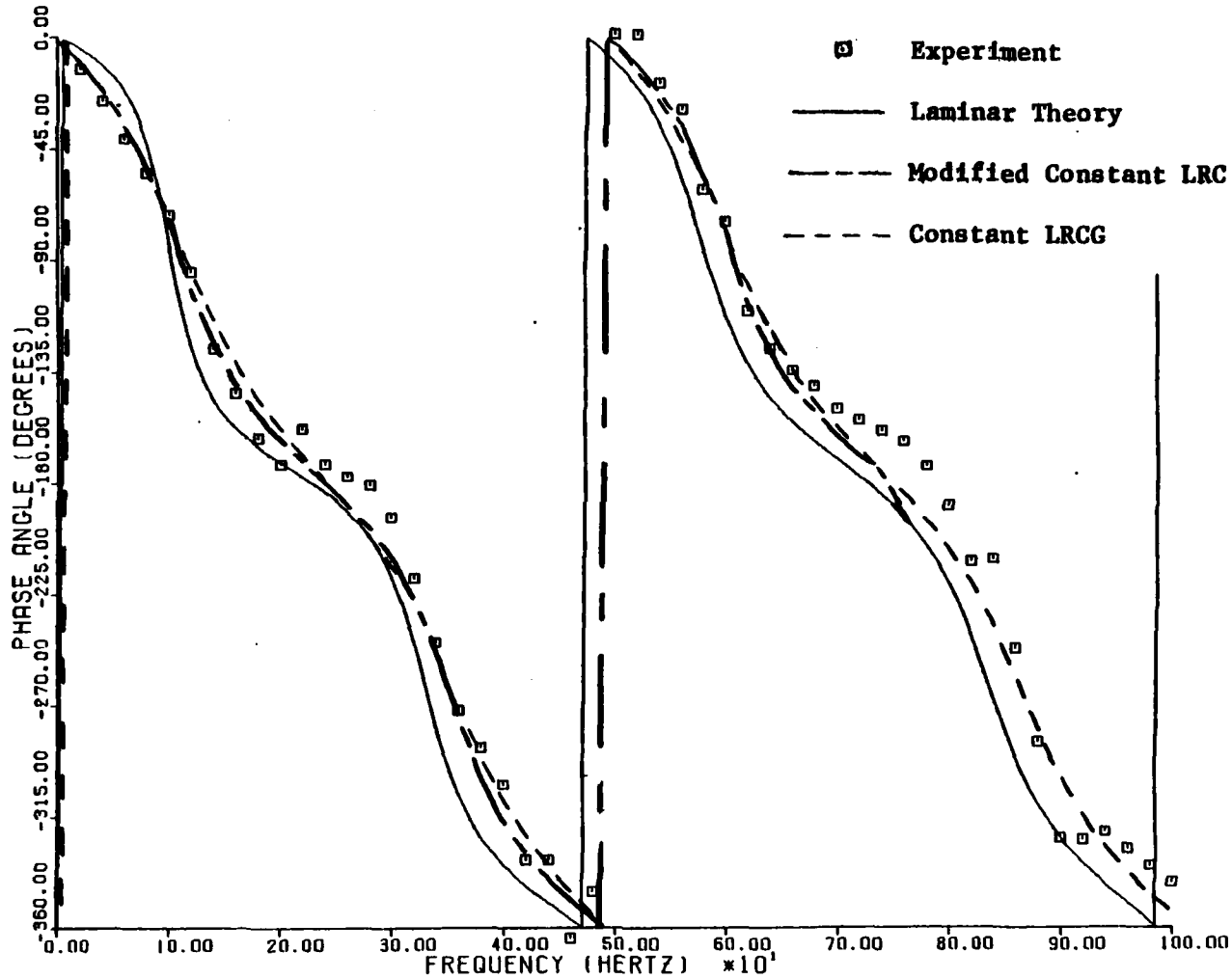

Figure 44 Experimental and Theoretical Phase vs Frequency for Case 11050

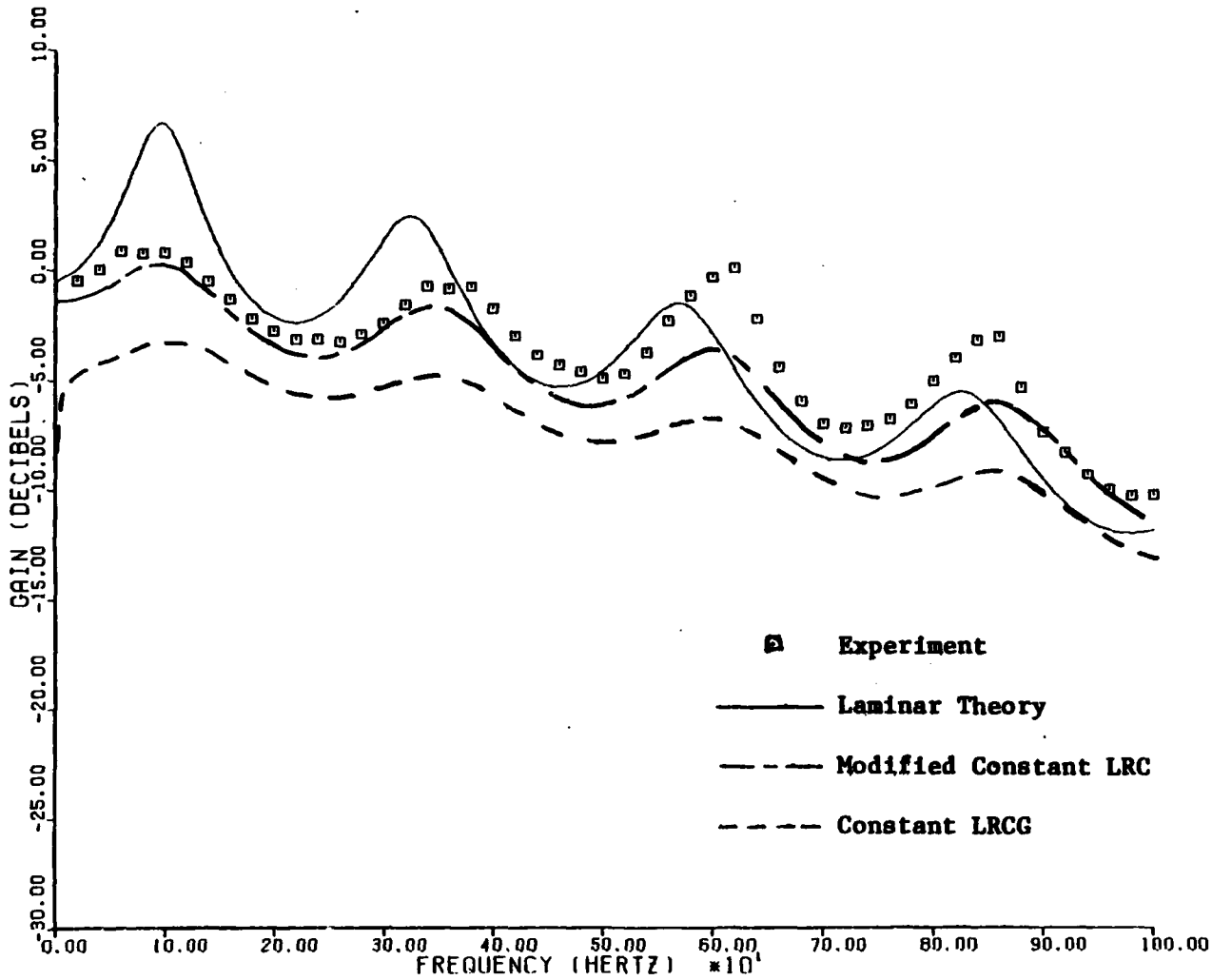

Figure 45 Experimental and Theoretical Gain vs Frequency for Case 12050

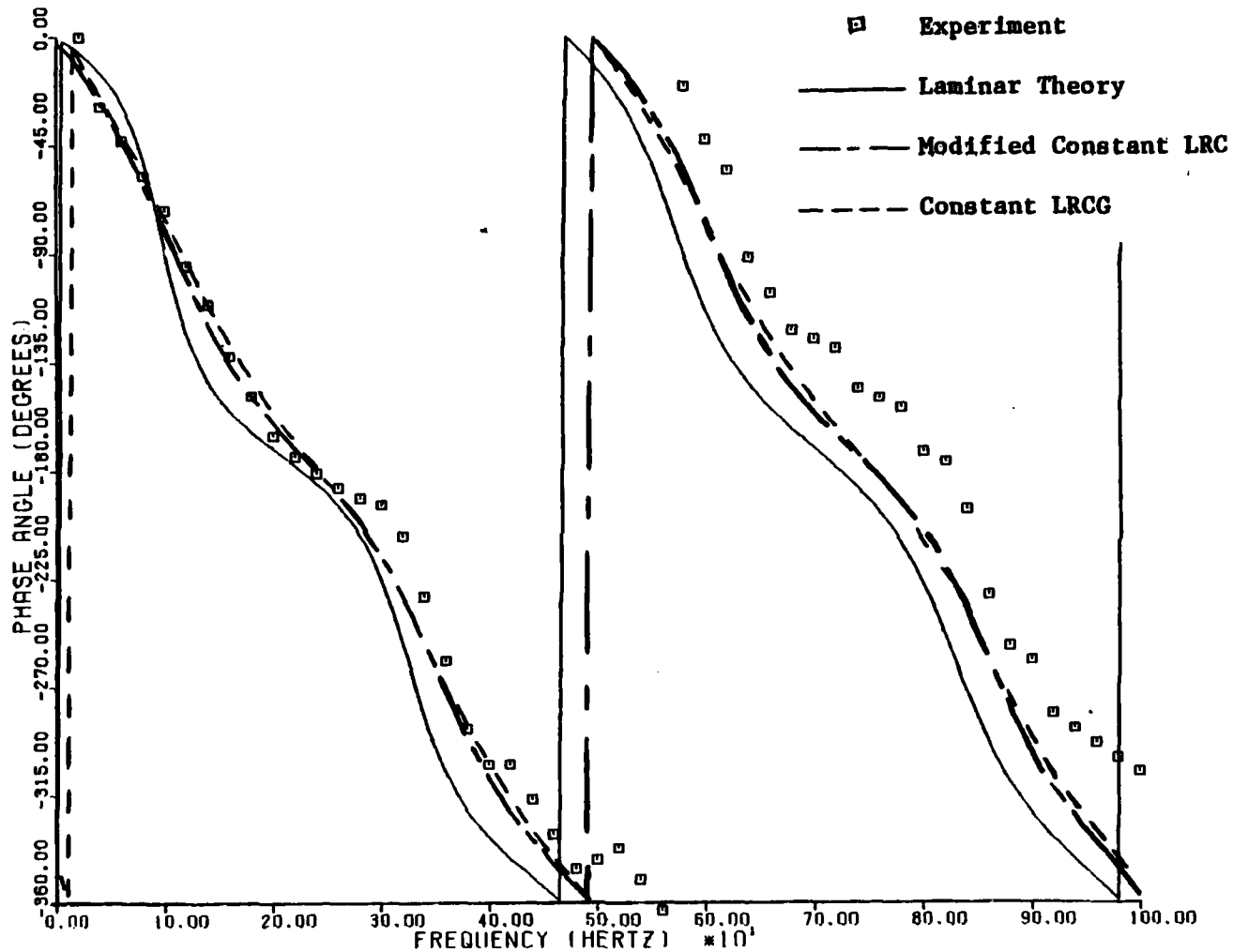

Figure 46 Experimental and Theoretical Phase vs Frequency for Case 12050

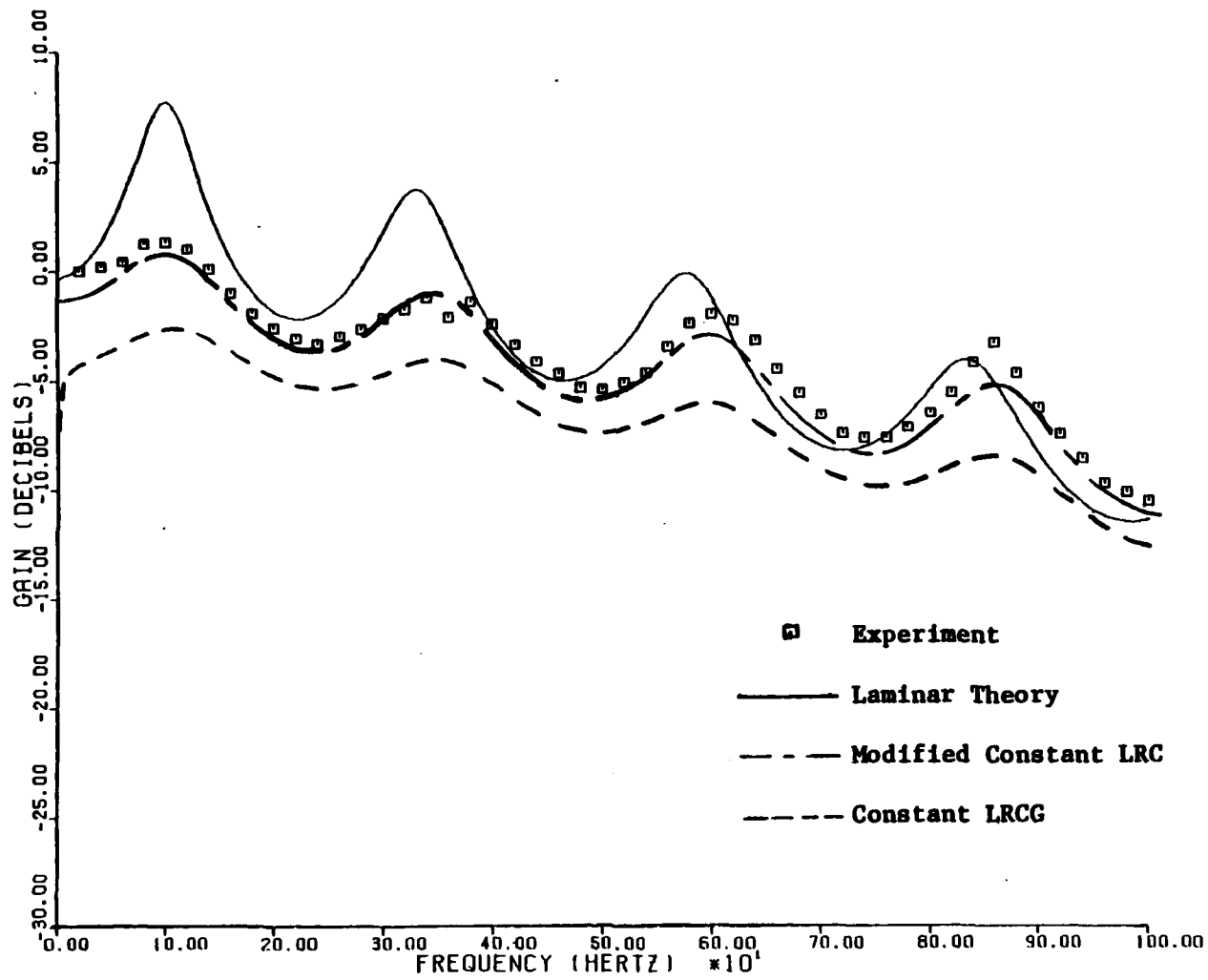

Figure 47 Experimental and Theoretical Gain vs Frequency for Case 12070

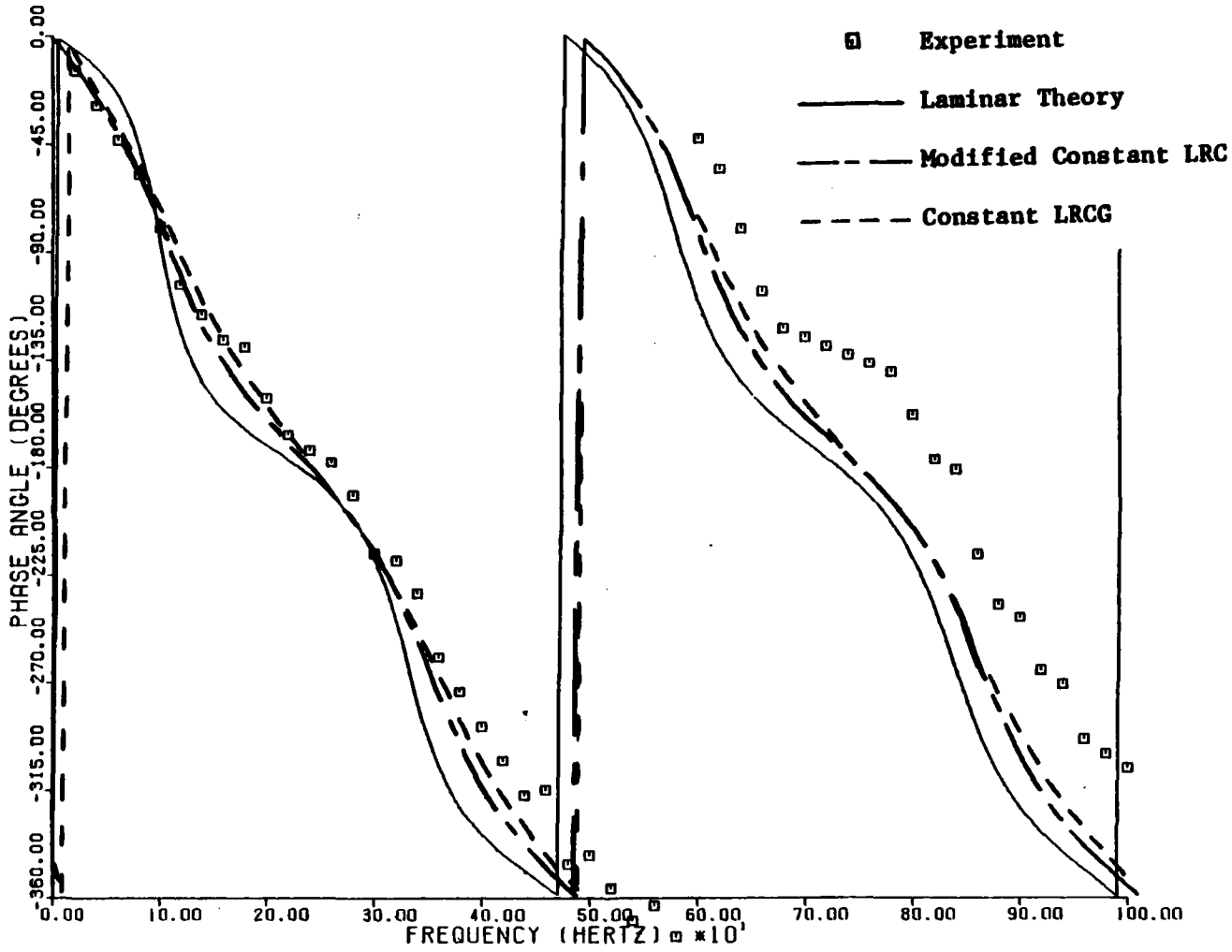

Figure 48 Experimental and Theoretical Phase vs Frequency for Case 12070

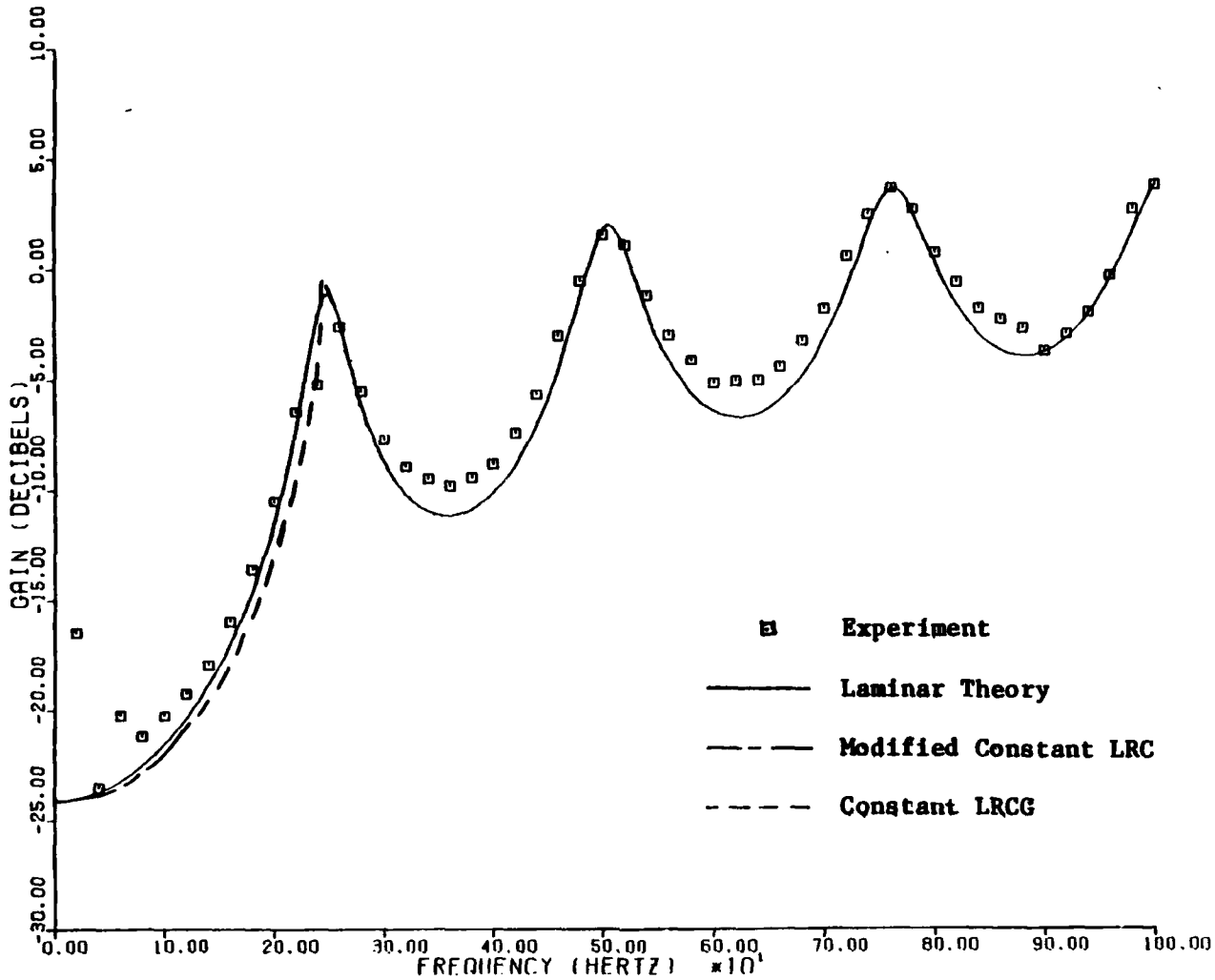

Figure 49 Experimental and Theoretical Gain vs Frequency for Case 23030

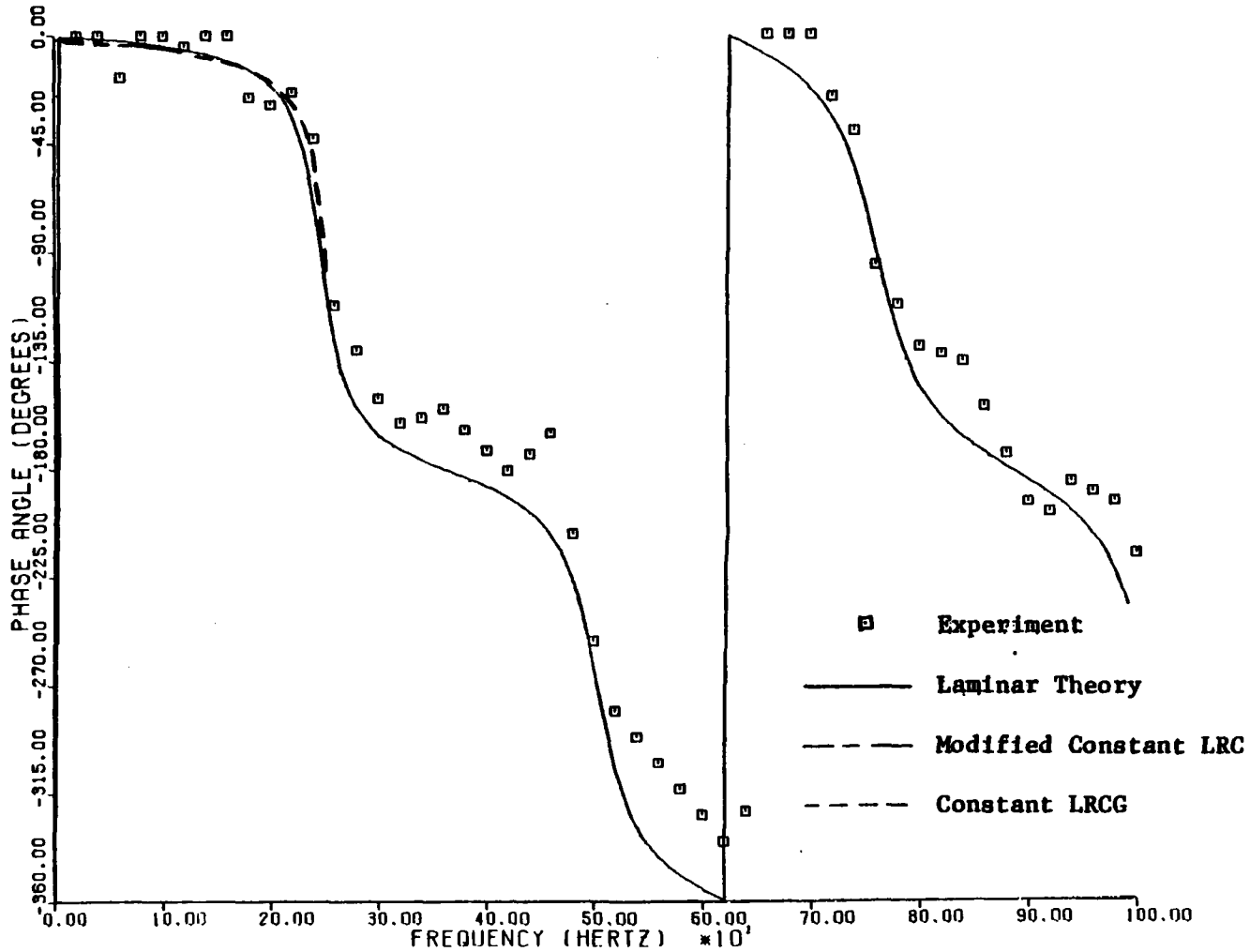

Figure 50 Experimental and Theoretical Phase vs Frequency for Case 23030

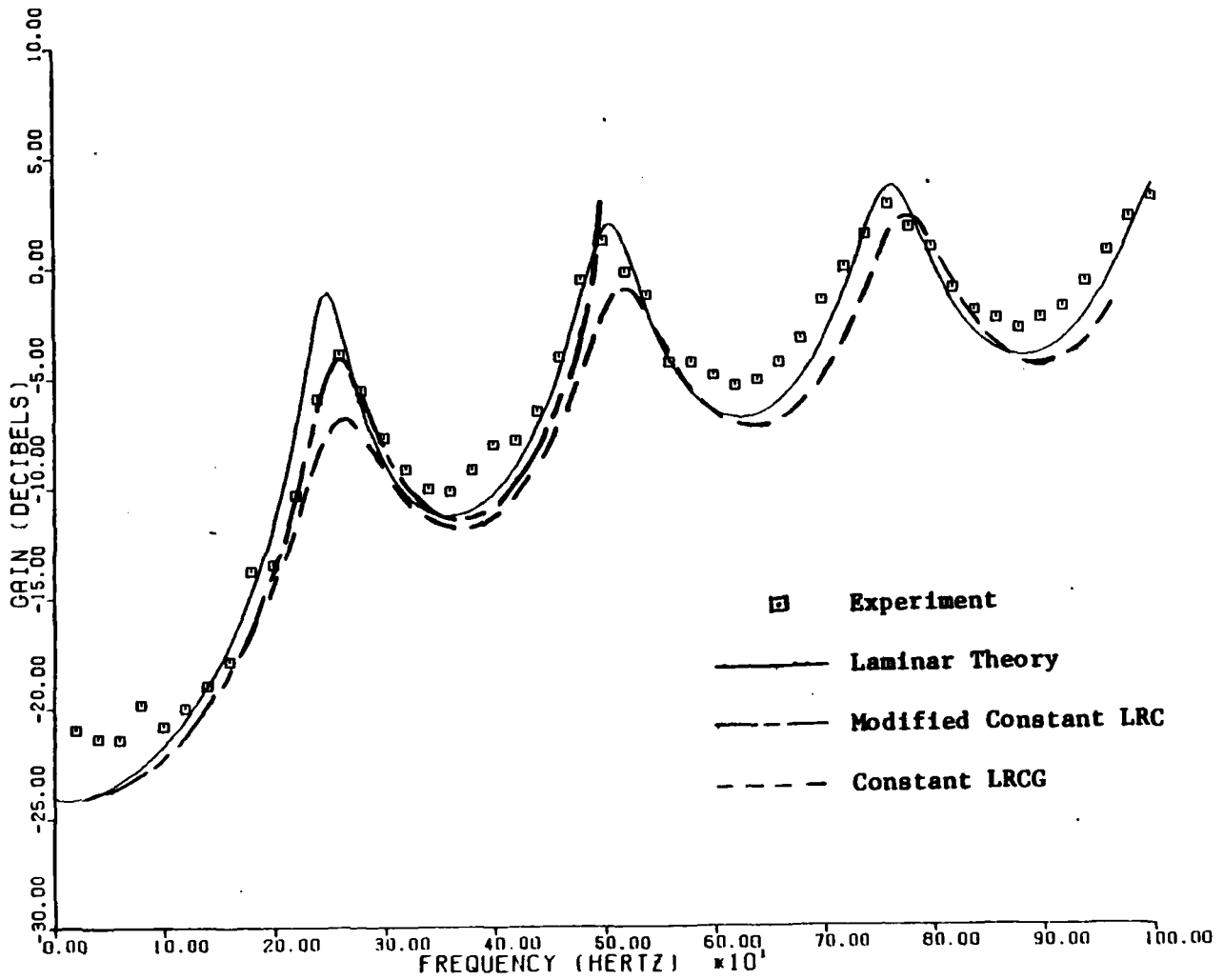

Figure 51 Experimental and Theoretical Gain vs Frequency for Case 23050

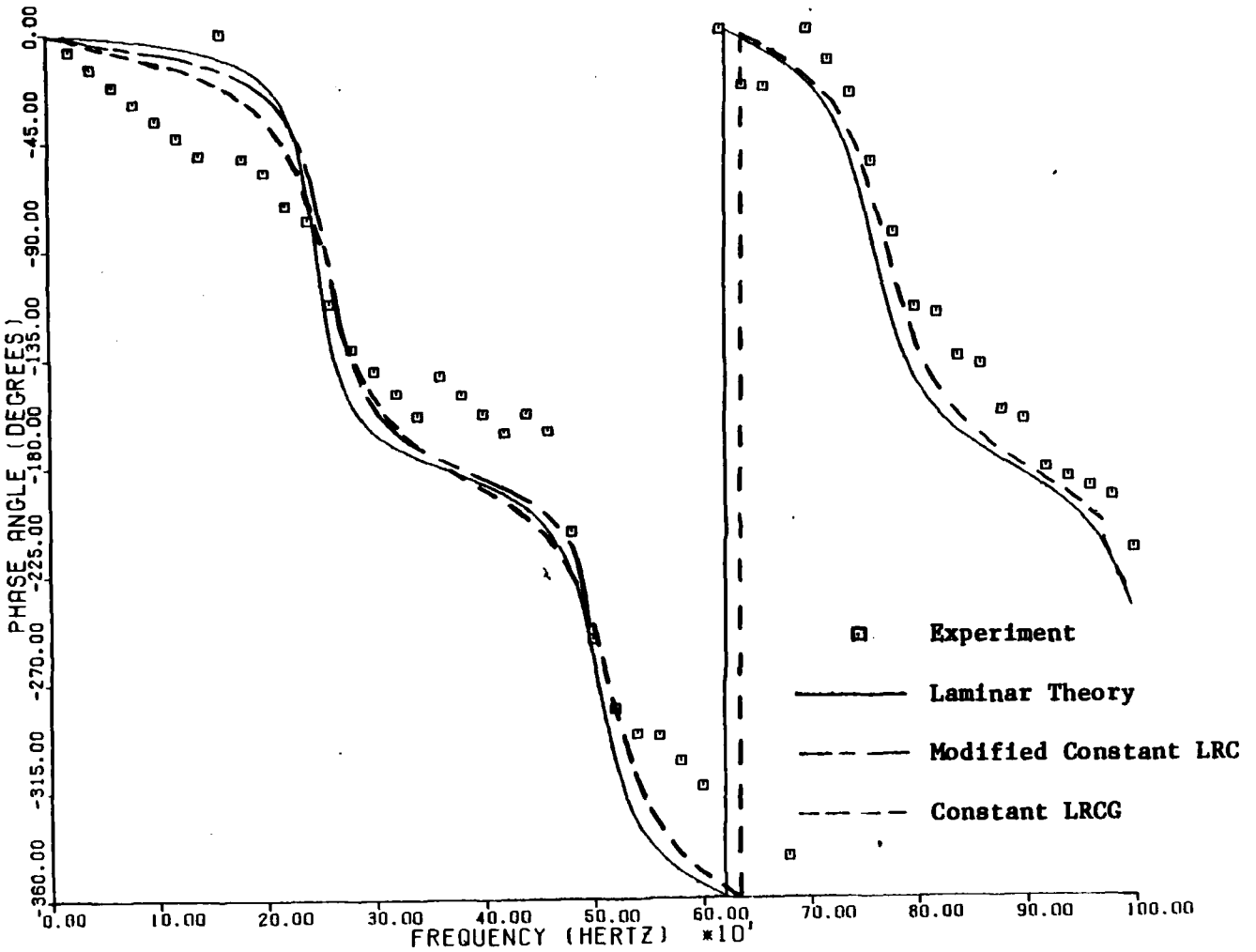

Figure 52 Experimental and Theoretical Phase vs Frequency for Case 23050

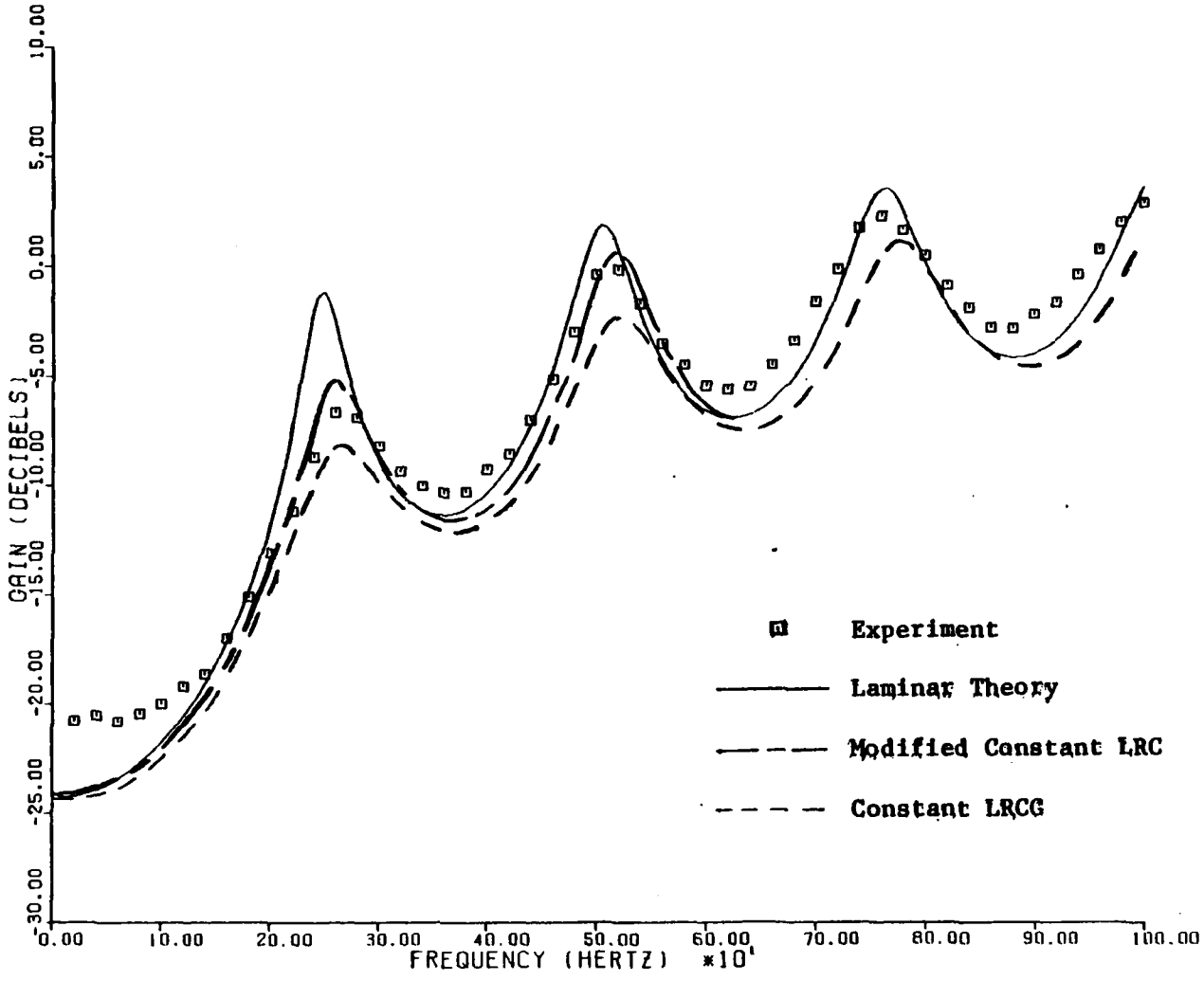

Figure 53 Experimental and Theoretical Gain vs Frequency for Case 23070

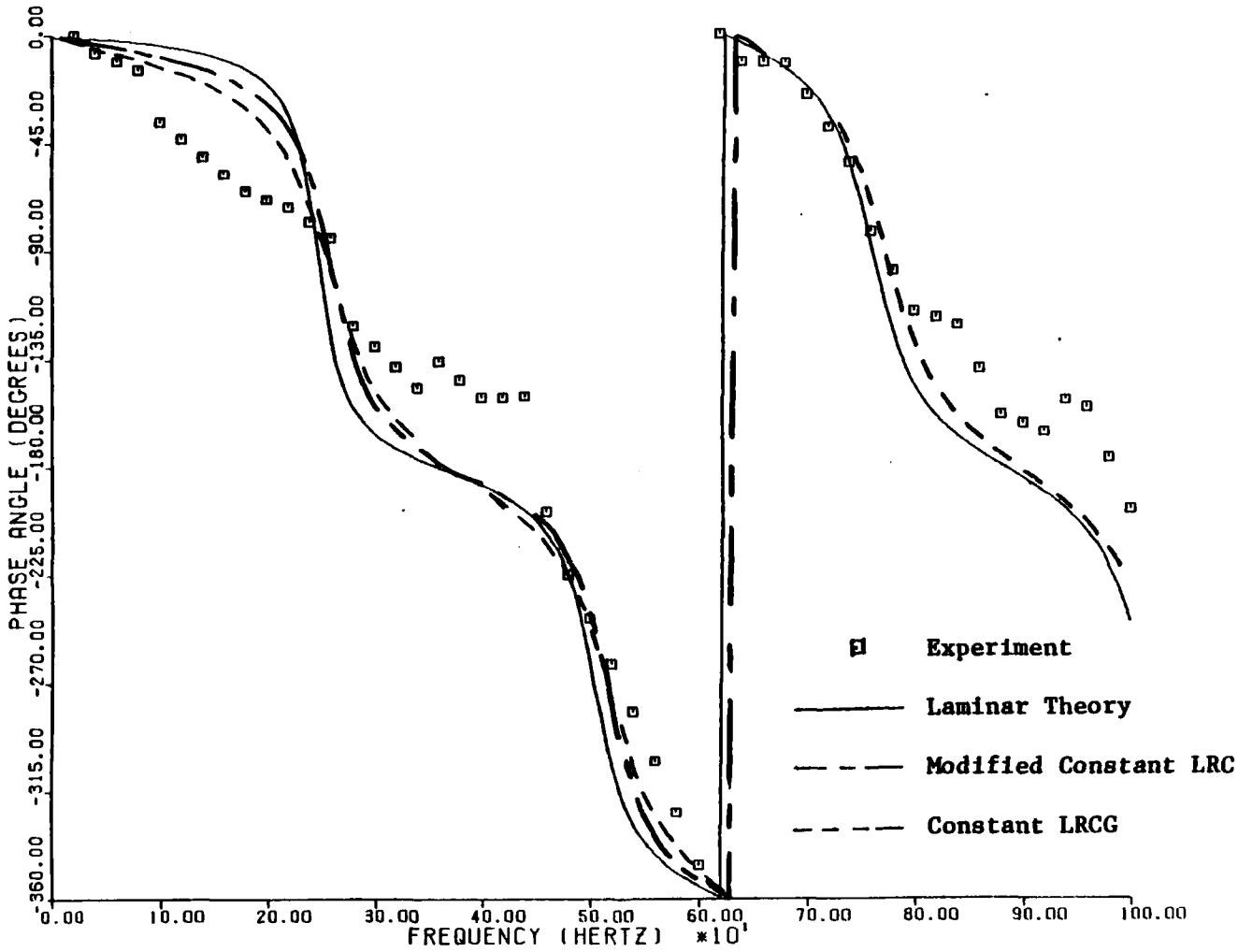

Figure 54 Experimental and Theoretical Phase vs Frequency for Case 23070

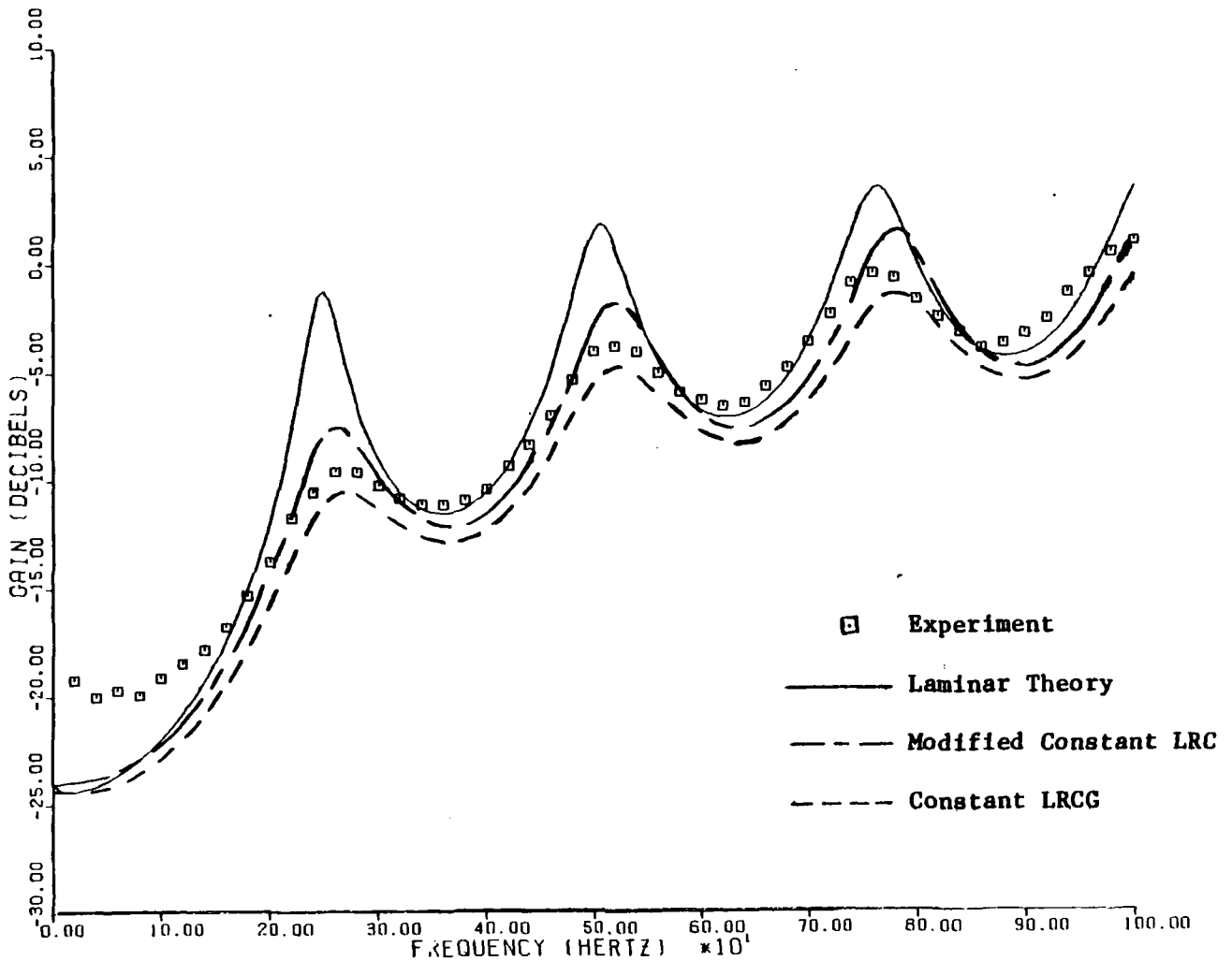

Figure 55 Experimental and Theoretical Gain vs Frequency for Case 23100

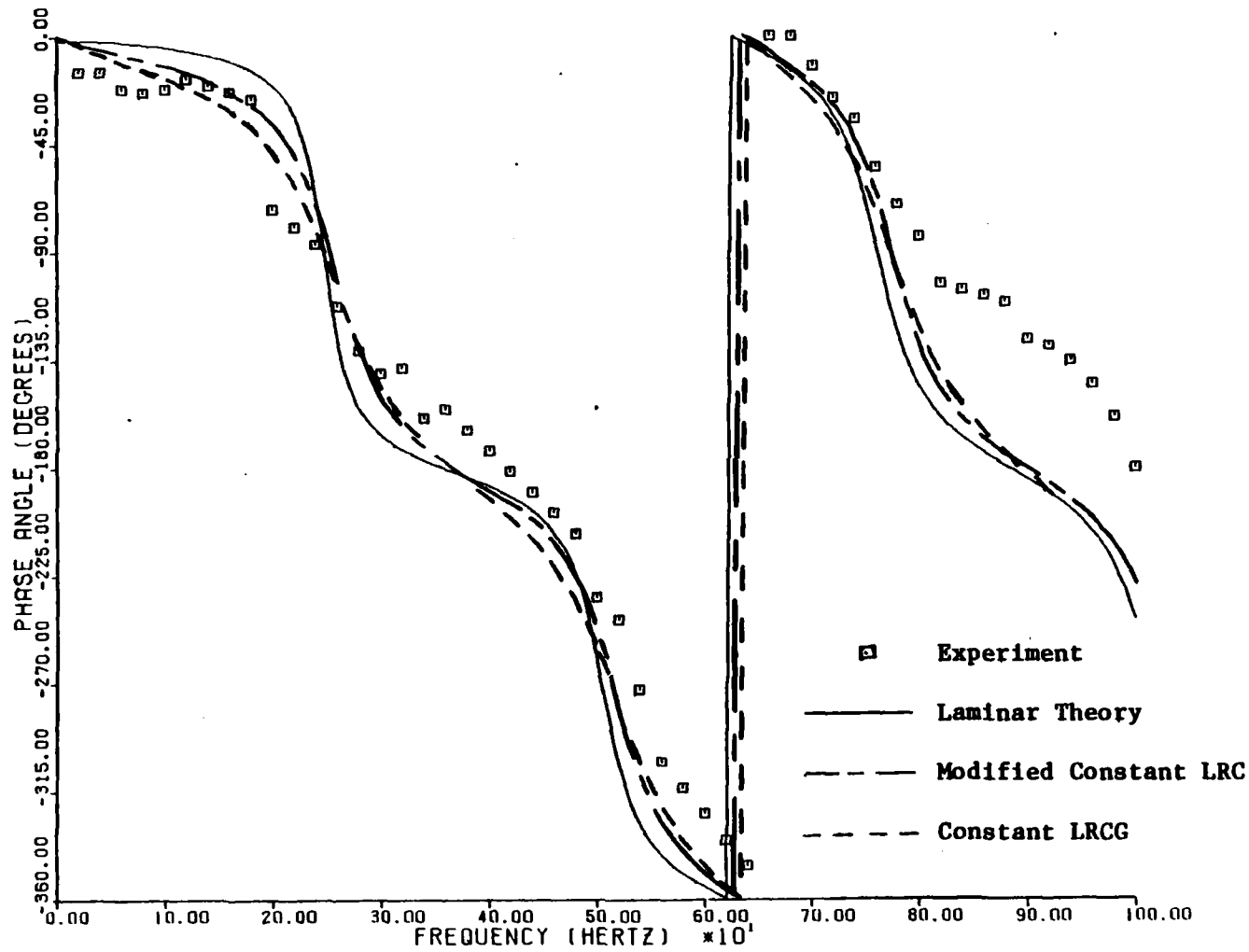

Figure 56 Experimental and Theoretical Phase vs Frequency for Case 23100

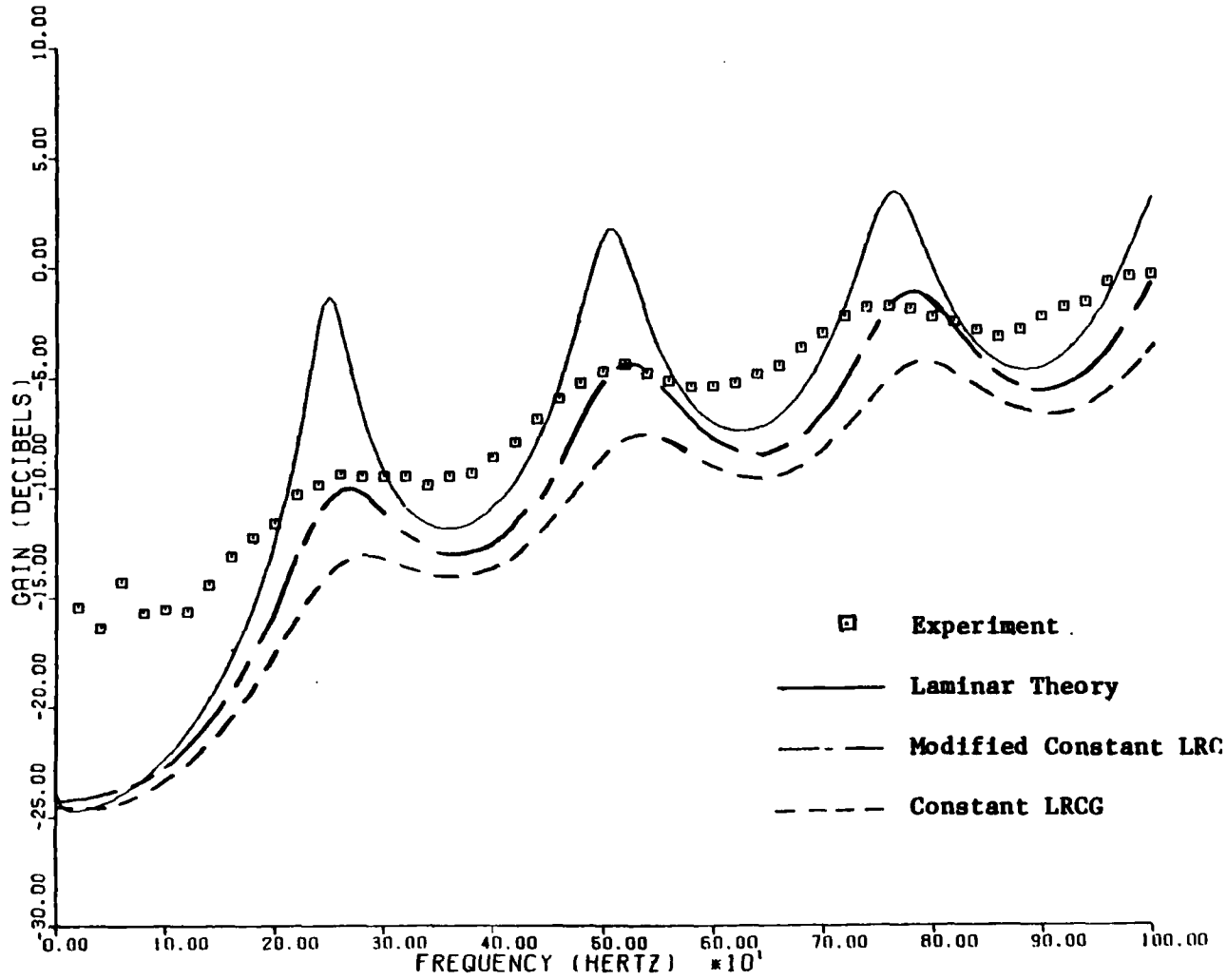

Figure 57 Experimental and Theoretical Gain vs Frequency for Case 23150

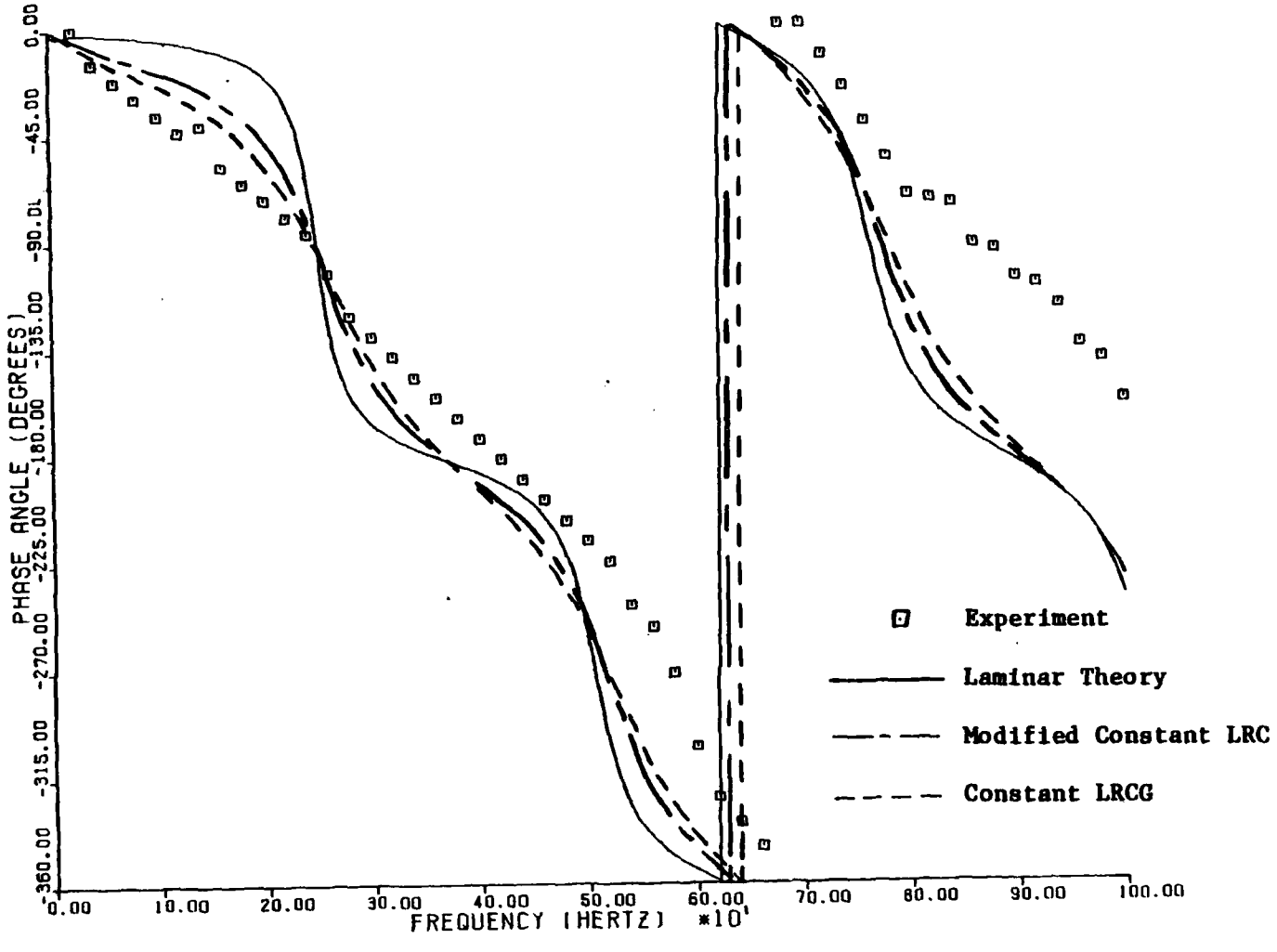

Figure 58 Experimental and Theoretical Phase vs Frequency for Case 23150

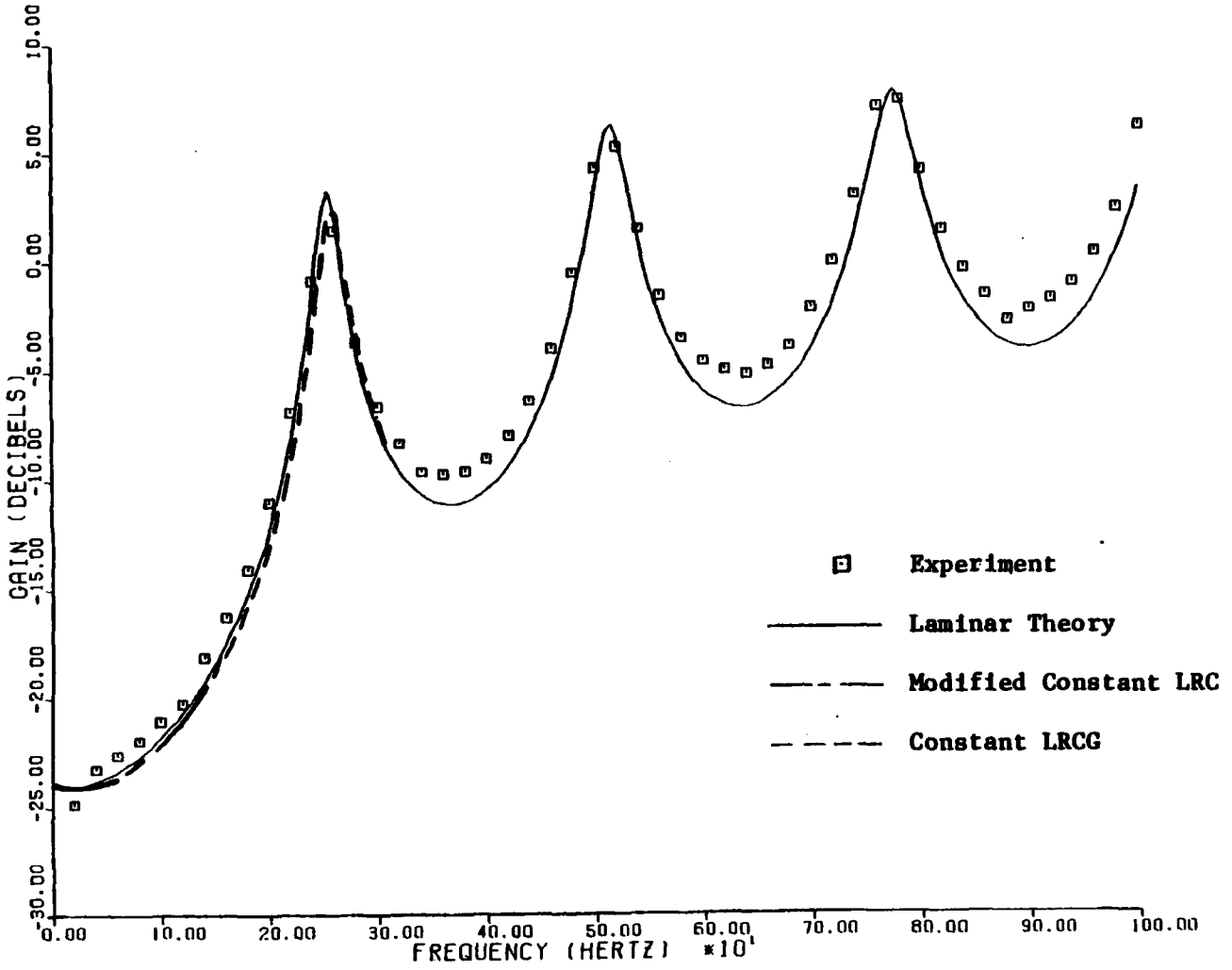

Figure 59 Experimental and Theoretical Gain vs Frequency for Case 33050

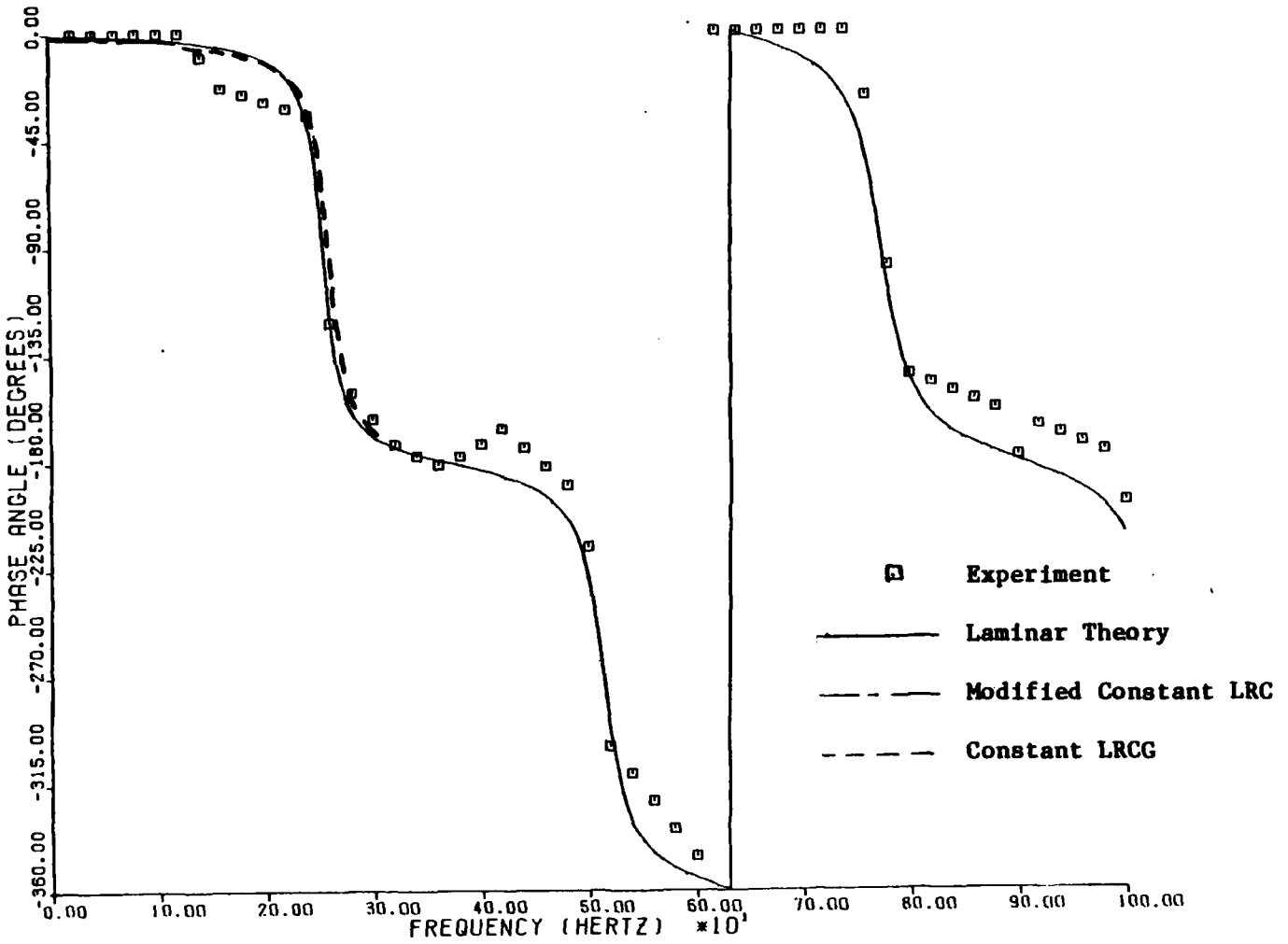

Figure 60 Experimental and Theoretical Phase vs Frequency for Case 33050

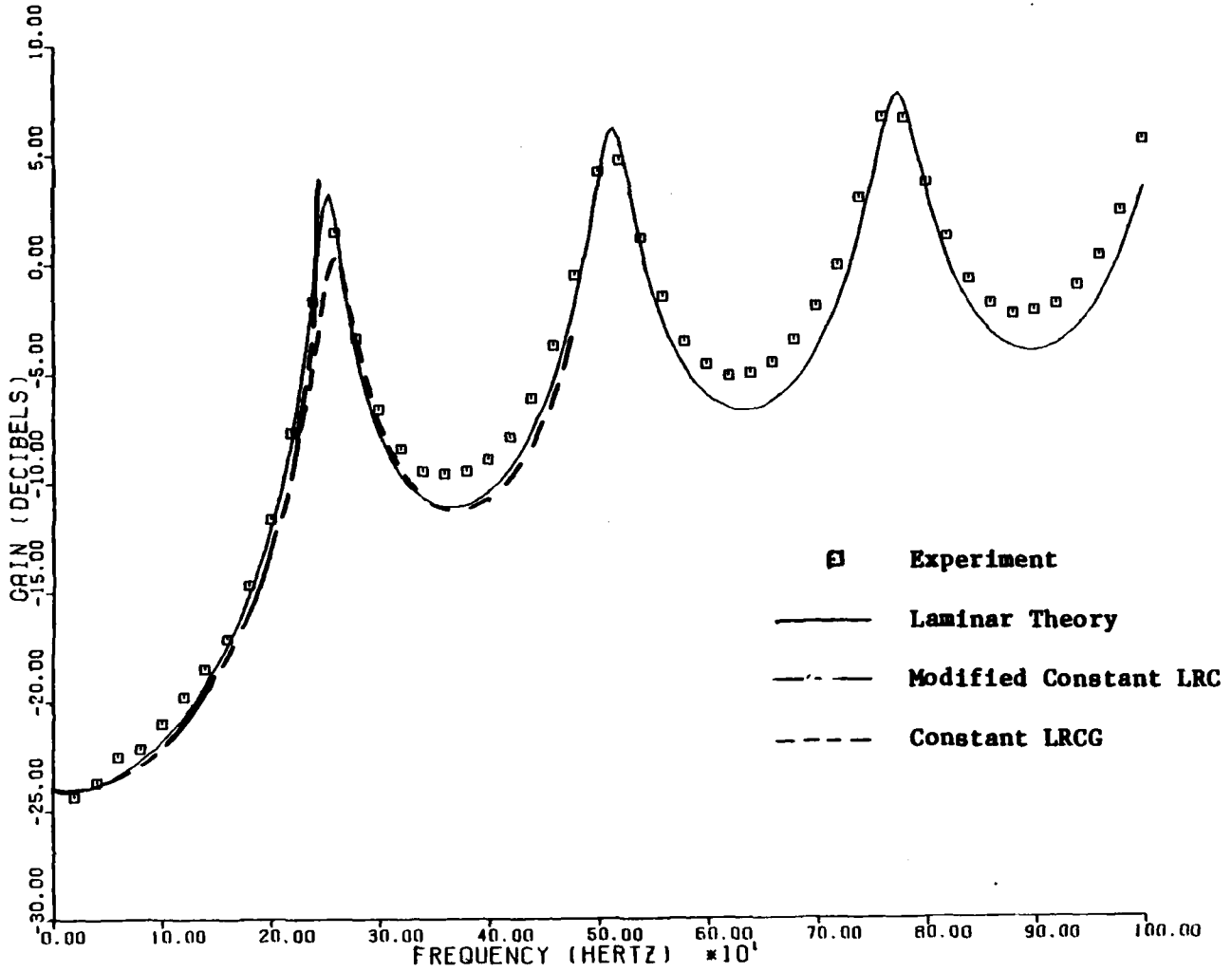

Figure 61 Experimental and Theoretical Gain vs Frequency for Case 33070

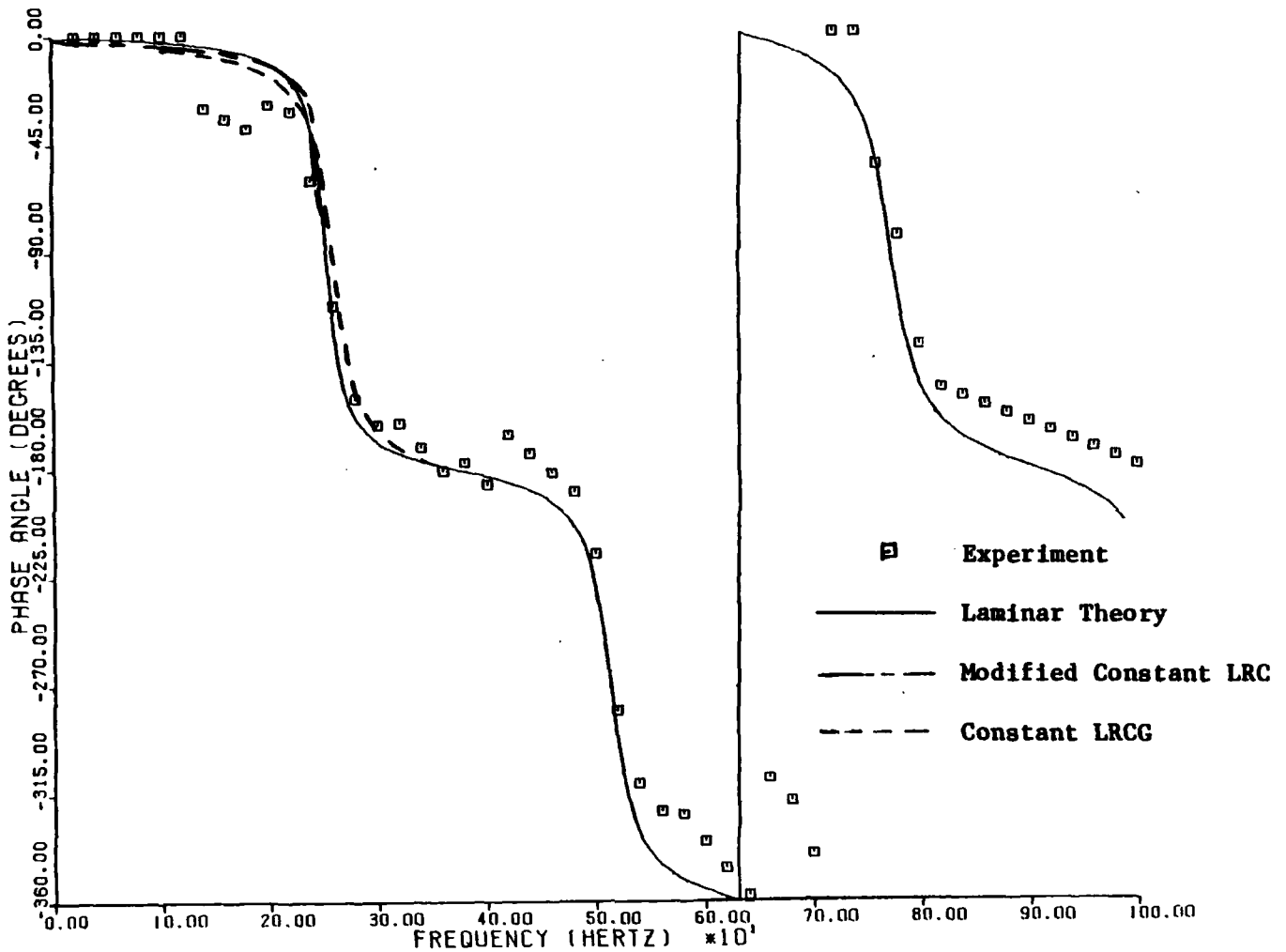

Figure 62 Experimental and Theoretical Phase vs Frequency for Case 33070

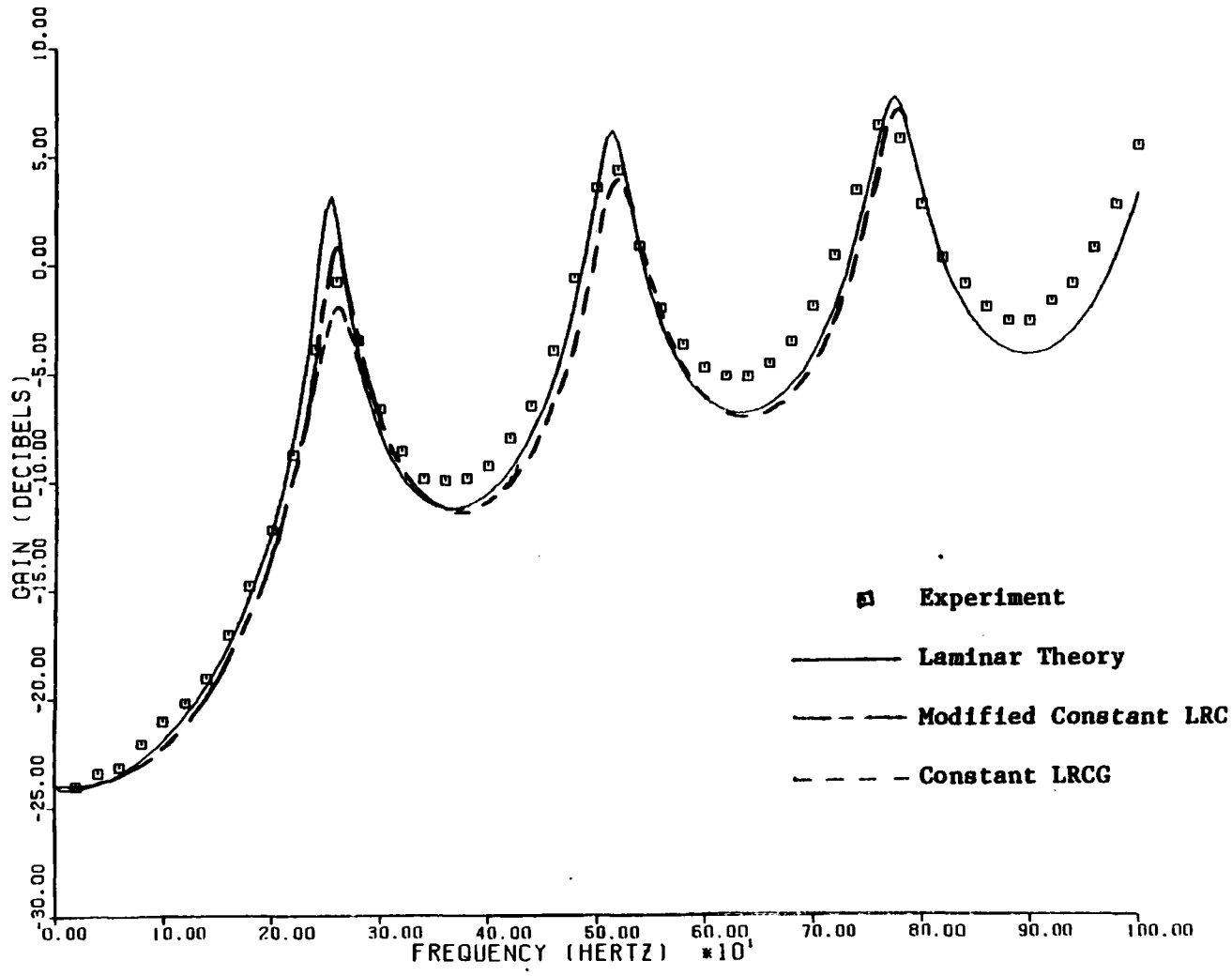

Figure 63 Experimental and Theoretical Gain vs Frequency for Case 33100

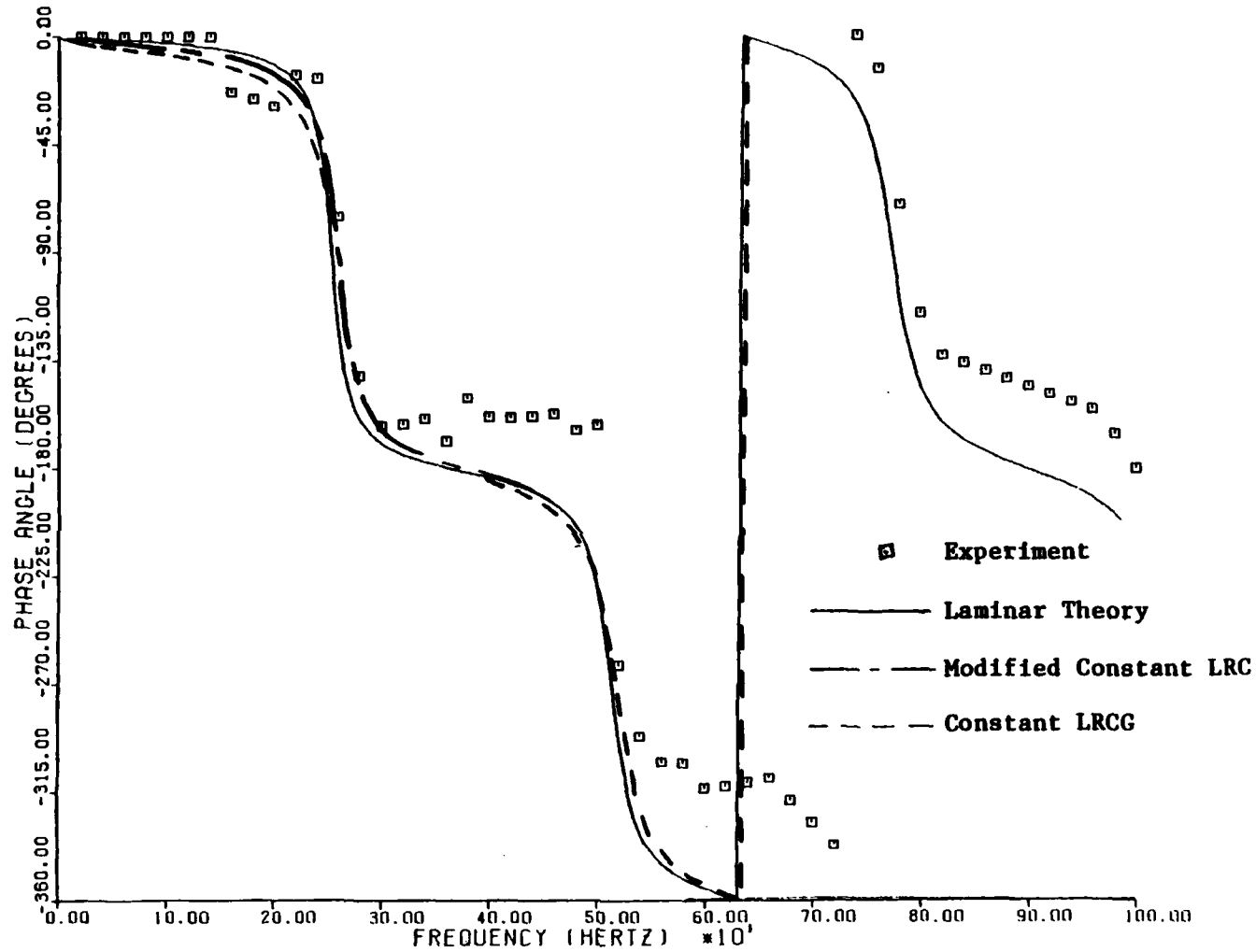

Figure 64 Experimental and Theoretical Phase vs Frequency for Case 33100

Appendix B

Orifice Models

A number of different methods were considered to determine the impedance of an orifice with through flow. The gain predictions of the various models are shown for case 22020 in Fig 65.

Model 1

Since the orifice diameter d is much smaller than the line diameter D, blocked line impedance was assumed

$$Z_L = \infty + j\,0 \tag{52}$$

Model 2

Equation (51) was used assuming constant density equal to that just before the orifice, negligible length and discharge coefficient of 0.6.

Model 3

The AC impedance of equation (51), seen to be twice the value obtained from equation (51), is used with the same assumptions as in Model 2.

Model 4

Model 2 was modified to use mean density by assuming the pressure in the orifice to be half the gauge pressure before the orifice.

Model 5

The same average density was used in conjunction with the AC impedance resulting in twice the impedance of Model 4.

Model 6

The steady state DC impedance of Model 2 is modified by assuming a sonic density in the orifice. The sonic density is found through the use of continuity to be

$$\text{sonic} = M/(A_o(\sqrt{kR_gT_a})) \tag{53}$$

where the Mach number has been taken as unity. Using the sonic density, the DC impedance can be expressed as

$$Z_L = P_L/Q_L = \left[\frac{MP_L}{(2(0.6)^2A^3(kR_gT_a)^{0.5}}\right]^{0.5} \tag{54}$$

Model 7

The AC impedance was calculated using as in Model 6, a Mach number of 1 in the orifice as in Model 6.

Model 8

This model assumes the flow to be isentropic and choked with the A^* value taken to be equal to the orifice area. Since d<<D, the flow in the line is very small and the properties upstream of the orifice are taken to be the stagnation values. With these assumptions, the DC impedance becomes

$$Z_L = \frac{\rho P_L}{\frac{PA^*}{(R_gT_a)^{0.5}}(k)^{0.5}\left(\frac{2}{k+1}\right)^{\frac{k+1}{2(k-1)}}} \tag{55}$$

Model 9

With the same assumptions as in Model 8, the AC impedance is again twice the DC value.

Model 10

Model 8 is used with the density take to be the average value previously mentioned.

Model 11

The AC impedance of Model 9 is calculated using the average density value.

Model 12

Model 8 is used with the sonic density to obtain a DC impedance.

Model 13

The sonic density is substituted for the constant density in Model 9.

Model 14

Funk, Wood and Chao (Ref 18) present an extension to the DC impedance of Model 2 by considering the axial length. The length of the orifice is taken to be 0.06 which is approximately 4 diameters in this case. The flow is assumed to be incompressible with a discharge coefficient of 0.6. The friction factor is found using a Reynolds number of 19000 in the orifice. The resistance

contributed by the orifice axial length is seen to increase the impedance by less than 5 percent.

Model 15

The above method is applied with a correction to the discharge coefficient for compressible flow. Shapiro (Ref 19) shows the discharge coefficient for sharp-edged orifices to vary in a non-linear fashion with the ratio of the downstream to upstream pressures. The discharge coefficient ranges from 0.6, as is assumed for incompressible flow, to approximately 0.85 as the pressure ratio goes from 1.0 to 0.2. Greater pressure differentials yield negligible increases beyond the 0.85 value. For this test case, the pressure ratio is 0.28 giving a discharge coefficient of 0.82. Model 14 is then calculated using this value.

On close examination under a microscope, the orifices used for this study were seen to be far different from sharp-edged or even square-edged models. Since the problem of compressible flow in an orifice is very difficult even when dealing with ideal models, alternative approaches to determining the impedance that do not require the orifice density and discharge coefficient are sought.

Model 16

The use of reflection coefficients is outlined in Section II. When a pressure wave propagating along a line

encounters an area change, as shown in Fig 4, a reflected wave is generated, the size and phase of which is determined by the area change. In the case of a blocked line, the original and reflected waves are identical. The reflection coefficient for this case is then defined to be 1. In the other extreme of an open line, the downstream area is infinite and the reflected pressure wave is equal and 180 degrees out of phase with the original. The corresponding reflection coefficient is -1. For the case where there is no area change, no reflected waves are generated and the reflection coefficient becomes 0. This is also seen to be the case when sonic flow exists as the reflected waves cannot propagate up stream against the mean flow.

To find the reflection coefficients for orifices,the cross-sectional area at the end of the line as seen by the pressure wave can be considered as three distinct regions. The orifice is split into two areas, a core area in which the flow is sonic, given a sufficient pressure ratio, and the remaining annular area which is open to the ambient conditions. The annular area around the orifice acts as a blocked line. The reflection coefficient of each region is then multiplied by its area to determine its contribution to an average reflection coefficient which can be used in equation (42) to find the impedance.

For unchoked cases, no core area exists and the model is reduced to two regions. For choked cases, it was believed that the vena-contracta area would be the core area. An attempt to determine this area using Schlieren flow visualization indicated a region of supersonic flow at the orifice exit. The flow pattern suggests the sonic flow had fully filled the orifice area before the exit plane thus allowing the use of a two region model where the core area is the entire orifice are.

Model 16

As the orifice diameter approaches the line diameter, the impedance tends towards that for an open line. The limiting case of the impedance equal to zero is shown for completeness.

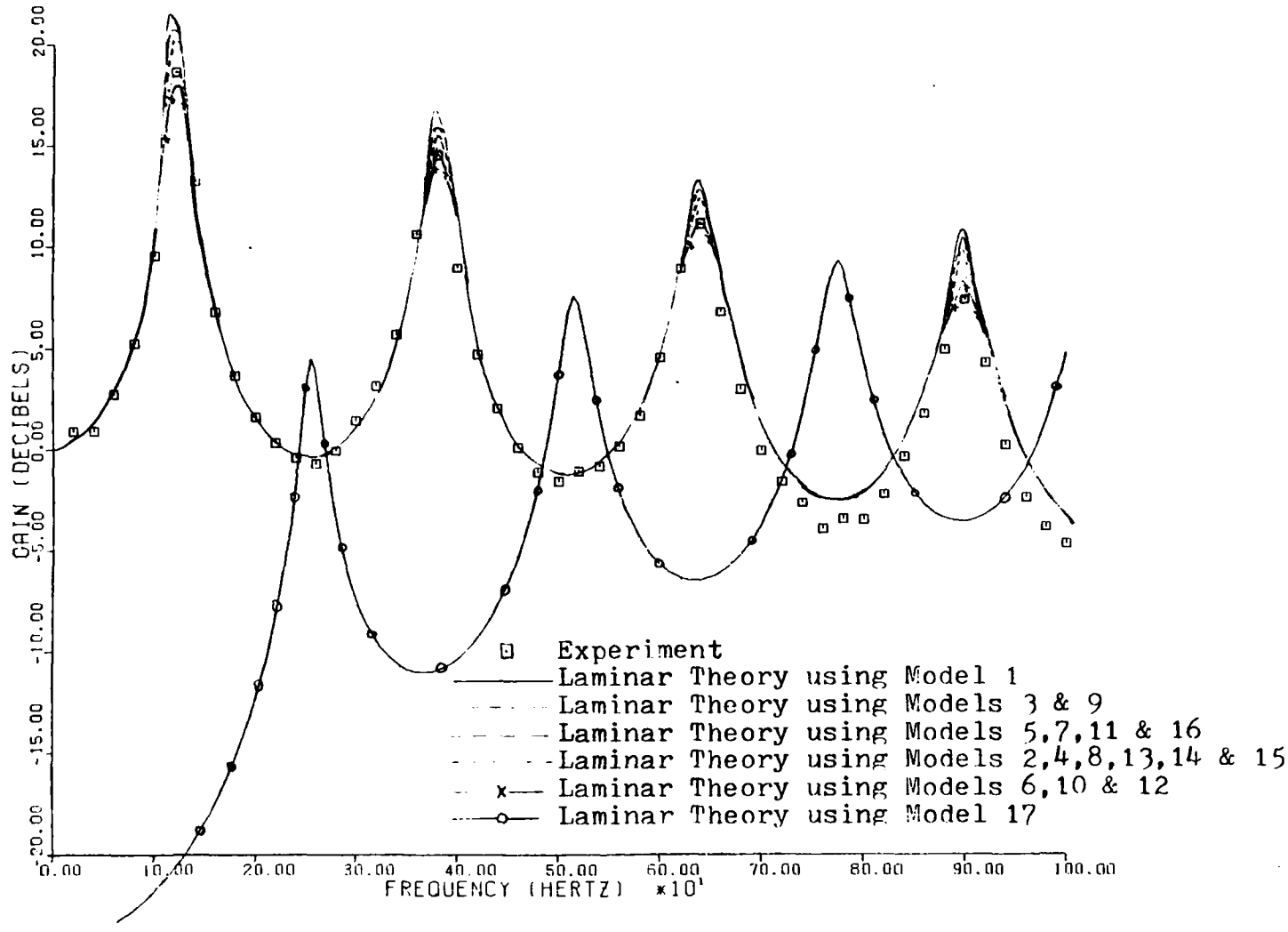

Figure 65 Experimental and Theoretical Gain versus Frequency for Case 22020

APPENDIX C

Computer Program

```
      PROGRAM MSB
      DIMENSION DBT(300),RVT(100),DI(100),AD(100),AR(100),
     1CV(100),OMT(100),CNA(100),GMA(100),AGM(100),FN(100),
     2RN(100),RN(100),GN(100),ALN(100),CN(100),AN(100),
     3BTN(100),AMC(100),AZRN(100),BZRN(100),AZIN(100),
     4BZIN(100),DC(100),DG(100),DD(100),P(100),RHO(100),
     5ANU(100),CA(100),QTCA(100),OMG(300),RTP(100),GP(100),
     6BETA(100),AZOT(100),BZOT(100),REY(100),Q(100),
     7BET(100),TURB(100)
      DIMENSION DB(300),OMGX(300),OMGP(300),PHASE(300),
     1PH(300),CASE(100)
      DATA PI/3.1415926/
      DATA TPI/6.2831853/
C
      OPEN(11,FILE='D1000')
      REWIND 11
      OPEN(12,FILE='ACROUT')
      REWIND 12
      CALL PLOTS(0.,0.,9)
C*****************************
C    TAPE 11 IS THE INPUT FILE CONTAINING THE FOLLOWING
C     ICAS IS THE CASE NUMBER
C     OP INDICATES OPEN LINE; 1.0 FOR OPEN LINE, ELSE 0.0
C     TF IS AMBIENT TEMPERATURE IN DEGREES F
C     PG IS THE BAROMETRIC PRESSURE (PSIA)
C     AMU IS THE DYNAMIC VISCOSITY (PSI-SEC)
C     RE IS THE GAS CONSTANT FOR AIR (IN /SEC / R)
C     GAM IS RATIO OF SPECIFIC HEATS
C     SIG IS SQUARE ROOT OF PRANDTL NUMBER
C     N IS NUMBER OF LINE SEGMENTS
C     CT IS THE TURBULENT CAPACITANCE/ADIABATIC CAPACITANCE
C     TL IS THE INERTANCE CONSTANT
C     FL IS THE MASS FLOW RATE (LBM/SEC)
C     D1 IS OUTSIDE DIAMETER OF LINE (IN)
C     PT IS STATIC LINE PRESSURE (PSIG)
C     ZEND IS REAL PART OF TERMINAL IMPEDANCE (PSI/CIS)
C     ZENDI IS IMAGINARY TERMINAL IMPEDANCE (PSI/CIS)
C     DI IS THE LINE SEGMENT DIAMETER (IN)
C     AD IS THE LINE SEGMENT LENGTH (IN)
C      THE FOLLOWING ARE USED BY THE CALCOMP PLOTTER
C         NPTS IS NUMBER OF EXPERIMENTAL POINTS INPUT
C         LSMB DESIGNATES PLOTTER SYMBOL (SEE USERS GUIDE)
C         FREQ IS EXPERIMENTAL FREQUENCY (HZ)
C         PS IS SENDING PRESSURE, EXPERIMENTAL
C         PR IS RECEIVING PRESSURE, EXPERIMENTAL
C         PHD IS EXPERIMENTAL PHASE DELAY IN MSEC
C*****************************
 110  READ(11,*)ICAS,OP
```

```
      READ(11,*)TF,PG,AMU,RE,GAM,SIG
      READ(11,*)N
      READ(11,*)CT,TL
      READ(11,*)FL
      READ(11,*)D1,PT
      READ(11,*)ZEND,ZENDI
      DO 898 I=1,N
      READ(11,*)DI(I),AD(I)
898   CONTINUE
      NPG=0
      ICT=0
      IND=0
      NNN=0
      M=0
      IF(OP.EQ.1.) GOTO 900
      REYT=1.22999E+06*FL/D1
897   CONTINUE
      PT=PT+PG
      IF(REYT.LT.2300.) THEN
      DP=PT-SQRT(PT**2.+2.27E-10*REYT*(TF+460.)/(D1**3.))
      ELSE
      DP=PT-SQRT(PT**2.+1.12226E-12*REYT**1.75*(TF+460.)/
     1(D1**3.))
      END IF
      P(N)=PT+DP-PG
      PF=P(N)
      DO 899 I=1,N-2
      IF(OP.EQ.1.) GOTO 895
      REYT=1.22999E+06*FL/DI(10)
895   CONTINUE
      PF=PF+PG
      K=N+1-I
      IF(REYT.LT.2300.) THEN
      DP=PF-SQRT(PF**2.+1.135E-10*AD(K)*REYT*(TF+460.)/
     1(D1(K)**3.))
      ELSE
      DP=PF-SQRT(PF**2.+5.61128E-13*REYT**1.75*AD(K)*
     1(TF+460.)/(D1(K)**3.))
      END IF
      P(N-I)=PF+DP-PG
      PF=P(N-I)
      PEND=P(2)
      IF(OP.EQ.1.) PEND=0.0
899   CONTINUE
      P(2)=P(5)
      P(1)=P(2)
      GOTO 903
900   CONTINUE
      TOTL=0.0
      DO 901 I=3,N
      TOTL=TOTL+AD(I)
901   CONTINUE
      TOTL=TOTL+2.
```

```
      REYT=PT*(PT/2.+PG)*(DI(N)**3.)/32./AMU/AMU
      REYT=REYT/TOTL/RE/(TF+460.)
      IF(REYT.LT.2300.) GOTO 902
      REYT=(REYT*32./.1582)**(4./7.)
902   CONTINUE
      GOTO 897
903   CONTINUE
      TOTL=0.0
      DO 2 I=3,N
2     CONTINUE
      RHO(N)=(PG+P(N))/(RE*(TF+460.))
      REYT=(P(N)-PEND)*((P(N)+PEND)/2.+PG)*(DI(N)**3.)/32./
     1AMU/AMU/TOTL/RE/(TF+460.)
      IF(REYT.LT.2300.) GOTO 3
      REYT=(REYT*32./.1582)**(4./7.)
3     QM=REYT*PI*DI(N)*AMU/4.
      DO 23 I=1,N
      PBR=P(I)+PG
      TBR=TF+460.
      RHO(I)=PBR/(RE*TBR)
      ANU(I)=AMU/RHO(I)
      CA(I)=SQRT(PBR*GAM/RHO(I))
      AR(I)=PI*DI(I)*DI(I)/4.
      CV(I)=(8.*PI*ANU(I))/AR(I)
      OMT(I)=CV(I)/SIG/SIG
      CNA(I)=(8.*PI*AMU)/AR(I)/AR(I)
      Q(I)=QM/RHO(I)
23    CONTINUE
      Q(1)=0.0
      Q(2)=0.0
      GMNI=.5*(GAM-1.)
      DO 26 I=1,N
      REY(I)=(4.*RHO(I)*Q(I)/(PI*DI(I)*AMU)
      PBR=P(I)+PG
      TEMP=GMNI/(GAM*PBR)
      GMA(I)=TEMP*AR(I)
      AGM(I)=AR(I)/(GAM*PBR)
      QTCA(I)=0.25*CA(I)
      RVT(I)=.3164*AMU/2./AR(I)/DI(I)/DI(I)*(REY(I)**.75)
      RVT(I)=RVT(I)*1.75
26    FN(I)=QTCA(I)/AD(I)
      NST=1
      DW=0.
      Y=1.
40    DO 80 J=1,NST
      M=M+1
      Y=Y+DW
      W=TPI*Y
      DO 27 I=1,N
      ARG=.5*SQRT(W/CV(I))
27    RN(I)=CNA(I)*(.375+ARG+(.375/(4.*ARG)))
      DO 28 I=1,N
      DC(I)=.25+SQRT(W/OMT(I)+.125*SQRT(OMT(I)/W)
```

```
      DG(I)=SQRT(W/OMT(I))-.125*SQRT(OMT(I)/W)
      DD(I)=DC(I)*DC(I)+DG(I)*DG(I)
 28   GN(I)=W*(GAM-1.)*AGM(I)*DG(I)/DD(I)
      DO 29 I=1,N
      ARG=.5*SQRT(CV(I)/W)
 29   ALN(I)=RHO(I)*(1.+ARG-(ARG*(15.*CV(I)/(W*64.))))/
     1AR(I)
      TEMP=GMNI/W
      DO 30 I=1,N
      TURB(I)=0
 30   CN(I)=AGM(I)*(1.+((GAM-1.)*DC(I)/DD(I)))
      TEMP=-W*W
      DO 31 I=1,N
      TEM1=RN(I)*GN(I)+TEMP*ALN(I)*CN(I)
      TEM2=W*(RN(I)*CN(I)+GN(I)ALN(I))
      CALL RTCMP(ARG1,ARG2,TEM1,TEM2)
      AN(I)=ARG1
      BTN(I)=ARG2
C****************************
C    NEXT 2 TERMS ARE DETERMINED BY THE TURBULENT MODEL
C    TEM1 IS THE REAL PART OF ZY
C    TEM2 IS IMAGINARY PART OF ZY
C    THE TERMS SHOWN ARE FOR THE CONSTANT LRCG MODEL
C    FOR MODIFIED CONSTANT LRC USE
C         TEM1=-W*W*TL*RHO(I)/AR(I)*CT*AGM(I)
C         TEM2=W*RVT(I)*CT*AGM(I)
C****************************
      TEM1=RVT(I)*RVT(I)*(GAM-1.)*CT*AGM(I)*AR(I)/RHO(I)/
     1TL/TL-W*W*TL*RHO(I)/AR(I)*CT*AGM(I)
      TEM2=W*RVT(I)*CT*AGM(I)+W*RVT(I)*(GAM-1.)*AGM(I)/TL
      CALL RTCMP(ARG1,ARG2,TEM1,TEM2)
      TAN=ARG1
      TBTN=ARG2
      IF(REY(I).LT.2300.) GOTO 31
      IF(AN(I).GE.TAN) GOTO 31
      AN(I)=TAN
      BTN(I)=TBTN
      TURB(I)=1
 31   AMC(I)=TPI/BTN(I)
      OX=AR(10)*W/ANU(10)/PI
      OY=AR(10)*CA(10)*AN(10)/PI/ANU(10)
C    CALCULATE Z0
      DO 32 I=1,N
      TEM1=W*ALN(I)
      TEM2=W*CN(I)
      TEM3=RN(I)
      TEM4=GN(I)
      CALL CMPDV(ARG1,ARG2,TEM3,TEM1,TEM4,TEM2)
      CALL RTCMP(AZRNI,BZRNI,ARG1,ARG2)
      AZRN(I)=AZRNI
      BZRN(I)=BZRNI
      IF(TURB(I).EQ.0) GOTO 32
      TEM1=RHO(I)*(P(I)+PG)/AR(I)/AR(I)
```

```
      TEM2=-RVT(I)*(P(I)+PG)/W/AR(I)
      CALL RTCMP(ARG1,ARG2,TEM1,TEM2)
      AZRN(I)=ARG1
      BZRN(I)=ARG2
 32   CONTINUE
C    CALCULATE Z IN 1
      I=1
      TEMP=AN(I)*AD(I)
      IF(TEMP.GT.88.) GOTO 80
      ARG1=COSH(TEMP)
      ARG2=SINH(TEMP)
      TEM5=BTN(I)*AD(I)
      TEMP=COS(TEM5)
      TEM1=ARG1*TEMP
      TEM3=ARG2*TEMP
      TEMP=SIN(TEM5)
      TEM2=ARG2*TEMP
      TEM4=ARG1*TEMP
      CALL CMPDV(ARG1,ARG2,TEM1,TEM2,TEM3,TEM4)
      TEM1=AZRN(I)
      TEM2=BZRN(I)
      CALL CMPMP(TEM3,TEM4,TEM1,TEM2,ARG1,ARG2)
      AZIN(I)=TEM3
      BZIN(I)=TEM4
C    CALCULATE Z IN 3
      I=3
      TEM1=AZRN(I)
      TEM2=BZRN(I)
      IF(OP.EQ.1.) THEN
      TEM3=0.0
      TEM4=-W*0.4*RHO(I)*DI(I)/AR(I)
      ELSE
      TEM3=ZEND
      TEM4=ZENDI
      END IF
      TEM5=AN(I)
      TEM6=AD(I)
      TEM7=BTN(I)
      CALL CALZIN(AARG,BARG,TEM1,TEM2,TEM3,TEM4,TEM5,TEM6,
     1TEM7)
      AZIN(I)=AARG
      BZIN(I)=BARG
C    CALCULATE Z IN 4 AND 5
      DO 34 I=4,5
      TEM1=AZRN(I)
      TEM2=BZRN(I)
      TEM3=AZIN(I-1)
      TEM4=BZIN(I-1)
      TEM5=AN(I)
      TEM6=AD(I)
      TEM7=BTN(I)
      CALL CALZIN(AARG,BARG,TEM1,TEM2,TEM3,TEM4,TEM5,TEM6,
     1TEM7)
```

```
      AZIN(I)=AARG
 34   BZIN(I)=BARG
C    CALCULATE Z IN 2
      I=2
      TEM1=AZRN(I)
      TEM2=BZRN(I)
      TEM3=AZIN(I-1)
      TEM4=BZIN(I-1)
      TEM5=AN(I)
      TEM6=AD(I)
      TEM7=BTN(I)
      CALL CALZIN(AARG,BARG,TEM1,TEM2,TEM3,TEM4,TEM5,TEM6,
     1TEM7)
      AZIN(I)=AARG
      BZIN(I)=BARG
C    CALCULATE RECEIVING Z FOR LINE 6
      I=6
      TEM1=AZIN(I-1)
      TEM2=BZIN(I-1)
      TEM3=AZIN(I-4)
      TEM4=BZIN(I-4)
      CALL ZEBRA(AZOTI,BZOTI,TEM1,TEM2,TEM3,TEM4)
      AZOT(I)=AZOTI
      BZOT(I)=BZOTI
C    CALCULATE Z IN 6
      TEM1=AZRN(I)
      TEM2=BZRN(I)
      TEM3=AN(I)
      TEM4=AD(I)
      TEM5=BTN(I)
      CALL CALZIN(AZINI,BZINI,TEM1,TEM2,AZOTI,BZOTI,TEM3,
     1TEM4,TEM5)
      AZIN(I)=AZINI
      BZIN(I)=BZINI
C    CALCULATE Z IN 7,8,9,10
      DO 39 I=7,10
      TEM1=AZRN(I)
      TEM2=BZRN(I)
      TEM3=AZIN(I-1)
      TEM4=BZIN(I-1)
      TEM5=AN(I)
      TEM6=AD(I)
      TEM7=BTN(I)
      CALL CALZIN(AZINI,BZINI,TEM1,TEM2,TEM3,TEM4,TEM5,
     1TEM6,TEM7)
      AZIN(I)=AZINI
 39   BZIN(I)=BZINI
C    CALCULATE P5/P6
      I=6
      TEMP=BTN(I)*AD(I)
      CSBI1=COS(TEMP)
      SNBI1=SIN(TEMP)
      TEMP=AN(I)*AD(I)
```

```
      ARG1=COSH(TEMP)
      ARG2=SINH(TEMP)
      TEM1=ARG1*CSBI1
      TEM2=ARG2*SNBI1
      AZOTI=AZOT(I)
      BZOTI=BZOT(I)
      AZINI=AZIN(I)
      BZINI=BZIN(I)
      CALL CMPDV(TEM7,TEM8,AZOTI,BZOTI,AZINI,BZINI)
      CALL CMPMP(TEM3,TEM4,TEM7,TEM8,TEM1,TEM2)
      TEM5=ARG2*CSBI1
      TEM6=ARG1*SNBI1
      TEM9=AZRN(I)
      TEM10=BZRN(I)
      CALL CMPDV(TEM7,TEM8,AZOTI,BZOTI,TEM9,TEM10)
      CALL CMPMP(TEM1,TEM2,TEM7,TEM8,TEM5,TEM6)
      TEM1=TEM3-TEM1
      TEM2=TEM4-TEM2
      TEMP=TEM1*TEM1+TEM2*TEM2
      BETA(I)=ATAN2(TEM2,TEM1)
      BET(I)=(180./PI)*BETA(I)
      RTP(I-1)=SQRT(TEMP)
      GP(I-1)=20.*ALOG10(RTP(I-1))
C     CALCULATE P6/P7, P7/P8, P8/P9, AND P9/P10
      DO 43 I=7,10
      TEMP=BTN(I)*AD(I)
      CSBI1=COS(TEMP)
      SNBI1=SIN(TEMP)
      TEMP=AN(I)*AD(I)
      ARG1=COSH(TEMP)
      ARG2=SINH(TEMP)
      TEM1=ARG1*CSBI1
      TEM2=ARG2*SNBI1
      AZINI1=AZIN(I-1)
      BZINI1=BZIN(I-1)
      AZINI=AZIN(I)
      BZINI=BZIN(I)
      CALL CMPDV(TEM7,TEM8,AZINI1,BZINI1,AZINI,BZINI)
      CALL CMPMP(TEM3,TEM4,TEM7,TEM8,TEM1,TEM2)
      TEM5=ARG2*CSBI1
      TEM6=ARG1*SNBI1
      TEM9=AZRN(I)
      TEM10=BZRN(I)
      CALL CMPDV(TEM7,TEM8,AZINI1,BZINI1,TEM9,TEM10)
      CALL CMPMP(TEM1,TEM2,TEM7,TEM8,TEM5,TEM6)
      TEM1-TEM3-TEM1
      TEM2=TEM4=TEM2
      TEMP=TEM1*TEM1+TEM2*TEM2
      BETA(I)=ATAN2(TEM2,TEM1)
      BET(I)=(180./PI)*BETA(I)
      RTP(I-1)=SQRT(TEMP)
 43   GP(I-1)=20.*ALOG10(RTP(I-1))
      RTPT=RTP(6)*RTP(7)*RTP(8)*RTP(9)*RTP(5)
```

```
      GPT=20.*ALOG10(RTPT)
      BETAR=BETA(6)+BETA(7)+BETA(8)+BETA(9)+BETA(10)
35    IF(BETAR.LE.O.) GOTO 36
      BETAR=BETAR-TPI
      GOTO 35
36    IF(BETAR.GT.-TPI) GOTO 37
      BETAR=BETAR+TPI
      GOTO 36
37    BETAD=(180./PI)*BETAR
      WRITE(12,700)Y,BETAD,RTPT,GPT
700   FORMAT(2X,6HFREQ =,F7.0,3X,11HBETA(DEG) =,F7.2,5X,
     16HGAIN =,1PE12.4,1X,2HOR,1X,1PE12.4,2HDB)
      WRITE(12,701)OX,OY
701   FORMAT(2X,6HOMEGA=,F7.2,3X,12HATTENUATION=,F7.2)
      DBT(M)=GPT
      OMG(M)=Y
      PHASE(M)=BETAD
      IF(NNN.GT.1) GOTO 80
      WRITE(12,810)
810   FORMAT(1H0,13X,6HLENGTH,9X,8HDIAMETER,7X,8HPRESSURE,
     19X,5HC ADB,10X,3HFN , 7X,7HDENSITY,5X,11HREYNOLDS NO
     2)
802   FORMAT(1H0,1X,5HLINE ,I2,3X, 8(1PE12.4,2X))
      DO 803 I=1,N
803   WRITE(12,802)I,AD(I),DI(I),P(I),CA(I),FN(I),RHO(I),
     1REY(I)
      NNN=2
80    CONTINUE
      GOTO (85,611),IND
85    Y=0.
      DW=5.
      NST=200
      IND=2
      GOTO 40
C     THE FOLLOWING SECTION IS FOR THE CALCOMP PLOTTER
611   IF(ICAS)502,502,610
610   CALL FACTOR(0.625)
      OMG(M+1)=0.
      OMG(M+2)=100.
      DBT(M+1)=-30.
      DBT(M+2)=5.0
      CALL AXIS(0.,0.,17HFREQUENCY (HERTZ),-17,10.0,0.,
     1OMG(M+1),OMG(M+2))
      CALL AXIS(0.,0.,15HGAIN (DECIBELS),15,8.,90.,
     1DBT(M+1),DBT(M+2))
      CALL LINE(OMG,DBT,M,1,0,4)
      READ(11,*)CASE(1)
      READ(11,*)NPTS,LSMB
      WRITE(12,207)
207   FORMAT(1H0,10X,1HN,4X,4HFREQ,10X,2HPS,10X,2HPR,
     110X,4HGAIN,10X,5HPHASE)
      J=0
      DO 69 I=1,NPTS
```

```
612   READ(11,*)FREQ,PS,PR,PHT
      GPX=20.*ALOG10(PR/PS)
      PHD=-PHT*FREQ*.36
      WRITE(12,209)I,FREQ,PS,PR,GPX,PHD
209   FORMAT(7X,I5,5F12.5)
      DB(I)=GPX
      OMGX(I)=FREQ
      IF(PHD.GT.0) GOTO 69
      J=J+1
      PH(J)=PHD
      OMGP(J)=FREQ
      JMAX=J
69    CONTINUE
      OMGX(NPTS+1)=OMG(M+1)
      DB(NPTS+1)=DBT(M+1)
      OMGX(NPTS+2)=OMG(M+2)
      DB(NPTS+2)=DBT(M+2)
      CALL LINE(OMGX,DB,NPTS,1,-1,LSMB)
      CALL PLOT(15.0,0,-3)
      CALL FACTOR(0.625)
      OMG(M+1)=0.
      OMG(M+2)=100.
      PHASE(M+1)=-360.
      PHASE(M+2)=45.
      CALL AXIS(0.,0.,17HFREQUENCY (HERTZ),-17,10.,0.,
     1OMG(M+1),OMG(M+2))
      CALL AXIS(0.,0.,21HPHASE ANGLE (DEGREES),21,8.,90.,
     1PHASE(M+1),PHASE(M+2))
      CALL LINE(OMG,PHASE,M,1,0,4)
      OMGP(JMAX+1)=OMG(M+1)
      OMGP(JMAX+2)=OMG(M+2)
      PH(JMAX+1)=PHASE(M+1)
      PH(JMAX+2)=PHASE(M+2)
      CALL LINE(OMGP,PH,JMAX,1,-1,LSMB)
      CALL SYMBOL(15.,5.,.165,5HCASE ,0.,5)
      CALL SYMBOL(16.,5.,.165,CASE(1),0.,2)
1003  CALL PLOT(10.0,0,-3)
501   CALL PLOTE
502   STOP
      END
C****************************
      SUBROUTINE RTCMP(X,Y,A,B)
      CALL ANGL(TEMP,A,B)
      TEMP=.5*TEMP
      Y=A*A+B*B
      X=SQRT(Y)
      X=SQRT(X)
      Y=X*SIN(TEMP)
      X=X*COS(TEMP)
      RETURN
      END
```

```
      SUBROUTINE CMPMP(X,Y,A1,A2,B1,B2)
      X=A1*B1-A2*B2
      Y=A1*B2+A2*B1
      RETURN
      END

      SUBROUTINE CMPDV(C1,C2,A1,A2,B1,B2)
      TEMP=B1*B1+B2*B2
      C1=A1*B1+A2*B2
      C1=C1/TEMP
      C2=B1*A2-A1*B2
      C2=C2/TEMP
      RETURN
      END

      SUBROUTINE HSINX(ARG,X)
      A=EXP(X)
      B=EXP(-X)
      A=A-B
      ARG=.5*A
      RETURN
      END

      SUBROUTINE HCOSX(ARG,X)
      A=EXP(X)
      B=EXP(-X)
      A=A+B
      ARG=.5*A
      RETURN
      END

      SUBROUTINE ANGL(C,A,B)
      DATA PI/3.1415926/
      C=ABS(B/A)
      C=ATAN(C)
      IF (A.GT.0.) GOTO 10
      IA=1
      GOTO 7
5     IA=0
7     IF (B.GT.0.) GOTO 10
      IB=2
      GOTO 15
10    IB=0
15    IA=IA+IB+1
      GOTO (35,30,25,20),IA
20    C=C-PI
      GOTO 35
25    C=-C
      GOTO 35
30    C=PI-C
      RETURN
      END
```

```
 SUBROUTINE CALZIN(AZINI,BZINI,AZRNI,BZRNI,AZIN2,
1BZIN2,AN1,DI1,BTN1)
 TEMP=AN1*DI1
 CALL HCOSX(ARG1,TEMP)
 CALL HSINX(ARG2,TEMP)
 TEMP=BTN1*DI1
 CSBI1=COS(TEMP)
 SNBI1=SIN(TEMP)
 ZR=0.
 CALL CMPMP(TEM1,TEM2,AZIN2,BZIN2,ARG1,ZR)
 CALL CMPMP(TEM3,TEM4,AZRN1,BZRN1,ARG2,ZR)
 CALL CMPMP(TEM5,TEM6,AZIN2,BZIN2,ARG2,ZR)
 CALL CMPMP(TEM7,TEM8,AZRN1,BZRN1,ARG1,ZR)
 A1=TEM1+TEM3
 B1=TEM2+TEM4
 A2=TEM5+TEM7
 B2=TEM6+TEM8
 CALL CMPMP(TEM1,TEM2,A1,B1,CSBI1,ZR)
 CALL CMPMP(TEM5,TEM6,A2,B2,CSBI1,ZR)
 CALL CMPMP(TEM7,TEM8,A1,B1,ZR,SNBI1)
 CALL CMPMP(TEM3,TEM4,A2,B2,ZR,SNBI1)
 TEM3=TEM3+TEM1
 TEM4=TEM4+TEM2
 TEM7=TEM7+TEM5
 TEM8=TEM8+TEM6
 CALL CMPDV(TEM1,TEM2,TEM3,TEM4,TEM7,TEM8)
 CALL CMPMP(AZIN1,BZIN1,TEM1,TEM2,AZRN1,BZRN1)
 RETURN
 END

 SUBROUTINE ZEBRA(C1,C2,A1,A2,B1,B2)
 D1=1.
 D2=0.
 CALL CMPDV(ARG1,ARG2,D1,D2,A1,A2)
 CALL CMPDV(ARG3,ARG4,D1,D2,B1,B2)
 ARG1=ARG1+ARG3
 ARG2=ARG2+ARG4
 CALL CMPDV(C1,C2,D1,D2,ARG1,ARG2)
 RETURN
 END
```

Appendix D

Experimental Equipment

Item	Make	Model	Serial Number
1) Pneumatic Driver Assembly	Bendix	PC-DCC -PS	001
2) Wave Analyzer	Hewlett Packard	302A	018-02012 018-01985
3) Oscilloscope	Tektronix	7613	4H4046
4) Pressure Transducer Dynamic	Kristal	701A	65079 65080
5) Pressure Transducer Static (0-50 psig)	Bell & Howell	1000-02	9302
6) Charge Amplifier	Kistler	568	704 1429
7) Digital Multimeter	Hewlett Packard	3466A	3230
8) DC Power Supply	Hewlett Packard	6205B	4646
9) Frequency Counter	Computer Measurement	726C	ENY0035
10) Rotometer	Brooks	Sho-Rate	9175-83
11) Bell Prover	Collins	Chain Compensated Gasometer	2683

Vita

Phillip G. Wilkins was born [redacted] the son of [redacted] After graduating from [redacted] in 1971, he attended Purdue University until enlisting in the U. S. Air Force in January 1976. He was granted a bachelor degree in engineering from Purdue University in 1978, awarded his commission and assigned to Eglin AFB, Florida in 1979. He was assigned to the Air Force Institute of Technology in June 1983.

Permanent Address: [redacted]

UNCLASSIFIED
SECURITY CLASSIFICATION OF THIS PAGE

REPORT DOCUMENTATION PAGE

1a. REPORT SECURITY CLASSIFICATION UNCLASSIFIED	1b. RESTRICTIVE MARKINGS
2a. SECURITY CLASSIFICATION AUTHORITY	3. DISTRIBUTION/AVAILABILITY OF REPORT Approved for public release; distribution unlimited
2b. DECLASSIFICATION/DOWNGRADING SCHEDULE	
4. PERFORMING ORGANIZATION REPORT NUMBER(S) AFIT/GAE/AA/84D-28	5. MONITORING ORGANIZATION REPORT NUMBER(S)
6a. NAME OF PERFORMING ORGANIZATION School of Engineering 6b. OFFICE SYMBOL (If applicable) AFIT/ENY	7a. NAME OF MONITORING ORGANIZATION
6c. ADDRESS (City, State and ZIP Code) Air Force Institute of Technology Wright-Patterson AFB, OH 45433	7b. ADDRESS (City, State and ZIP Code)
8a. NAME OF FUNDING/SPONSORING ORGANIZATION 8b. OFFICE SYMBOL (If applicable)	9. PROCUREMENT INSTRUMENT IDENTIFICATION NUMBER
8c. ADDRESS (City, State and ZIP Code)	10. SOURCE OF FUNDING NOS. PROGRAM ELEMENT NO. / PROJECT NO. / TASK NO. / WORK UNIT NO.
11. TITLE (Include Security Classification) See Box 19	

12. PERSONAL AUTHOR(S)
Phillip G. Wilkins, B.S., Capt., USAF

13a. TYPE OF REPORT	13b. TIME COVERED	14. DATE OF REPORT (Yr., Mo., Day)	15. PAGE COUNT
MS Thesis	FROM _____ TO _____	1984 December	137

16. SUPPLEMENTARY NOTATION

17. COSATI CODES			18. SUBJECT TERMS (Continue on reverse if necessary and identify by block number)
FIELD	GROUP	SUB. GR.	Fluidics, Fluid Transmission Lines, Frequency Response, Pneumatic Transmission Lines
20	04		

19. ABSTRACT (Continue on reverse if necessary and identify by block number)

Title: DYNAMIC RESPONSE OF FLUID TRANSMISSION LINES

Thesis Chairman: Dr. Milton E. Franke

Approved for public release IAW AFR 190-17.
Dean for Research and Professional Development
Air Force Institute of Technology (AIC)
Wright-Patterson AFB OH 45433

20. DISTRIBUTION/AVAILABILITY OF ABSTRACT	21. ABSTRACT SECURITY CLASSIFICATION
UNCLASSIFIED/UNLIMITED ☒ SAME AS RPT. ☐ DTIC USERS ☐	UNCLASSIFIED

22a. NAME OF RESPONSIBLE INDIVIDUAL	22b. TELEPHONE NUMBER (Include Area Code)	22c. OFFICE SYMBOL
Dr. Milton E. Franke	(513) 255-2362	AFIT/ENY

DD FORM 1473, 83 APR EDITION OF 1 JAN 73 IS OBSOLETE.

UNCLASSIFIED
SECURITY CLASSIFICATION OF THIS PAGE

Experimental frequency response data were obtained for straight pneumatic transmission lines of circular cross-section. Three 24 in. long lines with inside diameters of 0.041, 0.119 and 0.195 in. were tested at Reynolds numbers varying from 0 to 15000.

The experimental data were compared with theoretical predictions obtained from the distributed parameter, small signal equations for the blocked and laminar mean flow cases. Several models were used to predict the effects of turbulent mean flow. The prediction capability and limitations of two turbulent flow models, that include the effects of the Reynolds number, but not frequency, were investigated and discussed.

Methods for determining the end impedance of open and orifice terminated lines with mean flow were studied. The relatively simple approach of reflection coefficients gave satisfactory results for both choked and unchoked flow in orifices. The radiation impedance associated with open lines was found to be negligible for all test cases.

ORIGINATOR - SUPPLIED KEY WORDS INCLUDE: